

https://dspace.org/

# Analysis of co-firing biomass with South African coal in pulverised coal boilers

**Pokothoane, Palo Sidwell**

**2011-05-12**
http://hdl.handle.net/10539/9744

Downloaded from a DSpace repository. https://dspace.org/

# ANALYSIS OF CO-FIRING BIOMASS WITH SOUTH AFRICAN COAL IN PULVERISED COAL BOILERS.

Palo Sidwell Pokothoane

A thesis submitted to the Faculty of Engineering and the Built Environment, University of the Witwatersrand, in fulfilment of the requirements for the degree of Doctor of Philosophy.

Johannesburg, 2010.

DECLARATION

I declare that this thesis is my own, unaided work. It is being submitted for the Degree of Doctor of Philosophy in the University of the Witwatersrand, Johannesburg. It has not been submitted before for any degree or examination in any other university.

_____day of_____(year)_____
(Signature of candidate)

ABSTRACT

In this study, the effect on the extent of emissions reduction with co-combustion of small proportions (0-20%) of biomass with coal in a pulverised fuel combustor, is investigated. Such emissions include $CO_2$, $SO_2$ and $NO_x$. South African coal has high ash content and low volatile content that affects its ignitability. The effect of biomass co-firing on ignitability and slagging is also investigated. While higher percentages of biomass could reduce emissions more and improve ignitability, biomass tends to increase the undesirable fouling and slagging propensities, hence limiting the amount of biomass that can be co-fired.

Two types of biomass, namely grass and sawdust (calorific value 16-18 MJ/kg), and one coal (calorific value 21 MJ/kg) were used in this study. Combustion tests were carried out using the Eskom 1 MW Pilot Scale combustion Test Facility (PSCTF). The coal chosen was representative of an average coal burned at the Eskom's coal-fired power stations. For each of the types of biomass, three blends of biomass and coal were used, resulting in seven different feed fuels including coal alone. The ratios of biomass to coal, on an energy basis, in the three blends were 10%:90%, 15%:85% and 20%:80%. Seven tests were also carried out with the same fuels using a drop tube furnace (DTF) to determine the reaction kinetics of the baseline coal and its three different blends with each type of biomass. The reaction parameters obtained from these tests were used as input data in numerical simulations of the tests. Simulation using CFD software was used to predict combustion characteristics of each fuel in the PSCTF, which in turn can be extrapolated to predict the performance in a full scale commercial boiler. The simulation results were validated by the experimental data from the PSCTF; comparison of the combustion and emissions characteristics with experimental data from the PSCTF showed that the simulation procedure was capable of predicting these characteristics with generally good accuracy.

The results coming out of this work are positive. Co-firing with grass at the PSCTF was found to reduce the emissions by between 13% and 50% for $NO_X$, between 12% and 23% for $CO_2$ and between 21% and 29% for $SO_2$ as the proportion of biomass increased from 10% to 20%. The maximum emissions reduction for sawdust occurred at 20% co-firing ratio; these are, 29% for $NO_x$, 17% for $CO_2$ and 15% for $SO_2$.

For grass based co-firing, the combustion efficiency of the coal used was improved by 0.55% and 0.62% for 15% and 20% co-firing ratios respectively; whereas that of sawdust was between 0.78% and 0.38% as co-firing ratio was increased from 10% to 20%. Combustion efficiency for 10% grass dropped by 0.65%. The DTF results indicate that both grass and sawdust were able to improve the ignitability of the coal used in a temperature range of 1000℃ to 1200℃. The combustion efficiency determined from DTF results for this range indicate an improvement of between 0.1% and 1.4% for grass and between 0.8% and 2.45% for sawdust. The QEMSCAN analysis of slag deposits when co-firing biomass indicated that they should generally be weak enough to be handled by soot blowing equipment.

In conclusion grass (herbaceous) biomass resulted in greater emissions reductions than sawdust (ligneous). It was also found that slagging would be less of a problem when using grass, because the slag deposits are more friable than those of sawdust. At higher co-firing ratios grass based co-firing was found to improve coal ignitability better than that can be achieved with sawdust. The optimum co-firing ratio with grass would appear to be about 15% on an energy basis.

This project was carried out to obtain fundamental technical information on some of the salient effects of using biomass co-firing with pulverised power station coal. Before any implementation can be carried out, the next step would be to conduct a detailed technical and economic feasibility

study into possible large-scale applications, using full systems engineering principles.

DEDICATION

To my wife, son and daughter who patiently endured my absence during the hard and trying times while pursuing this study. *Kea leboha Matebele*.

ACKNOWLEDGEMENTS

I would like to thank my supervisor Professor John Sheer who gave me professional guidance throughout the duration of this research project. My thanks also go to Eskom Corporate Services Division, for funding this project and allowing me to use their Pilot Scale Combustion Test Facility (PSCTF) and the Drop Tube Furnace (DTF). I also want to express my sincere gratitude to the Eskom staff for their unfailing support throughout this project, without which the project would not have been a success. In particular I would like to thank Professor Mark Van der Riet for his advice and guidance during the early stages of this project, Bonny Nyangwa for identifying slots for my tests on the PSCTF and providing moral support, Priven Rajoo for helping me to run the tests on PSCTF, Dr. Chris Van Alphen for slag analysis and technical advice, Ali Thipe and Deborah Carpede for enabling me to run tests in the Drop Tube Furnace and finally, the efforts of Maria Kgaphola and her staff for coal sampling at the mine, milling of the grass and for physical and chemical analyses of various samples. The contribution of Professor Rosemary Falcon in providing technical advice is very much appreciated.

## CONTENTS


1 INTRODUCTION ..... 1
1.1 Background ..... 1
1.2 Statement of the Problem ..... 4
1.3 Scope and Objectives ..... 6
1.4 Envisaged Contribution to Knowledge ..... 7
1.5 Outline of the Report ..... 9
2 LITERATURE REVIEW ..... 11
2.1 Pulverised Fuel Boilers (PFB) ..... 11
2.2 Emissions From Pulverised Fuel Boilers ..... 12
2.2.1 $NO_x$ Formation ..... 12
2.2.2 Sulphur Dioxide ($SO_2$) and Carbon Dioxide ($CO_2$) Emissions 15
2.3 Emissions Control ..... 15
2.3.1 Control of $NO_x$ Formation ..... 15
2.3.2 Fly Ash Control ..... 16
2.4 Ash Deposition and Surface Corrosion ..... 16
2.4.1 Slagging ..... 17
2.4.2 Fouling ..... 19
2.4.3 Corrosion ..... 20
2.5 Effect of Co-firing Biomass with Coal on Emissions and Ash ..... 22
2.5.1 Effect of co-firing on $NO_X$ Emissions ..... 22
2.5.2 Effect of co-firing on $SO_2$ emissions ..... 23
2.5.3 Effect of co-firing on $CO_2$ emissions ..... 24
2.5.4 Effect of co-firing on ash deposition (Slagging and fouling) .. 25
2.5.5 Effect of co-firing on Ignition and Flame Stability ..... 27
2.6 Fuel Preparation ..... 30
2.6.1 Biomass Storage ..... 30
2.6.2 Grinding of Biomass ..... 30
2.6.3 Particle Size, Burnout and Residence Time ..... 31
2.7 Fuel injection methods ..... 32
2.7.1 Blending or co-milling ..... 32
2.7.2 Direct Injection ..... 33
2.8 Biomass availability as a sustainable fuel ..... 34
2.9 Impact on boiler efficiency ..... 36
3 NUMERICAL SIMULATION ..... 37

3.1 Inert Heating ..... 38
3.2 Devolatilisation ..... 39
3.3 Heat transfer to the particles during devolatilisation ..... 40
3.4 Char Reaction Model ..... 40
3.5 The Radiation Model ..... 42
3.6 Turbulence Model ..... 43
3.7 Discrete Phase Model ..... 44
3.7.1 Particle Force Balance ..... 44
3.7.2 Stochastic Tracking – Discrete Random Walk Model ..... 46
3.8 Setting up Discrete Phase Model ..... 47
3.8.1 Particle Tracking and Dragging Parameters ..... 47
3.8.2 Defining Injections ..... 49
3.9 Modelling $NO_X$ Formation ..... 56
3.9.1 Distribution of Nitrogen in Fuel Between Volatiles and Char 56
3.9.2 Partitioning of Volatile-N and Char-N into HCN and $NH_3$ ..... 59
3.10 $SO_2$ Formation ..... 60
4 EXPERIMENTAL PROCEDURE AND APPARATUS ..... 62
4.1 Fuel Preparation and Sampling ..... 62
4.1.1 Fuel Sourcing and Preparation ..... 62
4.1.2 Preparing a Representative Sample ..... 65
4.1.3 Size Grading ..... 68
4.2 Setting up the Pilot Scale Combustion Test Facility for Tests ..... 70
4.2.1 Description of the Pilot Scale Combustion Test Facility ..... 70
4.2.2 Biomass Vibratory Feeder ..... 75
4.2.3 Chemical and Physical Analyses ..... 77
4.2.4 Sample Calculation of Air Flow requirements for Test 13 (Table 5.2) ..... 78
4.2.5 Excess Air ..... 82
4.2.6 Data Recording and Sampling ..... 82
4.3 Conducting Tests in the Drop Tube Furnace (DTF) ..... 84
4.3.1 Description of the Drop Tube Furnace ..... 84
4.3.2 Procedure for running tests in the DTF ..... 85
4.3.3 Determination of Reaction Kinetics ..... 90
4.3.4 Sample Calculation of Kinetics for 15% Grass (See Appendix J, page L-14 for comparison). ..... 91
4.3.5 Calculation of Combustion Efficiency ..... 96

5 RESULTS ..... 98
5.1 Chemical Analysis Results ..... 98
5.2 Results From The Pilot Scale Combustion Test Facility ..... 99
5.3 Drop Tube Furnace (DTF) Results ..... 105
6 DISCUSSION OF RESULTS ..... 111
6.1 Experimental Results – Emissions ..... 111
6.1.1 $NO_X$ ..... 111
6.1.2 Repeat Tests (Coal B and Sawdust only) ..... 117
6.1.3 $SO_2$ ..... 121
6.1.4 $CO_2$ ..... 128
6.1.5 Ignition Behaviour Shown by the Results from the ERID/ESKOM Pilot Scale Combustion Test Facility ..... 131
6.1.6 Ignition Behaviour shown by DTF results ..... 136
6.1.7 Analysis of slag deposits ..... 145
6.2 Model validation ..... 154
6.2.1 Nitrogen Oxide ($NO_X$) Emissions ..... 154
6.2.2 Carbon dioxide ($CO_2$) Emissions ..... 156
6.2.3 Sulphur Dioxide ($SO_2$) Emissions ..... 157
6.2.4 Temperature Profiles ..... 159
7 CONCLUSION and recommendations ..... 165
7.1 CONCLUSIONS ..... 165
7.1.1 Percentage Reduction as Function of Co-firing Ratio ..... 165
7.1.2 Best Type of Biomass Based on Percentage Reduction in Emissions With Tolerable Slagging and Fouling Propensities ..... 166
7.1.3 Optimum Biomass Ratio Based on Carbon Burnout for the Best Type of Biomass ..... 166
7.1.4 The Effect of Biomass on the Ignitability of Low-volatile Coal 167
7.1.5 Validation of Simulation Technique Using the Experimental Results 167
7.2 RECOMMENDATIONS ..... 167
8 LIST OF REFERENCES ..... 171
9 LIST OF APPENDICES ..... 180

**LIST OF FIGURES**

Figure 2.1 *Pulverised fuel boiler* (Sabastian, 2002) ..... 11

Figure 2.2 Multi-fuel burner configuration for co-firing biomass with coal (Sami et al, 2001) ..... 34

Figure 3.1 The Discrete Phase Model data entry panel. ..... 47

Figure 3.2 Discrete Phase Injections data input panel ..... 50

Figure 3.3 Rosin-Rammler particle size distribution for sawdust..... 55

Figure 3.4 First mechanism: $NO_X$ formation all char N converts to the intermediate species (adapted from Fluent (2006) ..... 58

Figure 3.5 Second mechanism 2: $NO_X$ formation all char N converts NO directly (adapted from Fluent (2006) ..... 58

Figure 4.1 Swing mill pot is held in position by pneumatically inflated rubber clamp during operation. ..... 64

Figure 4.2 Swing mill pot opened to show the sliding grinder ..... 64

Figure 4.3 The splitter used to mix or subdivide samples ..... 67

Figure 4.4 Fuel and air flows through the PSCTF low-NOX burner ..... 71

Figure 4.5 Eskom Pilot Scale Combustion Test Facility..... 72

Figure 4.6 A Diagrammatic representation of the PSCTF burner..... 73

Figure 4.7 Dimensions of the Eskom Pilot Scale Combustion Test Facility ..... 74

Figure 4.8 Feeding of biomass into the PSCTF burner using a vibratory feeder ..... 77

Figure 4.9 Fly ash sampling at port 9 and slagging probe on the floor. The Slagging probe was used to take slag samples which were sent to Van Alphen Consultancy for detailed analysis. ..... 84

Figure 4.10 Eskom DTF top half showing pre-heater and water cooled injection probe. ..... 86

Figure 4.11 Eskom Drop Tube Furnace Schematic (source: Eskom Fuel and Combustion Technology Brochure, 2005)..... 87

Figure 4.12 Eskom DTF Showing bottom-half with water cooled sampling probe ..... 87

Figure 4.13 Sampling probe positions from the DTF combustion chamber entry. ..... 88

Figure 4.14 Best fitting line drawn through DTF experimentally derived data points. ..... 94

Figure 6.1 Effect of Sawdust on Emissions from the Baseline (Original test nos. 11, 13-15) ..... 112

Figure 6.2 The effect of grass on emissions from the baseline (Original test nos. 11, 16-18) ..... 112

Figure 6.3 The effect of sawdust on emissions from the baseline (Repeated test Nos. 1-4) ..... 113

Figure 6.4 Correlation of peak flue gas temperature and excess air for tests nos. 11, 13-18 and 1-4. ..... 114

Figure 6.5 Correlation of $NO_x$ emissions and excess air for tests nos. 11, 13-18 and 1-4 ..... 115

Figure 6.6 Correlation of $NO_x$ emissions and peak flue gas temperature and excess air for tests nos. 11, 13-18 and 1-4 ..... 115

Figure 6.7 Effect of fluctuations in coal flow rate on $SO_2$ emissions for sawdust-based co-firing. ..... 125

Figure 6.8 Effect of fluctuations in coal flow rate on $SO_2$ emissions for grass-based co-firing. ..... 125

Figure 6.9 Effect of fluctuations in coal flow rate on $CO_2$ emissions and the actual excess air for sawdust-based co-firing. ..... 129

Figure 6.10 Effect of fluctuations in coal flow rate on $CO_2$ emissions and the actual excess air for grass-based co-firing. ..... 129

Figure 6.11 Effect of sawdust on flue gas temperature profiles and combustion efficiency (Original Test nos. 11, 13-15) ..... 132

Figure 6.12 Effect of sawdust on flue gas temperature profiles and combustion efficiency (Repeated Test nos. 1-4) ..... 133

Figure 6.13 Effect of grass on flue gas temperature profiles and combustion efficiency (Original test nos. 11, 16-18). ..... 134

Figure 6.14 Sawdust based co-firing burnout profiles from the DTF ..... 140

Figure 6.15 Grass-based co-firing burnout profiles from the DTF at ..... 140

Figure 6.16 Sawdust based co-firing combustion efficiency profiles ..... 141

Figure 6.17 Grass based co-firing combustion efficiency profiles from .. 141
Figure 6.18 Sawdust based co-firing combustion efficiency profiles from DTF at 1400 ℃ ..... 144

Figure 6.19 Grass based co-firing combustion efficiency profiles from DTF at 1400 ℃ ..... 144

Figure 6.20 Test 14: 85% coal and 15% sawdust. Solid clinker samples dominated by Ca-Fe aluminosilicate and Ca-Fe quartz glass (van Alphen, 2008). ..... 149

Figure 6.21 Test 15 80% coal and 20% sawdust. Note the “consolidated” clinker deposit (bottom left) compared to the clinker deposit with a high proportion of voids (van Alphen, 2008). ..... 150

Figure 6.22 Test 16: 10% Grass and 90% Coal. Clinker deposit mainly consists of thin walled- cenospheres. Consolidated clinker deposit appears at the bottom of the deposit (van Alphen, 2008). ..... 151

Figure 6.23 Backscatter electron micrograph of T18 clinker deposit. Note the spherical Fe-oxide grains (light grey), angular quartz (Q), aluminosilicate (Ka) and anorthite laths in light grey “glass”. Scale bar is 500 μm. The dark background is epoxy resin (van Alphen, 2008). ..... 152

Figure 6.24 $NO_X$ profiles for sawdust/coal co-firing ..... 155

Figure 6.25 $NO_X$ profiles for grass/coal co-firing ..... 155

Figure 6.26 $CO_2$ profiles for sawdust/coal co-firing ..... 156

Figure 6.27 $CO_2$ profiles for grass/coal co-firing ..... 156

Figure 6.28 $SO_2$ profiles for sawdust/coal co-firing ..... 158

Figure 6.29 $SO_2$ profiles for grass/coal co-firing ..... 158

Figure 6.30 Temperature distribution for baseline coal A ..... 161

Figure 6.31 Temperature distribution for 10% sawdust / 90% coal A ..... 162

Figure 6.32 Temperature distribution for 20% sawdust / 80% coal A ..... 163

Figure 6.33 Temperature distribution for 10% grass / 90% coal A ..... 163

Figure 6.34 Temperature distribution for 15% grass / 85% coal A ..... 164

Figure 6.35 Temperature distribution for baseline coal A..... 164

## LIST OF TABLES

Table 2.1 Relationship between fouling index and fouling tendencies ..... 20

Table 3.1 Flow rates and mass weighted shape factors for different co-firing ratios ..... 49

Table 3.2 Sawdust size grading presented in Rosin-Rammler format ..... 50

Table 3.3 Discrete phase parameters entered in the injections panel..... 51

Table 3.4 Properties of coal used for the simulation of tests run at the Pilot Scale Combustion Test Facility (PSCTF)..... 52

Table 3.5 Properties of sawdust used for the simulation of tests run at Pilot Scale Combustion Test Facility (PSCTF)..... 53

Table 3.6 Properties of grass used for the simulation of tests run at Pilot Scale Combustion Test Facility (PSCTF)..... 54

Table 3.7 Fuel-N Parameters for Simulation of Sawdust-based Co-firing 57

Table 3.8 Fuel-N Parameters for Simulation of Grass-based Co-firing .... 57

Table 3.9 Partition of HCN and NH3 in Volatile-N and Char-N ..... 59

Table 3.10 Fuel-S Parameters for Simulation of Sawdust-based Co-firing ..... 61

Table 3.11 Fuel-S Parameters for Simulation of Grass-based Co-firing .. 61

Table 4.1 Calorific values of coals from various Eskom power stations... 65

Table 4.2 Properties of selected possible coals ..... 66

Table 4.3 Biomass size grading ..... 69

Table 4.4 Sample calculation for stoichiometric mass of air required to burn sawdust. ..... 79

Table 4.5 Sample calculation for stoichiometric mass of air required to burn coal A..... 80

Table 4.6 Sampling ports used, their distance from the burner mouth and the quantities sampled ..... 83

Table 4.7 Gas temperature and wall temperature calibration data for DTF ..... 89

Table 4.8 Temperature and surface reaction rate coefficient values for 15% grass ..... 94

Table 5.1 Chemical and Physical Properties of Fuels and Ashes (Air-dried basis) ..... 98

Table 5.2 Co-firing tests done on the PSCTF ..... 99

Table 5.3 Summary of the data obtained from the Pilot Scale Combustion Test Facility using the original coal sample (coal A). ..... 101

Table 5.4 Summary of the data obtained from the PSCTF for the additional tests using the second coal sample (coal B) ..... 102

Table 5.5 Percentage unburned carbon for the test done on the PSCTF ..... 104

Table 5.6 Tests that were done at the DTF ..... 105

Table 5.7 Mass of respective raw fuels required to prepare blends to be co-fired ..... 105

Table 5.8 Raw fuels analysis results ..... 107

Table 5.9 Char analysis results ..... 108

Table 5.10 Unburned carbon determined from the combustible residue at each testing position. ..... 109

Table 5.11 Combustion efficiency calculated at each testing position. .. 109

Table 5.12 Char particle diameter and density ..... 110

Table 6.1 Excess air, peak flue gas temperature and $NO_X$ for all tests run on PSCTF ..... 116

Table 6.2 Comparison of original sawdust results (Sep 2007) and the results of repeated tests (Aug 2008). ..... 119

Table 6.3 Comparison of original sawdust results (Sep 2007) and the results of repeated tests (Aug 2008). ..... 120

Table 6.4 Standard deviation of the logged data for original and repeat tests. ..... 123

Table 6.5 Normalized values of coal flow rate standard deviation and $SO_2$ meter readings. ..... 124

Table 6.6 Normalized values of coal flow rate standard deviation, $CO_2$ meter readings and % excess air..... 128

Table 6.7 Ignition parameters of the fuels combusted in the DTF..... 137

Table 6.8 Calculated normative mineral proportions based on chemical analysis (van Alphen, 2008)..... 146

Table 6.9 Clinker deposit mineral and phase proportions - volume % (van Alphen, 2008) ..... 148

Table 6.10 Percentage error in predicting flue gas temperatures. ..... 159

Table 7.1 Emissions of grass and sawdust at 20%..... 165

Table 7.2 Unburned carbon for 15% and 20% grass along the radiative section ..... 166

## LIST OF SYMBOLS

| | | |
|---|---|---|
| $\bar{d}$ | = mean diameter | (m) |
| a | = absorption coefficient | |
| $A_1$ | = pre-exponential factor | ($s^{-1}$) |
| $A_p$ | = surface area of the particle | ($m^2$) |
| $a_p$ | = equivalent absorption coefficient | |
| $A_p$ | = particle surface area | ($m^2$) |
| $A_{pn}$ | = projected area of the nth particle | ($m^2$) |
| $C_1$ | = mass diffusion-limited rate constant | ($s^{-1}$) |
| $C_2$ | = kinetics-limited rate pre-exponential factor | ($kg/m^2$ s Pa) |
| $C_D$ | = drag coefficient | |
| $c_p$ | = heat capacity of the particle | (J/kg-K) |
| $D_o$ | = diffusion rate coefficient | ($m^2/s$) |
| $d_p$ | = current particle diameter | (m) |
| $d_p$ | = particle diameter | (m) |
| $d_{p,0}$ | = original particle diameter | (m) |
| $d_{pn}$ | = diameter of the nth particle | (m) |
| $E$ | = activation energy | (J/mol) |
| $E_k$ | = kinetics-limited rate activation energy | (J/mol) |
| $E_p$ | = equivalent emission of particles | |
| $F_{char}$ | = mass fraction of char in fuel (dry-ash-free basis (daf)) | |
| $F_{char}$ | = mass fraction of char in fuel (daf) | |
| $f_{pn}$ | = scattering factor of the nth particle | |
| $f_{v,0}$ | = mass fraction of volatiles initially present in the particle | |
| $F_{vol}$ | = mass fraction of volatiles in fuel (daf) | |
| $F_{vol}$ | = mass fraction of volatiles in fuel (daf) | |
| $f_{w,0}$ | = mass fraction of evaporating/boiling material | |
| $F_x$ | = additional acceleration (force/unit particle mass) term | ($m/s^2$) |

| | | |
|---|---|---|
| $G$ | = the incident radiation | ($W/m^2$) |
| $G_b$ | = generation of turbulence kinetic energy due to buoyancy | |
| $G_k$ | = generation of turbulence kinetic energy due to the mean velocity gradients | |
| $h$ | = convective heat transfer coefficient is predominantly carbon | ($W/m^2$-K) |
| $k$ | = kinetic rate | ($s^{-1}$) |
| $m_B$ | = mass flow rate of biomass (sawdust or grass) | (kg/h). |
| $m_C$ | = mass flow rate of coal | (kg/h). |
| $m_p$ | = mass of the particle | (kg) |
| $m_{p,0}$ | = initial particle mass | (kg) |
| $n$ | = spread factor | |
| $N_{split}$ | = split of nitrogen between volatiles and char | |
| $P_{Nc}$ | = percentage by mass of nitrogen in char (Char-N) | |
| $P_{Nv}$ | = percentage by mass of nitrogen in volatiles (Volatile-N) | |
| $P_{ox}$ | = oxidant partial pressure | |
| $P_{Sc}$ | = percentage by mass of sulphur in char (Char-S) | |
| $P_{Sv}$ | = percentage by mass of sulphur in volatiles (Volatile-S) | |
| $R$ | = universal gas constant | (J/mol K) |
| $R_k$ | = kinetic rate | ($s^{-1}$) |
| $S$ | = actual surface area of the particle | ($m^2$) |
| $s$ | = surface area of the sphere having the same volume as the particle | ($m^2$) |
| $S_b$ | = stoichiometric mass of oxygen required to burn 1 kg of char | |
| $S_k$ | = user defined source term | |

| | | |
|---|---|---|
| $S_{split}$ | = split of sulphur between volatiles and char | |
| $S_\varepsilon$ | = user defined source term | |
| $T_\infty$ | = temperature of the gas surrounding the particle | (K) |
| $TN_{fuel}$ | = percentage by mass of nitrogen in fuel (daf) to the overall dissipation rate | |
| $T_L$ | = Lagrangian integral time | (s) |
| $T_P$ | = particle temperature | (K) |
| $TS_{fuel}$ | = percentage by mass of sulphur in fuel (daf) | |
| u | = component of flow velocity perpendicular to gravitational vector | (m/s) |
| $u'$ | = Gaussian distributed random velocity fluctuation | (m/s) |
| $u_f$ | = fluid phase velocity | (m/s) |
| $u_p$ | = particle velocity | (m/s) |
| *v* | = component of flow velocity parallel to gravitational vector. | |
| $Y_M$ | = contribution of the fluctuating dilation in compressive turbulence | |
| $\varepsilon_p$ | = particle emissivity | |
| $\varepsilon_{pn}$ | = emissivity of the nth particle | |
| $\theta_R$ | = radiation temperature | (K) |
| $\mu$ | = molecular viscosity of the fluid | ($m^2/s$) |
| $\rho$ | = fluid density | ($kg/m^3$) |
| $\rho_p$ | = density of the particle | ($kg/m^3$) |
| $\sigma_B$ | = Stefan-Boltzmann constant | ($W/m^2\text{-}K^4$) |
| $\sigma$ | = scattering coefficient | |
| $\sigma_k$ | = turbulent Prandtl number for k | |
| $\sigma_\varepsilon$ | = turbulent Prandtl number for $\varepsilon$ | |
| $\tau_e$ | = eddie life time | (s) |
| $\phi_B$ | = shape factor of biomass | |
| $\phi_C$ | = shape factor of coal | |
| $\Phi$ | = is the shape factor | |
| $\zeta$ | = normal distributed random number | |

# 1 INTRODUCTION

## 1.1 Background

The threat of increased global warming, resulted in the ratification of the 1997 Kyoto protocol in 2004. The Kyoto protocol requires that major polluters that have signed the protocol, should meet a 5% reduction in the greenhouse gas emissions by 2012, relative to 1990 values (Kyoto Protocol, Article 3). Although South Africa is not among the countries required to comply with this deadline, the Government has however pledged to start towards meeting this target.

Coal is the primary fuel produced and consumed in South Africa. The country has 54.6 billion short tons (approximately 5% of the world total) of recoverable coal reserves (EIA, 2005). It is the sixth largest coal producer in the world. The coal contains low levels of sulphur and has high ash content. The coal is mainly used for electricity generation and production of synthetic fuels from Sasol's coal liquefaction plants at Secunda and Sasolburg. Eskom, a parastatal company, is one of the largest utilities in the world generating nearly all of South Africa's electricity and exporting some to the neighbouring countries (EIA, 2005).

Combustion of coal, however, contributes to the accumulation of greenhouse gases and toxic pollutants in the atmosphere. The mounting pressure from the international community to cut down on emissions translates into reducing the amount of coal used in power stations. Since demand for electrical energy keeps on increasing, an alternative greener fuel has to substitute for some coal in order to meet the current and future electricity demand. Recent research has shown that the use of biomass alone or with coal can reduce emissions. The partial replacement of coal by biomass in conventional pulverized fuel boilers is regarded as a green

energy technology eligible for carbon credits. The strong financial incentive (carbon trading) to invest in renewable energy technology is also a driving force for biomass co-firing.

The technology of using biomass for electricity generation is still being developed through research work, especially in the United States and Europe (Chapter 2). Here in South Africa, the Star Biomass Pellet company uses waste material from the Zululand timber industry to produce wood pellets for consumption in the European market for electricity generation. The Mondi company is also engaged in a project involving the recovery of biomass waste (previously land filled at a Richards Bay municipal landfill site) for use in power boilers as an alternative fuel to coal to generate steam at Mondi Kraft, Richards Bay. The project will achieve reduced carbon dioxide emissions due to displaced coal fuel and there will no longer be methane emissions from land filled biomass (Mondi, 2005). Except for the efforts of the Mondi Paper company, no research has been done on the use of biomass for electricity generation in South Africa and this project is the first on using biomass with coal in South African pulverised coal boilers.

South African coal was formed during the Permian era about 280 to 300 million years ago under cool temperate climatic conditions, whereas North American and European coals were formed earlier during the Carboniferous era, about 300 to 350 million years ago, under hot, steamy and swampy climatic conditions (Falcon, 2007). This has resulted in the fundamental difference in the maceral structure of the Permian and Carboniferous coals. The Carboniferous coals tend to have higher vitrinite content making them very reactive (Falcon, 2007). Their reactivity can be seen from the cenospheric chars that result from their pyrolysis. Vitrinite combustion behaviour can be characterised as releasing higher volatiles, having good swelling properties, higher surface area for reaction, easy ignition and fast burn-out. On the other hand Permian coals are less

reactive due to their maceral composition which is mainly inertinite. The chars from these coals are not as porous as those of carboniferous coals. Permian coals require about 50% more residence time to reach burnout than carboniferous coals (Falcon, 2006). Inertinite is characterised by low volatiles, no swelling, poor ignition, slow combustion and poor burnout.

Apart from the less reactive maceral composition, South African coal has low sulphur content, low volatile content, low calorific value and high ash content. The high ash content does not only reduce the calorific value of the coal but can inhibit the diffusion of oxygen into the coal particle, further reducing the reactivity of the coal.

The co-combustion of biomass with coal and its various impacts on power plant operation have been studied in Europe, US and Australia for over a decade. There have been major collaborative full power and pilot scale investigations to assess the impact of the co-combustion of biomass with coal. Examples include IEA Bioenergy Task 32, UK DTI Cleaner Coal R &D, TNO Netherlands to mention a few. In these studies, few (Wigley et al, 2007, Kupka et al, 2008, Gil et al, 2009, Molcan et al, 2009) include South African coal. Even so, the South African coal used in those tests is an export coal which is of higher quality than the one used for local consumption. This is so because of the good price offered by European markets. The turnover is so good that it enables the mines to subsidise production costs for lower quality coal and sell it for local consumption very cheaply (Falcon, 2006). The best coal reserves for long term export contracts are gradually being mined out, leaving poorer grades of coal for electricity generation and other industries. These low grade coals are sometimes incompatible with older generating plants which were originally designed for higher-grade coals, and this poses problems such as reduced combustion efficiency due to poor ignition and increased dust burden due to higher ash content. Over the years there has been a

gradual decline in the quality of coal used for electricity generation and this will continue to be the case as long as coal is exported (Falcon, 2006).

To sum up, although considerable research has been carried out in the Northern hemisphere on co-firing biomass with coal, the findings cannot simply be applied wholesale to the South African case, especially with regard to pulverised fuel boilers. Few studies (None of the studies has looked into the co-firing of biomass with inertenite rich South African coal characterised by high ash content and low volatiles with regard to emissions (NOX, $SO_2$ and $CO_2$), ignitability, fouling and slagging.

## 1.2 Statement of the Problem

The purpose of the research project was to analyse the effects of direct co-firing of biomass with South African coal, on emissions, fouling, slagging, ignitability and flame stability.

The main gaseous emissions involved with coal combustion are carbon dioxide ($CO_2$), sulphur dioxide ($SO_2$) and nitrogen oxides ($NO_x$). $NO_x$ refers to either nitric oxide (NO) or nitrogen dioxide ($NO_2$), both of which are considered toxic and play a major role in the formation of acid rain, smog and ground level ozone. Co-firing of biomass with coal as a greenhouse mitigating strategy can reduce these emissions and create biomass energy markets. Biomass recycles $CO_2$ because during its combustion, it releases the same amount as it absorbed during its growth (Demirbas, 2003). Compared to coal, biomass also has generally lower sulphur and nitrogen contents, hence it can be expected to have lower sulphur ($SO_2$) and nitrogen ($NO_x$) related emissions. The reduction of $NO_x$ emissions is not only due to lower fuel-bound nitrogen, but also due to the changes in stoichiometry at the near-burner region, caused by the rapid release of the large volatile content of the biomass fuel.

Fouling and slagging obstructs the flow of energy from the furnace to the steam in the water wall in the convective section, thus reducing thermal efficiency. It is therefore important to monitor and keep fouling and slagging to a minimum. A higher ratio of biomass to coal means increased reduction in emissions (Spliethoff et al, 1998; Tillman, 2000; Demirbas 2004) but more fouling and slagging, so an optimum operating point must exist.

The coal used in pulverised fuel boilers in South Africa has low volatile matter and high ash content, which has a negative impact on ignitability and flame stability. It is hoped that the use of biomass will be able to anchor the flame and improve its stability.

**Patrick Muanza's MSc Dissertation**

The investigation of fly ash particulate behaviour ($PM_{>10}$, $PM_{10}$, $PM_{2.5}$ and $PM_{1.0}$) when biomass is co-fired with a typical pulverized South African coal was part of the overall project sponsored by Eskom and was reported in the MSc Dissertation (Muanza, 2009). $PM_x$ means particulate matter whose particle diameter is less than x (stands for 10, 2.5 or 1.0) microns. The main objectives of this study (Muanza, 2009) were to:

1. Analyse the particle size distribution of fly ash sampled from the experiments and observe its mineralogy variation with the co-firing ratio;

2. Compare both grass and sawdust experiments on the basis of particulate matter particle size distribution produced and its blending ratio with coal;

3. Compare the results of fly ash particulate formation modelling by means of computational fluid dynamics methods with the experimental results from the Pilot Scale Combustion Test Facility.

The conclusion drawn from Muanza, (2009) were:

1. The fine coal excluded grains caused a shift of the fly ash particle size distribution towards the coarse mode, and coarse coal excluded grains towards fine fly ash particle size distribution.

2. The experimental results of grass and sawdust blends showed that the percentages of $PM_{10}$ and $PM_{2.5}$ fly ash particles generally decreased with increasing co-firing ratio.

3. There was a good agreement between experimental data and simulation except for the potassium sulphate concentrations. The difference between the predicted and measured $K_2SO_4$ concentration seemed very large. The discrepancies of the $K_2SO_4$ and $SO_3$ mass fractions during the grass/coal A and sawdust/coal A blends tests could be associated with the effect of its dilution by oxygen present in the flue gas.

## 1.3 Scope and Objectives

This PhD project was concerned with the effect of co-firing a small percentage (0-20%) of biomass with coal on emissions, combustion efficiency and slagging propensity. These emissions were in particular $NO_X$, $SO_2$, and $CO_2$. The project involved an experimental part and a computer simulation. The experimental part was accomplished by running 7 tests at the Eskom Pilot Scale Combustion Test Facility (PSCTF)(1 $MW_t$) and 7 tests at the Drop Tube Furnace (DTF) at Rosherville near Germiston in Johannesburg. The commercial computational fluid dynamics Fluent$^{TM}$ code was used for performing computer simulations which were validated by the data from the PSCTF.

The objectives of this project were to:

1. Investigate the percentage reduction of $NO_x$,$SO_2$ and $CO_2$ as a function of proportion of biomass replacing coal for two biomass types (sawdust and grass) by carrying out tests on the PSCTF.
2. Determine the best type of biomass based on percentage reduction in emissions and tolerable slagging and fouling propensities.
3. Determine, for the biomass selected in 2 above, the optimum biomass percentage that can be co-fired without adversely affecting slagging and fouling tendencies.
4. Investigate the effect of biomass on the ignitability of the low-grade coal by carrying out tests using the PSCTF and the DTF.
5. Carry out computer simulations to enable prediction of combustion and emissions characteristics when coal is burned together with a small proportion of biomass in pulverised fuel boilers.
6. Validate the simulation technique using the experimental results from the PSCTF.

## 1.4 Envisaged Contribution to Knowledge

Most researchers (Pederson et al, 1996; Spliethoff et al, 1998; Battista et al, 2000; Boylan et al, 2000; Hus et al, 2000; Tillman, 2000; Annamalai et al, 2003b; Demirbas 2004; Kwong et al, 2007, Narayanan et al, 2007) have indicated that biomass can reduce $NO_X$ emissions, while others argue that the influence of biomass on $NO_X$ could not be clearly identified (Skodras et al, 2002, Gani et al, 2005; Kazagic et al, 2009; Gil et al, 2009). Some researchers report modest (Wieck-Hansen at al, 2000) or conditional reduction or increase (Savolainen et al., 2003; Baxter et al, 2005) of $NO_X$ emissions. The detailed figures showing quantities of $NO_X$ reduction results are few and far between. Few studies (Annamalai et al,

2003b; Kwong et al, 2007; Narayanan et al, 2007) actually quote the cofirng ratios and the percentage reductions in emissions.

Many researchers (Pedersen et al, 1996; Spliethoff et al, 1998; Tillman, 2000; Sami et al, 2001, Skodras et al, 2002; Robinson et al, 2003; Savolainen et al, 2003; Baxter et al, 2005; Demirbas 2004; Kwong et al, 2007; Narayanan et al, 2007; Kazagic et al, 2009) indicate that there is a reduction in $SO_2$ emissions when biomass is co-fired with coal but only a few (Narayanan et al, 2007; Kazagic et al, 2009) give details of how much reductions and at which co-firing ratios. The extend to which $SO_2$ and $NO_X$ emissions reductions occur as a function of biomass added are are not adequately covered.

$CO_2$ reductions refer to avoiding fossil $CO_2$ emissions from fossil fuels not $CO_2$ emissions coming out of the stack. Even if the $CO_2$ stack emissions can be more than those of coal alone, fossil $CO_2$ would still have been avoided because carbon in the biomass fuel is part of the active carbon cycle (Robinson et al, 2003). If however there are actual stack reductions, then the $CO_2$ emissions would be further reduced. The reports of how much stack emissions exceeded or were below readings of coal alone are few (Kazagic et al, 2009). It may not be useful to simply state that there are reductions, but rather there is a need to quantify $CO_2$ values in order to allow policy makers on emissions control to make informed decisions.

Slagging and fouling have been reported as some of the negative aspects of co-firing coal with biomass. Some researchers (Heinzel et al, 1998; Wigley et al, 2007; Annamalai et al, 2003a, Fradson, 2005; Pronobis 2005, Zheng et al, 2007) report increased deposition rates when biomass was co-fired with coal while others (Pederson et al, 1996; Robinson et al, 1998; Heinzel et al, 1998; Kazagic et al, 2007) report modest or no changes. One study (Kupka et al, 2008) found that addition of sawdust to South African export coal from Middleburg seems to have positive influence on

deposition behaviour. The lack of consensus in this area indicated that it was still not well understood.

Su et al, (2001) gives a comprehensive account on ignition of blends of coals, which could be extended to biomass/coal blends. Moghtaderi, (2007) indicated that blending of coal with biomass increases the likelihood of char extinction resulting in decreasing the level of char burnout. On the other hand Vamvuka et al, 2003 and Savolainen, 2003, Molcan et al, 2009) have actually indicated that solid bio-fuels could support the combustion of poor coals. In some studies (Pan et al, 1996; Meesri et al, 2002), addition of biomass did not result in any synergistic effects. So far research work in this area is required to fully define the combustion behaviour of biomass-coal mixtures.

The results of emissions and deposition rates reported are based on variety of testing equipment such as laboratory scale, pilot scale and full scale commercial plants.

The envisaged contribution to knowledge was to establish the extent to which the two types of biomass chosen can reduce (if at all) baseline coal emissions ($NO_X$, $SO_2$ and $CO_2$) without adversely affecting slagging and fouling tendencies; and to assert the type of dependence of emissions on biomass co-firing ratio. It was also to be able to show that biomass can be used to improve ignitability of coal of low volatile coal and to prove that the combustion and emissions characteristics could be predicted through numerical modelling.

## 1.5 Outline of the Report

**Chapter 2** presents the literature survey on co-firing biomass with coal in pulverised fuel boilers, focusing in particular on the emissions, ignition and

ash deposition. **Chapter 3** describes the numerical simulation approach and the parameters used as material properties and boundary conditions. **Chapter 4** deals with fuel preparation, experimental apparatus and the data used to set the air flow requirements. **Chapter 5** presents the results obtained from the chemical analysis, and from tests using Eskom's Pilot Scale Combustion Test Facility and Drop Tube Furnace. **Chapter 6** discusses the results presented in Chapter 5. **Chapter 7** presents the conclusions drawn from this study and outlines the recommendations.

# 2 LITERATURE REVIEW

## 2.1 Pulverised Fuel Boilers (PFB)

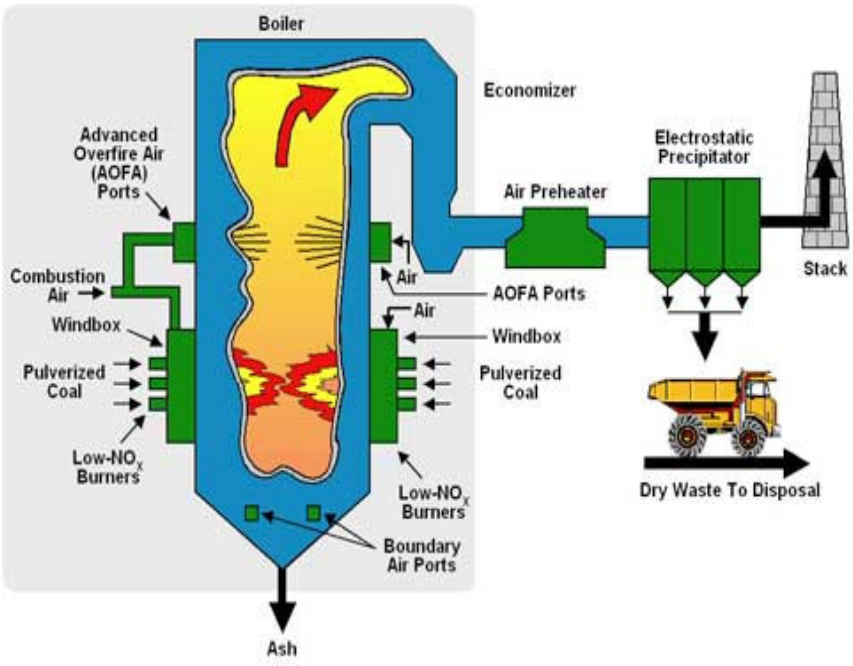


Figure 2.1 *Pulverised fuel boiler* (Sabastian, 2002)

In this type of boiler, a solid fuel is crushed into a powder and fed through jet burners with air into the combustion chamber as shown in figure 2.1. The air used to transport the fuel into the furnace is called the primary air and usually enters the furnace through the centre duct of the burner. For boilers with low-$NO_x$ burners additional air, usually called secondary air, is supplied through an annular duct around the primary air duct to promote complete combustion. Pulverised fuel boilers (PFB), which are the most popular utility boilers today, have a high efficiency but costly $SO_2$ and $NO_x$ control. The PFB technology has enabled the increase of boiler unit size from 100 MW in the 1950's to over 1000 MW electrical. The inorganic particles remain as ash and slag and increase the need for particle filters of the flue gas and promote the wear and tear of furnace tubes (Sabastian, 2002).

Eskom uses pulverised fuel boilers in thirteen power stations. South African coal is considered as a fuel with low sulphur content and hence relatively low sulphur related emissions can be expected. These power stations are burning low grade coal which sometimes present problems associated with ignition and unburned carbon in ash. Slagging is not a major problem for most of the power stations. At least 7 power stations have no slagging problems (Tarr et al, 2006). Some stations including Hendrina, have problems with slagging.

Originally when the power stations were built, a mine was tied to a power station which was then optimised for that particular coal from the mine. At that time, the coals were generally of better quality than they are now. Currently not all power stations are tied to one mine, some can source coal wherever they can and transport it in trucks, so long as the coal is within the power station design parameters. This variable fuel supply coupled with blending of coals to make the resulting blend compliant with power station design parameters, necessitated the procurement of the Pilot Scale Combustion Test Facility (PSCTF) and the Drop Tube Furnace (DTF) located at Rosherville. This afforded Eskom the opportunity to test the fuels for suitability before signing contracts with suppliers.

## 2.2 Emissions From Pulverised Fuel Boilers

### 2.2.1 $NO_x$ Formation

$NO_x$ can be formed through any of three mechanisms: fuel $NO_x$, thermal $NO_x$ and prompt $NO_x$.

**Fuel $NO_x$ Formation Mechanism**

The nitrogen contained in the fuel is converted to $NO_x$ through a series of elementary steps called the fuel $NO_x$ mechanisms. The important intermediate species in this process are ammonia ($NH_3$) and hydrogen

cyanide (HCN) both of which get converted to $NO_x$ through different routes. The ratio of HCN to $NH_3$ depends on the type of fuel. The fuel nitrogen in biomass, exists in aliphatic chains as compared to that in coal, which exists in aromatic rings. This results in nitrogen from biomass preferably forming more ammonia ($NH_3$) than hydrogen cyanide (HCN) which readily forms from coal-bound nitrogen (Spliethoff et al, 1998). For example bituminous coal tends to favour more production of HCN than $NH_3$ resulting in a typical HCN/$NH_3$ ratio of 9:1 (Winter et al in Fluent, 2006). The ratio is the reverse for biomass fuels i.e. 1:9 (Liu and Gibbs in Fluent manual, 2006).

Some researchers (Phong-Anant et al, 1985, Sliethoff et al, 1998, Annamalai et al, 2003b, Di Nola et al, 2008, Stubenberger et al, 2008) have also found that fuel nitrogen in coal mostly converts to HCN and that in biomass predominantly converts to $NH_3$. The reason attributed to this behaviour is that nitrogen in coal exists in aromatic rings while that in biomass exists in aliphatic chains. Other researchers (Leppälahti J., 1995) however argue that this may not be the main route for formation of $NH_3$. They argue that $NH_3$ is also produced by hydrogenation of HCN in gas phase or on the char surface. Li et al, (2000) on the other hand believe that the direct hydrogenation of the nitrogen (and not HCN) in the pyrolysing coal or char particle is the main route for the formation of $NH_3$. The presence of potassium has also been found to promote N-conversion to both $NH_3$ and HCN (Ren et al, 2008). There seems to be a continuing debate on the mechanisms underlying formation of $NO_X$ precursors, but at the moment more researchers agree that HCN forms in the flames of bituminous and higher rank coals especially when rate of pyrolysis is high (Tsubouchi et al, 2007) while $NH_3$ dominates N-containing species in lignite and biomass flames.

### Thermal $NO_x$ Mechanism

Thermal $NO_x$ results from the reaction of nitrogen in the air with excess oxygen at temperatures greater than 1500 ℃ (Obernberger, 1998). At these temperatures, both nitrogen ($N_2$) and oxygen ($O_2$) are dissociated into atoms that react by the extended Zeldovich mechanism (Kuo, 1986):

$$N_2 + O \leftrightarrow NO + N$$

$$N + O_2 \leftrightarrow NO + O$$

$$N + OH \leftrightarrow NO + H$$

Thermal $NO_X$ is influenced by the near-burner combustion dynamics such as flame temperature, residence time (or degree of air/fuel mixing) and the concentrations of nitrogen and excess oxygen in that area. The longer the combusting fuel is kept in the flame zone at high temperature and in the presence of excess oxygen, the higher the heat release rate. High heat release rate at early stages of combustion increases flame temperature which favours thermal $NO_x$ production. Little excess air can promote thermal $NO_x$ formation while too much excess air acts as a heat sink and tends to lower temperature (Burd in Berber et al., 2002). This would suggest that beyond some optimum point the effect of excess air in lowering the flame temperature (Van Loo et al, 2002) by absorbing the heat, outperforms its contribution towards $NO_X$ formation by fixation (Baukal, 2001).

### Prompt $NO_x$ Mechanism

Prompt $NO_x$ is formed when nitrogen under fuel-rich conditions reacts with hydrocarbon CH to form HCN, which then follows the reaction steps of fuel $NO_x$. This mechanism is less temperature dependent and much faster than that of thermal $NO_x$. Although the actual formation of prompt $NO_x$

involves a complex series of reactions and a number of intermediate species, major contribution comes from the hydrocarbons CH and $CH_2$ through reactions:

$$CH + N_2 \leftrightarrow HCN + N$$
$$CH_2 + N_2 \leftrightarrow HCN + NH$$

The Prompt $NO_x$ mechanism has not been found to be of significant importance in biomass combustion applications as compared to those of coal (Van Loo et al, 2002).

### 2.2.2 Sulphur Dioxide ($SO_2$) and Carbon Dioxide ($CO_2$) Emissions

The $SO_2$ and $CO_2$ emissions are produced from the oxidation of fuel-bound sulphur and carbon respectively. Unlike the case of $NO_X$, the mechanisms by which these emissions are produced almost depend on the chemical composition of fuel only. The presence of these gases in the flue gas therefore should be proportional to the amount of sulphur and carbon in the fuel. In the presence of $SO_2$, biomass char has been found to be more reactive than that of coal when reducing NO (Dong et al, 2007). The result implies that biomass combustion whose flue gas is rich in $SO_2$ may provide greater opportunities for NO reduction .

## 2.3 Emissions Control

### 2.3.1 Control of $NO_x$ Formation

$NO_x$ formation in boiler burners can be reduced by either pre-combustion or post combustion technologies. Post-combustion technology allows $NO_x$ to form and then breaks it down in the exhaust gases through either Selective Non-Catalytic Reduction (SNCR) or Selective Catalytic Reduction (SCR) processes. Pre-combustion technologies prevent $NO_x$

from forming in the first place. This is accomplished by either combustion staging or flue gas re-circulation (FGR) processes.

**Combustion Staging (air staging and fuel staging)**

Combustion staging is a process in which some of the fuel is ignited in an oxygen lean environment to create a fuel rich mixture. This helps to keep the flame temperature down by limiting the rate of oxidation and hence reduce formation of thermal $NO_x$. Thermal $NO_x$ emissions do not form in significant amounts until flame temperature reaches about 1500 ℃, beyond which any further rise in temperature causes a rapid increase in the rate of $NO_x$ formation (Obernberger, 1998; Kokkinos et al, 2002; Wistrom, 2005).

**Flue Gas Recirculation**

The flue gas recirculation method recycles some of the flue gas back to the combustion chamber. The reduced oxygen content of the flue gas limits the reaction and therefore lowers the flame temperature in the combustion zone, thereby reducing $NO_x$ formation. The reduction in flame temperature potentially limits the maximum heating capacity of the unit.

### 2.3.2 Fly Ash Control

The inorganic material in the solid fuel emerges from the combustion process as ash. While some ash will be collected as bottom ash, most of it gets carried away with the flue gas as fly ash to the smoke stack. It is therefore necessary to install air pollution control devices to remove the fly ash before it reaches the atmosphere. Such devices are fabric filters and electrostatic precipitators (ESP).

## 2.4 Ash Deposition and Surface Corrosion

### 2.4.1 Slagging

Slagging is the formation of molten or semi-molten deposits on the furnace walls in the radiative section. It is formed when molten ash reaches the heat transfer surface before it could cool down to solid state and hence sticks to the surface. Ash does not have a definite melting point like ice because of its composition with different elements that melt at different temperatures. This results in a semi-molten substance with high viscosity at the onset of deformation, to a molten substance with lower viscosity at higher temperatures (Hatt, 1990).

Slagging depends on ash fusion temperatures of the fuel used. Ash fusion temperatures (AFT) provide an indication of the temperature range over which portions of the ash will be a molten fluid or in a semi-molten, plastic state. Fuels with lower ash fusion temperatures have higher slagging propensity than those with higher fusion temperatures. A high ash fusion temperature indicates that ash released in the furnace will cool quickly to a non-sticky state resulting in minimal potential for slagging. Conversely, low ash fusion temperatures indicate that ash will remain in a molten or plastic state longer, exposing more of the furnace to potential deposition.

The eight principal oxides frequently found in coal ash: $SiO_2$, $AL_2O_3$, $TiO_2$, $Fe_2O_3$, CaO, MgO, $Na_2O$ and $K_2O$. The oxides fall under base or acid categories. The basic constituents are oxides of: iron, the alkaline earth metals calcium and magnesium, and the alkali metals sodium and potassium. Acidic constituents are oxides of: silicon, aluminium and titanium. It was believed that the basic constituents tend to lower fusion temperatures and promote slagging while acidic ones tend to increase them, thereby inhibiting slagging (Hatt, 1990).

A number of slagging indices based on ash elemental analysis and ash fusion temperatures have been used to predict slagging propensity of

northern hemisphere coals. These include silica ratio, base/acid ratio, iron index, iron+calcium, calculated viscosity, multi-viscosity index, slagging factor and slagging temperature (Van Alphen, 2005).

The use of these indices was on the premise that ash fusion temperatures and by extension slagging depends on composition of ash alone. But these indices have been shown to be inaccurate by Van Aphen (2005) at least for the South African coals tested. In a study by Van Dyk et al (2005) selected South African coals were subjected to chemical fractionation tests to isolate certain mineral species in order to correlate their impact with the ash fusion temperatures. Five indices (eqns. 2.1-2.5) were considered. It was found from this study that for the range of indices considered, dolomite ratio gave a best correlation factor of 0.81, while those of eqns. 2.1, 2.2, 2.3 and 2.5 were 0.7, 0.71, 0.71 and 0.54 respectively (Van Dyk, 2005).

$$\%Base = Na_2O + K_2O + CaO + MgO + Fe_2O_3 \quad (2.1)$$

$$\%Acid = SiO_2 + Al_2O_3 + TiO_2 \quad (2.2)$$

$$Silica\ value = \frac{SiO_2}{SiO_2+Fe_2O_3+CaO+Mgo} \quad (2.3)$$

$$\text{Dolomite ratio} = \frac{CaO+MgO}{Fe_2O_3+CaO+Mgo+Na_2O+K_2O} \quad (2.4)$$

$$\text{Acidity} = \frac{SiO_2+Al_2O_3}{Fe_2O_3+CaO+Mgo+Na_2O+K_2O} \quad (2.5)$$

The study concluded that the ash fusion temperature behaviour of coal cannot be explained accurately by composition of ash alone but depends on complex interactions between different mineral elements. In view of the shortcomings in the traditional indices, Van Alphen (2005) developed a new slagging index to pedict the slagging propensity. The traditional slagging indices are based on bulk analysis and do not take into account the impact of size and viscosity of individual fly ash particles (Van Alphen, 2005). The developed model uses data from detailed analysis of

pulverised coal using CCSEM-based technology developed by Van Alphen, (2005) to predict mineral phases in the individual fly ash particles. The information of mineral phase proportions, size, and viscosity of each fly ash is used to assess the slagging propensity. Slag-developing fly ash phases were identified as kaolinite (carbonate), kaolinite (carbonate, pyrite) and kaolinite (pyrite) (Van Alphen, 2005). Kaolinite is a generic term for metakiolinite, mullite and silicon spinel. Kaolinite (carbonate) is an alumino-silicate phase with minor to trace elements of Ca and Mg. Kaolinite (pyrite) is an alumino-silicate phase with minor to trace elements of Fe while kaolinite (carbonate, pyrite) is Ca-Fe bearing alumino-silicate phase. The particles that were most likely to stick are those with phases stated above, coarser than 38 µm and having a viscosity of less than or equal to 80 poise (Van Alphen, 2005).

Although Van Alphen model would have been ideal, the detailed mineral associations analysis of the pulverised fuel required and the use of proprietary software used in the model, had implications on time and cost, which in view of limited budget could not be justified for quick initial assessment of slagging required in section 4.1.1. On the other hand dolomite ratio (Van Dyk, 2005) which gave reasonable correlation for South African coals could be used to choose coal in section 4.1.1.

### 2.4.2 Fouling

Fouling is generally caused by the vaporization of volatile inorganic elements in the coal during combustion. When heat is absorbed and temperatures decrease in the convection area of the boiler, compounds formed by these elements condense on ash particles and the heating surface, forming glue, which initiates deposition.

Volatile forms of alkali metals, sodium and potassium are vaporized in the furnace at combustion temperature and react with sulphur in the flue gas

and other elements in the ash to form compounds that deposit on convection surfaces (Hatt, 1990). Northern hemisphere coals can have significant amounts of sodium and/or potassium (Bryers, 1996) but southern hemisphere coals, in particular, Australian and South African Permian coals have low levels of sodium and potassium making them less likely to foul (Kershaw et al, 1992).

An empirical index of fouling (Rf), is a measure of fuel's propensity to cause fouling. It is calculated as follows:

$$R_f = \frac{Fe_2O_3+CaO+Mgo+Na_2O+K_2O}{SiO_2+Al_2O_3+TiO_2} \times (Na_2O + K_2O) \qquad (2.6)$$

Table 2.1 Relationship between fouling index and fouling tendencies

| | **Range** | **Fouling Intensity** |
|---|---|---|
| **Rf** | <0.6 | No fouling |
| **Rf** | 0.6 – 40 | Strong fouling |
| **Rf** | >40 | Very strong fouling |

Eqn. 2.6 and Table 2.1 were used in Table 4.2 to assess fouling propensities of the coals considered.

### 2.4.3 Corrosion

During combustion, fuel-bound chlorine may be partly devolatilised into the gas phase as HCl or alkali chlorides (potassium chloride (KCl) and sodium chloride (NaCl)) (Salmenoja et al, 1996). Volatilised chlorine-enriched compounds may condense on superheater tubes by various mechanisms: brownian diffusion, electrophoresis, thermophoresis, inertial impaction and gravity settling (Kauffman et al, 2000). In a study by Michelsen et al, (1998), deposition measurements on the superheaters showed deposits rich in potassium and chlorine making up 40–80 wt.% of the deposits.

In temperature range 1600 – 1300 ℃, the chlorine content of the fuel seems to have a decisive effect on alkali/ash reactions (Nutulapati et al, 2007). If the K/Cl molar ratio >1, more potassium is found in the condensed phase of alkali silicates or alkali alumino-silicates, whereas when it is less than unity, more potassium appears in the form of gas phase KCl instead of alkali silicates and KOH (Nutulapati et al, 2007).

Biomass fuels such as straw tend to have high chlorine content, raising concerns about corrosion but co-firing of straw with sulphur-containing fuels can sometimes decrease the corrosion, because the tight layer of $K_2SO_4$ that may form can protect the tubes (Pronobis, 2006). Experiments show that sulphur from the coal reacts with alkali chlorides from the straw to create alkali sulphates, consequently releasing chlorine to the gas phase, primarily as hydrogen chloride (HCL). The effects of these reactions reduce or potentially eliminate condensed phase chlorides from deposits (Robinson et al, 2002a). In relation to corrosion, it is positive to have chlorine existing as HCL in the flue gas as opposed to forming potassium chloride (KCL), which causes corrosion (Wieck-Hansen et al, 2000). Protective effect of sulphates does not always occur, which proves that this phenomenon may also depend on other parameters (Pronobis, 2006). When the S/Cl molar ratio is higher than 4.0, the fuel can be regarded as noncorrosive; and when S/Cl is less than 2.0 the corrosion of superheaters occurs almost inevitably (Pronobis, 2006).

A mechanism proposed for chlorine-induced corrosion based on thermodynamic equilibrium, predicts that chlorine in deposits should decrease sharply with increasing sulphur content. However, since more chlorine has been observed in deposits than predicted by the equilibrium, the conversion of alkali chlorides to alkali sulphates is apparently limited by kinetic or transport effects (Sondreal et al, 2001).

## 2.5 Effect of Co-firing Biomass with Coal on Emissions and Ash

### 2.5.1 Effect of co-firing on $NO_X$ Emissions

Most researchers (Pederson et al, 1996; Spliethoff et al, 1998; Battista et al, 2000; Boylan et al, 2000; Hus et al, 2000; Tillman, 2000; Annamalai et al, 2003b; Demirbas 2004; Kwong et al, 2007; Narayanan et al, 2007) have indicated that when biomass is mixed in small proportions to the baseline coal can reduce $NO_X$ emissions. Co-firing biomass with coal offers a technique for reducing $NO_x$ emissions by 10-30% depending on boiler type, base coal, biofuel and co-firing technique (Battista et al, 2000; Sami et al, 2001). Factors influencing biomass fuels' success in reducing $NO_x$ that would be produced by burning coal alone, are lower fuel nitrogen in biomass (Pederson et al, 1996; Boylan et al, 2000; Hus et al, 2000; Demirbas 2004; Kwong et al, 2007) and high volatile content of biomass (Hus et al, 2000, Tillman, 2000, Battista et al, 2000 Annamalai et al, 2003a). The high volatile content promotes more gas-phase combustion than gas-solid oxidation associated with coal, and relatively higher volatile/fixed carbon ratio than that of coal (Tillman, 2000). In the gas phase, the volatile biomass fuel nitrogen preferably forms ammonia ($NH_3$) in contrast to hydrogen cyanide (HCN) formed by bituminous coal nitrogen (Spliethoff et al, 1998). The ammonia reduces NO to molecular nitrogen, essentially providing an in-situ thermal DeNOX source (Sami et al, 2001).

Other researchers however (Skodras et al, 2002, Gani et al, 2005; Kazagic et al, 2009) argue that the influence of biomass on $NO_X$ reduction could not be clearly identified. They concluded that fuel nitrogen seem to have no influence on production of $NO_x$. For instance Gani et al, (2005) report that there was no change in $NO_x$ emissions even if biomass had half fuel-N as the coal. Kazagic et al, (2009) however found that excess air ratio exerts a strong influence on $NO_X$ emissions for both coals and coal-biomass blends. When excess air ratio was varied between 0.95 to 1.1 at

1250 ℃, for a blend of 80% coal 20% sawdust, $NO_x$ increased from 150 ppm to 750 ppm. Wieck-Hansen at. al., (2000) reports modest changes due to small change in gas temperature between firing coal and that when co-firing.

Larry Baxter et al, (2005) indicate that $NO_X$ may increase, decrease, or remain the same depending on fuel, firing conditions and operating conditions. For instance moisture content can increase $NO_X$ emissions due to delayed combustion (Savolainen et al., 2003), or it can reduce $NO_X$ emissions by lowering flame temperature (Baxter et al, 2005). Although biomass fuels have lower heating value, rapid release of volatiles may locally increase temperature near the burner compared to coal-only combustion. Such an increase in temperature may increase production of thermal $NO_X$ (Sami et al, 2001), this however, is offset by the moisture content of biomass which tends to lower the peak temperature (Baxter et al, 2005). Fuel volatility may be influenced by particle size. Smaller particles release more volatiles, and will release them more rapidly than bigger ones (Tillman, 2000). Kwong et al, (2007) however reported that the biomass grinding size did not seem to have a significant impact to the combustion performance.

$NO_X$ behaviour during co-firing biomass with coal is a multi-pronged issue depending on complicated matrix of chemical, physical and combustion variables to fully define it. The arguments on impact of co-firing coal and biomass on $NO_X$ formation are on-going and more research is needed to fully understand $NO_X$ behaviour under these conditions.

### 2.5.2 Effect of co-firing on $SO_2$ emissions

A number of researchers (Pedersen et al, 1996; Spliethoff et al, 1998; Tillman, 2000; Sami et al, 2001, Skodras et al, 2002; Robinson et al, 2003; Savolainen et al., 2003; Baxter et al, 2005; Demirbas 2004; Kwong et al,

2007; Narayanan et al, 2007; Kazagic et al, 2009) agree that co-combustion of biomass with coal reduces $SO_2$ emissions due to typically low sulphur content associated with biomass fuels. Most of these researchers indicate that there is a reduction in $SO_2$ emissions when biomass is co-fired with coal but only a few (Narayanan et al, 2007; Kazagic et al, 2009) give details of how much reductions and at which co-firing ratios. The extend to which these reductions occur as a function of biomass added are not adequately covered.

The reduction in $SO_2$ emissions is often greater than would result from simple dilution because of reactions between sulphur from the coal and alkali and alkaline species from the biomass, which form sulphates that are collected in the particulate control system (Pedersen et al, 1996; Spliethoff et al, 1998; Wieck-Hansen et al, 2000).

Reduction in $SO_2$ emissions depend on how big the difference is between the sulphur content of coal and the biomass with which it is co-fired and the calorific value of biomass (Narayanan, 2007). It also depends on the calcium and potassium in the ash and whether the temperature is low enough for the capture of $SO_2$ to occur (Kazagic et al, 2009).

### 2.5.3 Effect of co-firing on $CO_2$ emissions

$CO_2$ reductions refer to avoiding fossil $CO_2$ emissions from fossil fuels not $CO_2$ emissions coming out of the stack. Even if the $CO_2$ stack emissions can be higher than those of coal alone, fossil $CO_2$ would still have been avoided because carbon in the biomass fuel is part of the active carbon cycle (Robinson et al, 2003). If however there are actual stack reductions, then the $CO_2$ emissions would be further reduced. The reports of how much stack emissions exceeded or were below readings of coal alone are few (Kazagic et al, 2009). It may not be useful to simply state that there

are reductions, but rather there is a need to quantify $CO_2$ values in order to allow policy makers on emissions control to make informed decisions.

### 2.5.4 Effect of co-firing on ash deposition (Slagging and fouling)

The negative aspects of biomass, especially some grasses and straws, are that it can contain more reactive potassium, sodium and chlorine than coal, encouraging corrosion and accelerated fouling and slagging in boilers (Robinson et al, 2003, Annamalai et al, 2003a).

Some researchers (Wigley et al, 2007; Annamalai et al, 2003a, Fradson, 2005; Pronobis 2005, Zheng et al, 2007) report increased deposition rates when biomass was co-fired with coal. The reason attributed to this, is the lowering of ash fusion temperature due to addition of fluxing elements from biomass ash such as potassium and sodium.

Coal ash is an alumino-silicate system with quartz as the principal mineral species. It also contains iron, magnesium, calcium, potassium and sodium. Coal ash can generally be regarded as having lower propensity to slag than that of biomass because of the relatively low levels of fluxing elements (iron, calcium, magnesium, potassium and sodium) responsible for the formation of hard glassy deposits on heat transfer surfaces. On the other hand, biomass is not an alumino-silicate system and can contain relatively higher levels of potassium, calcium, magnesium and sodium salts, principally in the form of phosphates, sulphates and chlorides. Biomass ash is therefore regarded as having higher propensity to slag and foul the boiler than coal. The addition of significant levels of fluxing elements into the mixed ash when co-firing, can have dramatic a effect on the propensity of the mixed ash to slag. The ash fusion temperature of the mixed ash can be 100-200 ˚C lower than that of the baseline coal ash (Van Loo et al, 2002).

Biomass fuels can release increased amounts of potassium and chlorine in the vapour phase, and their subsequent condensation on boiler surfaces can lead to enrichment of potassium chloride at the ash deposit interface. This enrichment can result in high temperature corrosion of the superheater and reheater sections of the boiler leading to rapid metal loss (Van Loo et al, 2002).

Deposition rate is dependent on coal with which co-firing is done. For instance in a study carried out by Wigley et al, (2007) using Russian coal and South African coal, for the same co-firing ratio and same type of biomass, higher deposition efficiency and greater degree of deposit sintering was reported for Russian coal than South African coal. The most sintered deposit for Russian coal was with Miscanthus, whereas for South African coal it was with sawmill. This shows that, it is possible for someone to report no slagging propensity while someone else for seemingly same set of biomass type and co-firing ratio can report severe slagging. The success of co-firing does not only depend on the quantity, physical properties and chemistry of biomass alone but on the interaction of species in the coal and biomass make-up as well. Zheng et al, 2007 conducted a study of coal/straw co-firing and found out that, deposition rate increased with co-firing ratios for coal with small ash content (5%) but was almost constant for all co-firing ratios when coal ash content was higher (15%). Some researchers (Pederson et al, 1996; Robinson et al, 1998; Heinzel et al, 1998; Kazagic et al, 2007) report modest or no changes in ash deposition. Pederson et al, 1996 reported that even though higher co-firing ratios of straw/coal increased potassium content in the blend, no significant increase in slagging or fouling was observed. In one study (Kupka et al, 2008) addition of the sawdust to South African export coal from Middleburg seems to result in a decrease (20%) in the deposition rate even at higher temperatures, and an improvement of ash fusibility behaviour.

The constituents primarily responsible for fouling include volatile sodium, potassium and chlorine. Since most Permian coals have low levels of sodium and potassium, fouling is not considered a serious problem (Kershaw et al, 1992). Biomass on the other hand usually has higher levels of potassium and chlorine than coal. The addition of biomass when co-firing may cause fouling problems. It has been noted however that the behaviour of fouling is dependant on the ash composition of the coal used as the primary fuel. Coals with high proportions of Al and SI such as South African coal reduces potassium by allowing it to bind to alumino-silicate (Aho et al, 2005; Bryers, 1996) as a result lowering fouling tendency.

Fouling and slagging are very complex phenomena depending upon the fuel type, mineral deportment, local gas temperatures, tube temperatures, temperature differentials, gas velocities, tube orientation, and local heat flux on each particle. Even though the ash content of biomass fuels is much less than that of steam coals, the different chemistry and mineralogy can have a significant impact on the coal ash. Since the end product of co-firing is a mixed ash, it is important to understand the behaviour of both the individual ash components as well as those of mixed ashes in order to predict the high temperature behaviour of the mixed ash.

### 2.5.5 Effect of co-firing on Ignition and Flame Stability

Grotkjær et al, (2003) define ignition as the transition from a negligible or slow fuel oxidation rate to a rapid oxidation of either the volatiles or the solid matrix. The classical thermal definition of ignition is provided by two statements (Essenhigh, 1989):

1. Heat loss is equal to heat generated by chemical reaction,
   $Q_{loss} = Q_{gen}$ (van't Hoff condition) and
2. The heat generation curve and the heat loss curve are tangent to each other on the heat –temperature (Q-T) plane,

$\frac{dQ_{loss}}{dT} = \frac{dQ_{gen}}{dT}$ (Taffanel and le Flotch condition).

The temperature at the point of tangency is the ignition temperature $T_i$.

Flame stability requires ignition and in addition, that the flame velocity is matched by the velocity of the material fed (Su et al, 2001). If the velocity of the fed material is too high the flame will be lifted from the burner mouth until it eventually blows off, whereas if it is too low the flame will flash back. The distance between the burner mouth and the root of the flame when it is lifted, is called the stand-off distance.

In the previous work reported in Essenhigh, (1989) ignition temperature increased with falling volatile matter which inferentially suggested that fuels with higher volatile matter would have lower ignition temperatures. This is confirmed by Grotjær et al, (2003) when he concluded that since the ignition temperatures of the biomass fuels tested were significantly lower than values obtained for coal under similar conditions, the relationship between volatile matter content (higher in biomass than coal) and ignition temperature exists.

At the early stages of pulverised fuel combustion, when fuel particles are heated by the radiation from the wall and the local gas convective heat transfer, volatiles evolve from the particles. Continued heating raises the temperature of the volatiles until it reaches the volatile's ignition temperature. At this stage volatiles combust in a flame that prevents char reaction by shielding it from access by oxygen (Essenhigh, 1989). When the combustion of volatiles is complete char combustion begins. Activation energy of the char is the energy that has to be supplied to it before it can spontaneously combust. For ignition to occur, the energy released from the volatiles should be high enough to overcome this activation energy of the char. This energy depends on the amount of volatiles (determined by the drop tube furnace (DTF)) and the calorific

value of the volatiles. The volatile matter of pulverised fuel reported by the proximate analysis, is not as appropriate as that of char determined by DTF because the heating rate in the DTF simulate the full scale furnace heating rate better. One of the important parameters Eskom uses is the energy ratio ($E_r$) which is the ratio of the amount of energy required for ignition relative to the amount of energy being liberated during combustion (Wagner, 2008).

Previous research work on blended coals has generally shown that volatile matter is a common index in predicting the ignitability of coal blends (Su et al, 2001). In a blend of two coals in which one has low volatile matter and the other has high volatile matter, the latter was able to improve the ignition properties of the former. It was also found that volatile matter is not the only factor affecting ignitability, other factors such as heating value also do because the high heating value is needed to maintain the flame intensity.

Carbon burnout is affected by the amount of volatile matter quickly released from the fuel, the porosity of the resultting char, particle size of the char, the reactant, the partial pressure of the reactant, furnace temperature and the residence time. Unburned carbon is the small proportion of the fuel that leaves the combustion chamber with fly ash in the form of unburned char. Increased unburned carbon does not only reduce combustion efficiency but negatively impacts the saleability of ash and reduces the efficiency of the electrostatic precipitators. Poor carbon burnout is indicative of poor ignition. The combustion efficiency using an ash tracer technique is given by:

$$\eta_c = \left[1 - \frac{A_0}{100 - A_0} \times \frac{100 - A_i}{A_i}\right] \times 100 \qquad (2.7)$$

Where $A_0$ = ash content of the feed fuel on dry basis and

$A_i$ = ash content of combustible residue on dry basis

(Su et al, 2001).

Moghtaderi, (2007) indicated that blending of coal with biomass increases the likelihood of char extinction resulting in decreasing the level of char burnout. Pallarés et al, (2009) reported decreasing combustion efficiency as co-firing ratio was increased. On the other hand Vamvuka et al, (2003) and Savolainen, (2003) have actually indicated that solid bio-fuels could support the combustion of poor coals. Molcan et. al, 2009 observed that the burnout increased with increasing co-firing ratio. In some studies (Pan et al, 1996; Meesri et al, 2002), addition of biomass did not result in any synergistic effects.

## 2.6 Fuel Preparation

### 2.6.1 Biomass Storage

Biomass fuels need significant provision for bulk handling and long-term storage. For woody biomass it is advisable to store it in the form of logs, even though it occupies more space, to avoid biological activity usually associated with storage in chip form, especially when moisture content exceeds 20% (Van Loo, 2002). Biological activity can lead to heating of the storage pile, loss of dry matter and physical deterioration of the fuel. Herbaceous biomass such as grass and straws usually have moisture content below 20 % and therefore are not subject to the biological activity to the same extent as wood and hence can be stored for longer periods without serious quality deterioration.

### 2.6.2 Grinding of Biomass

Grinding of biomass is a challenging exercise because of the non-friable nature of biomass and its moisture content. For biomass fuels with maximum particle size of 5mm (when co-firing at 5-15% on energy basis) and a moisture content below 25%, the amount of energy to grind biomass is in the range 0.5-2% of the heating value (Van Loo et al, 2002). This is

higher than that required for coals which is 0.9-1.2% of the heating value (Robinson et al, 2002b). With the moisture content in excess of 25%, the fuel must be dried before grinding. When grinding biomass to particle sizes less than 1 mm, energy requirements increase significantly (>20% of the heating value) and this is uneconomical (Robinson et al, 2002b). Bigger particle size may raise concern of carbon burnout, but particle sizes up to 6 mm have been found to burn successfully (see section 2.6.3).

In The Netherlands, grinding of biomass by agricultural equipment was found to be inadequate such that equipment that would meet co-firing requirements had to be developed. Such equipment is still not available in South Africa. Comminution of biomass feedstock may require it to be passed through a cascade of size reduction stages until the required top-size is achieved.

### 2.6.3 Particle Size, Burnout and Residence Time

Complete burnout depends on residence time at high temperatures and particle size. If residence time is long enough and particle size is fine, the burnout increases with increasing biomass share. However, if the residence time is too short and the biomass particles are too coarse, the burnout deteriorates with increasing biomass share (Spliethoff et al, 1998).

For pilot scale tests, the maximum particle size that will burn out completely was found to be about 6 mm for straw and grass (Spliethoff et al, 1998; Demirbas, 2003; Tillman, 2000; Robinson et al, 2003; Baxter L, 2005), and about 4 mm for woody biomass (Spliethoff et al, 1998). Some tests show that even larger particles for straw or grass can be tolerated in commercial plants due to their high volatile content and rapid kinetics

(Kwong et al, 2007), as well as aerodynamic factors that can allow large particles to achieve considerably longer residence times inside the boiler (Tillman, 2000; Robinson et al, 2002b).

## 2.7 Fuel injection methods

The economics of co-firing in pulverised coal boilers are closely tied to the biomass transportation and preparation costs such as drying and milling. The most critical terms in the cost of co-firing are the fuel cost and the capital cost of retrofitting the power plant to enable biomass to be co-fired with the coal. The fuel cost is the difference between the cost of biomass and that of coal displaced by the biomass (Hughes, 2000). Retrofitting costs are dependent on whether the biomass is blended with coal, fired separately from coal or used as a reburn fuel.

### 2.7.1 Blending or co-milling

Blending or co-milling requires no separate flow because biomass is mixed with coal and fed together into the pulverising mill. This approach allows simultaneous size reduction and drying of both fuels before feeding their blend into the combustion chamber through the same channel used for coal. Blending is much lower in costs than separate flow. Although blending biomass with coal is least expensive, there is an upper limit to the quantities of biomass employed, generally up to 5% biomass on mass basis (Battista at al, 2000). There is a limitation because blending tends to reduce mill outlet temperatures, increase pulveriser load and reduce feeder speeds.

Biomass heating values generally are lower than those of coal, particle densities are about half those of coal and bulk densities are about one-fifth those of coal. This is equivalent to an overall fuel density of roughly one tenth that of coal (Baxter L, 2005), as a result the blend flow rate has to be

increased in order to have a heat throughput the same as in the coal-only case.

This increased fuel flow rate may cause the flame to move away from the burner mouth, thereby creating a flame stability problem (Sami et al, 2001). Lifted flames are also known to cause higher $NO_X$ levels (Sami et al, 2001).

### 2.7.2 Direct Injection

Separate injection involves setting up a separate line for milling and conveying the biomass to the furnace. This has the advantage that biomass does not affect the flow, milling and classification of coal. Either dedicated biomass burners or multi-fuel burners are used. Multi-fuel burners consist of a central pipe for injecting one fuel and an annular concentric pipe for the other fuel. A third annular pipe may be added for swirl air. Fig. 2.2 shows different configurations of a multi-fuel burner. Injecting biomass through the central pipe has a different effect on $NO_X$ emissions than when injecting it through an annular pipe. Introduction of biomass through the center of the burner releases volatiles readily enough to cause early ignition of the entire mass of fuel. Also it consumes additional oxygen from the air supply, thus increasing fuel staging within the flame zone (Tillman, 2000). This approach is more capital intensive than the limited modifications required for a co-milling installation.

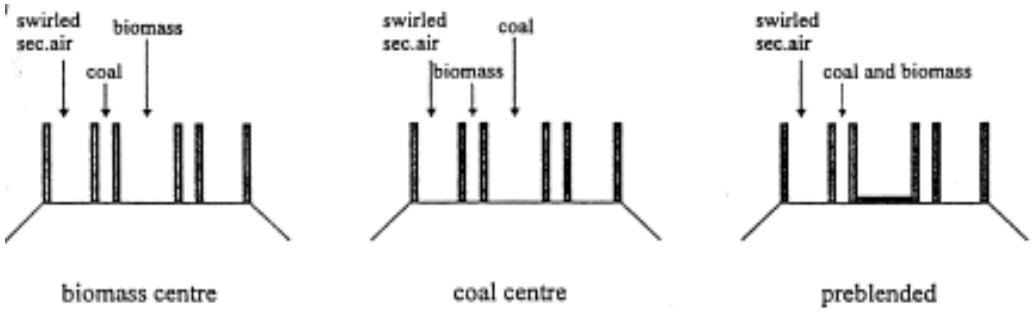


Figure 2.2 Multi-fuel burner configuration for co-firing biomass with coal (Sami et al, 2001)

**Re-burning**

Another option is to inject biomass downstream of the primary coal combustion zone as a re-burn fuel. The local concentration of hydrocarbons from volatiles released creates fuel rich conditions that favour $NO_x$ reduction to molecular nitrogen. The higher the volatile matter content, the larger the reduction in $NO_x$. Coal contains 30-50 % volatile matter and biomass contains up to 80% volatile matter on a dry-ash-free (DAF) basis, hence biomass has the potential to be a very effective re-burn fuel when coal is used as a primary fuel (Sami et al, 2001). Up to 60 % reduction in $NO_x$ can be achieved when injecting biomass as a re-burn fuel (Sami et al, 2001; Robinson et al, 2003).

## 2.8 Biomass availability as a sustainable fuel

The sustainable availability of biomass in the vicinity of the power stations could cut transportation costs and improve reliability, but since the power stations were originally built with availability of coal in mind, they are not always near biomass sources. In the US, wood grows at a rate that increases forest biomass by about 3%, the annual net increase after subtracting the annual harvest (Hughes, 2000). Forests alone are not adequate and may not always be near the power stations such that they

are augmented with farm and pasture land for short-rotation agro-forestry production, in order to have a sustainable supply of biomass (Hughes, 2000).

Energy crops are relatively expensive compared to residues, resulting in higher operating costs for energy crops. Many residues are nominally free at the point of their generation, but transportation, preparation and on-site handling typically increases their effective cost per unit energy such that it is equal to or exceeds that of coal (Baxter L, 2005).

A general conclusion is that biomass co-firing is commonly slightly more expensive than a dedicated coal system. The rationale for co-firing is justified by the motivation to reduce $CO_2$ emissions which is rewarded by carbon credit incentives. In this respect, the more relevant cost comparison is that with other renewable options such as wind and solar, in which case co-firing, where it is feasible, is by far the cheapest means of power generation. Feasibility is determined by biomass resources and coal-based power plants being located in the same region (Baxter L., 2005).

The ideal situation for South Africa would have been when all the biomass resources spread all over the country were concentrated in the Mpumalanga area where the power stations are clustered. The cost of collection and transportation could be prohibitive. There is already a significant biomass industry from paper and sugar cane, however most of it is used by the companies themselves for local co-generation projects. Production of bioenergy as crops can ensure reliability of fuel supply, however there are limiting conditions when it comes to availability of suitable land for energy crops. Conditions such as protected land (international conventions), areas with steep slopes, areas set aside for crops, wetlands, areas with unsuitable soils and rainfall will limit biomass production. Crops such as bagasse, sweet sorghum could be grown to

supplement the biomass which is collected as waste. According to research that is being done by the University of Kwazulu Natal regarding GIS data that assesses the suitability of land in the SADC region for suitability of sugar cane and sweet sorghum, the SADC region is the one with the highest potential in the world to grow bioenergy crops (Watson et al, 2008). South Africa itself does not have high potential, but the neighbouring countries such as Zambia, Mozambique and Malawi have a high potential (Watson et al, 2008). There is a possibility of South Africa importing these biomass fuels in the form of pellets to improve volume to mass ratio in order to lower transportation costs. When controls on emissions become tighter this could be a cheaper option, in comparison to importing biomass from South Africa by European power utilities.

## 2.9 Impact on boiler efficiency

Biomass fuels, which originate from plants or animals, generally contain moisture content, which acts as a heat sink that can lower the boiler efficiency. Co-firing of biomass materials, and particularly of wet biomass, can have an impact on the maximum achievable boiler load and on the boiler efficiency. However, some studies show modest or no reductions in boiler efficiency when firing low moisture (<10% moisture) biomass fuels at low levels of co-firing (Robinson et al, 2003; Sondreal et al, 2001; Baxter L, 2005; Maciejewska et al, 2006).

# 3 NUMERICAL SIMULATION

The approach adopted in this project was to run a simulation of the combustion process on a 2-D grid of the Pilot Scale Combustion Test Facility at Rosherville. The 2-D grid was found to be accurate enough for this type of problem because the conclusions that could be drawn from it, are the same as those which could be drawn from a more time-consuming 3-D grid. The simulation of the combustion process was implemented using the commercial software FLUENT© (Fluent, 2006). Chemical and physical properties of the fuels and the furnace operating conditions are set as inputs or boundary conditions into the model. The combustion process was modelled as a two-phase flow, namely the continuous gas phase flow and the discrete phase flow. The continuous phase consists of primary and secondary air as well as the volatiles evolved from the combusting particles, while the combusting particles themselves form the discrete phase. The continuous phase is determined by solving the transport equations for the conserved scalar, mixture fraction. On the other hand, the discrete phase is solved in the Lagrangian reference frame to determine particle trajectories and heat interaction in the combustion chamber. Since there is an interaction between the two phases, after certain iterations of the continuous phase, the discrete phase has to be updated.

The following models or sub-models were used: P1 radiation model to calculate heat transfer, the viscous model for turbulence interaction, energy model for transport equations, non-premixed model and probability density function (PDF) equilibrium chemistry model for the thermo-chemical interaction of species, $NO_X$ and $SO_X$ sub-models for the calculation of pollutant formation.

The modelling approach was to solve the main combustion problem and calculate the $NO_X$ and $SO_X$ formation from the converged solution via post processing.

The combustion models of solid fuels use three steps: heating up, devolatilisation, volatile combustion and char combustion. Sub-models include those describing pollutant formation, fluid flow and heat transfer, as described below.

## 3.1 Inert Heating

Inert heating law applies to a particle before its devolatilisation temperature (defined by user) is reached. Devolatilisation temperature $T_{vap}$ is used to define the onset of devolatilisation. When the combusting particle becomes ash after burning, the inert heating law also applies. When using this law, heat balance is used to relate the particle temperature, to the convective heat transfer and the absorption (or emission) of radiation at the particle surface.

$$m_p c_p \frac{dT_p}{dt} = hA_p\left(T_\infty - T_p\right) + A_p \varepsilon_p \sigma_B \left(\theta_R{}^4 - T_p{}^4\right) \qquad (3.1)$$

This law is applicable when $T_p < T_{vap}$ or $m_p \leq (1-f_{v,0})m_{po.}$

where

$m_p$ = mass of the particle (kg)

$c_p$ = heat capacity of the particle (J/kg-K)

$A_p$ = surface area of the particle ($m^2$)

$T_\infty$ = temperature of the gas surrounding the particle (K)

$T_P$ = particle temperature (K)

h = convective heat transfer coefficient ($W/m^2$-K)

$\varepsilon_p$ = particle emissivity (dimensionless)

$\sigma_B$ = Stefan-Boltzmann constant ($5.67 \times 10^{-8}$ $W/m^2$-$K^4$)

$\theta_R$ = radiation temperature (K)

$f_{v,0}$ = mass fraction of volatiles initially present in the particle

$m_{p,0}$ = initial particle mass (kg)

## 3.2 Devolatilisation

The devolatilisation model assumes that the rate of devolatilisation is first-order dependent on the amount of volatiles remaining in the particle.

$$-\frac{dm_p}{dt} = k\left[m_p - \left(1 - f_{v,0}\right)\left(1 - f_{w,0}\right)m_{p,0}\right] \tag{3.2}$$

Where

The kinetic rate is defined by an Arrhenius type expression

$$k = A_1 e^{-\frac{E}{RT_p}} \tag{3.3}$$

Where

$f_{w,0}$ = mass fraction of evaporating/boiling material

$k$ = kinetic rate ($s^{-1}$)

$A_1$ = pre-exponential factor ($s^{-1}$)

$E$ = activation energy (J/mol)

$R$ = universal gas constant (J/mol K)

During devolatilisation, particle diameter changes depending on swelling coefficient $C_{sw}$. When swelling coefficient is equal to one, the particle diameter remains constant. When the swelling coefficient is equal to two, the final particle diameter doubles when all of the volatile component has vaporised. Swelling coefficient is user defined and is applied in the following equation:

$$\frac{d_p}{d_{p,0}} = 1 + (C_{sw} - 1)\frac{\left(1 - f_{w,0}\right)m_{p,0} - m_p}{f_{v,0}(1 - f_{w,0})m_{p,0}} \tag{3.4}$$

$d_p$ = current particle diameter (m)

$d_{p,0}$ = original particle diameter (m)

## 3.3 Heat transfer to the particles during devolatilisation

Heat transfer to the particles during devolatilisation includes the contribution from convection, radiation and the heat consumed during the devolatilisation and it is given by:

$$m_p c_p \frac{dT_p}{dt} = hA_p\left(T_\infty - T_p\right) + \frac{dm}{dt} h_{fg} + A_p \varepsilon_p \sigma_B \left(\theta_R{}^4 - T_p{}^4\right) \tag{3.5}$$

$h_{fg}$ = latent heat of devolatilisation (J/kg)

## 3.4 Char Reaction Model

When devolatilisation is complete, the heterogeneous surface char reaction begins which consumes the combustible fraction $f_{comb}$, of the particle. Devolatilisation is complete when the following condition holds:

$$m_p < (1-f_{v,0})\,(1-f_{w,0})m_{p,0} \tag{3.6}$$

The surface reaction will continue while eqn (3.6) holds until the following condition is true:

$$m_p > (1- f_{v,0} - f_{comb})\,(1-f_{w,0})m_{p,0} \tag{3.7}$$

The combustion of the reactive content of the particle is governed by the stoichiometric requirement , $S_b$, of the following surface reation:

$$\text{Char(s)} + S_b\, O_2\text{(g)} \rightarrow \text{Products(g)} \tag{3.8}$$

$S_b$ = stoichiometric mass of oxygen required to burn 1 kg of char which is predominantly carbon.

For the char reaction, the Kinetic/Diffusion Surface Reaction Rate Model is used (Baum et al in Fluent, 2006). This model assumes that the surface reaction rate is determined either by chemical kinetics or by the diffusion of gaseous oxidant to the surface of the particle. The rate of mass loss by combustion, depends on particle density, diameter, and the ratio of the reacting surface to the external surface of the particle which is assumed to be spherical.

$$\frac{dm_p}{dt} = -A_p P_{ox} \frac{D_o R_k}{D_o + R_k} \tag{3.9}$$

where

$A_p$ = particle surface area ($m^2$)

$P_{ox}$ = oxidant partial pressure (Pa)

$R_k$ = kinetic rate ($kg/m^2$ s Pa)

$D_o$ = diffusion rate coefficient ($m^2/s$)

$$D_o = \frac{C_1 \left[ \left( T_p + T_\infty \right) / 2 \right]^{0.75}}{d_p} \tag{3.10}$$

$$R_k = C_2 e^{-\frac{E_k}{RT_p}} \tag{3.11}$$

where

$C_1$ = mass diffusion-limited rate constant ($s^{-1}$)

$C_2$ = kinetics-limited rate pre-exponential factor ($kg/m^2$ s Pa)

$E_k$ = kinetics-limited rate activation energy (J/kg mol)

$C_2$ and E are obtained from the Drop Tube Furnace (DTF) tests (see section 4.3.3).

## 3.5 The Radiation Model

The solid fuel particles can be treated as absorbing, emitting and scattering medium and the transport equation for the incident radiation can be written as:

$$\nabla \bullet (\Gamma \nabla G) + 4\pi \left( a \frac{\sigma T_P^{\ 4}}{\pi} + E_p \right) - (a + a_p) G = 0 \tag{3.12}$$

where

G = the incident radiation ($W/m^2$)
a = absorption coefficient
σ = scattering coefficient
$E_p$ = equivalent emission of particles
$a_p$ = equivalent absorption coefficient

$$E_P = \lim_{V \to 0} \sum_{n=1}^{N} \varepsilon_{Pn} A_{Pn} \frac{\sigma T_{Pn}^4}{\pi V} \tag{3.13}$$

$$\Gamma = \frac{1}{3(a + a_p + \sigma_p)} \tag{3.14}$$

$$\sigma_P = \lim_{V \to 0} \sum_{n=1}^{N} (1 - f_{pn})(1 - \varepsilon_{pn}) \frac{A_{pn}}{V} \tag{3.15}$$

$$a_P = \lim_{V \to 0} \sum_{n=1}^{N} \varepsilon_{Pn} \frac{A_{pn}}{\pi V} \tag{3.16}$$

$$A_{pn} = \frac{\pi d_{pn}^2}{4} \tag{3.17}$$

where

$f_{pn}$ = scattering factor of the nth particle

$\varepsilon_{pn}$ = emissivity of the nth particle

$A_{pn}$ = projected area of the nth particle ($m^2$)

$d_{pn}$ = diameter of the nth particle (m)

## 3.6 Turbulence Model

For turbulence interaction, a standard k-ε model was used, where k is turbulence kinetic energy and ε is the rate of dissipation of turbulence kinetic energy (Launder et al in Fluent (2006)).

k and ε are obtained from the following transport equations:

$$\frac{\partial}{\partial t}(\rho k)+\frac{\partial}{\partial x_i}(\rho k u_i)=\frac{\partial}{\partial x_j}\left[\left(\mu+\frac{\mu_t}{\sigma_k}\right)\frac{\partial k}{\partial x_i}\right]+G_k+G_b-\rho\varepsilon-Y_M+S_k \qquad (3.18)$$

$$\frac{\partial}{\partial t}(\rho \varepsilon)+\frac{\partial}{\partial x_i}(\rho \varepsilon u_i)=\frac{\partial}{\partial x_j}\left[\left(\mu+\frac{\mu_t}{\sigma_\varepsilon}\right)\frac{\partial \varepsilon}{\partial x_j}\right]+C_{1\varepsilon}\frac{\varepsilon}{k}(G_k+C_{3\varepsilon}G_b)-C_{2\varepsilon}\rho\frac{\varepsilon^2}{k}+S_\varepsilon \qquad (3.19)$$

where

$G_k$ = generation of turbulence kinetic energy due to the mean velocity gradients.

$G_b$ = generation of turbulence kinetic energy due to buoyancy.

$Y_M$ = contribution of the fluctuating dilation in compressive turbulence to the overall dissipation rate.

$\sigma_k$ = turbulent Prandtl number for k.

$\sigma_\varepsilon$ = turbulent Prandtl number for ε.

$S_\varepsilon$ = user defined source term.

$S_k$ = user defined source term.

$v$ = component of flow velocity parallel to gravitational vector.

u = component of flow velocity perpendicular to gravitational vector.

Turbulent or eddy viscosity

$$\mu_t = \rho c_\mu \frac{k^2}{\varepsilon} \tag{3.20}$$

$C_{1\varepsilon}$, $C_{2\varepsilon}$, $C_\mu$, $\sigma_k$, and $\sigma_\varepsilon$ are model constants with the following values:

$C_{1\varepsilon}$= 1.44 $C_{2\varepsilon}$ = 1.92 $C_\mu$ = 0.09 $\sigma_k$ = 1.0 and $\sigma_\varepsilon$ = 1.3 (Launder et al in Fluent (2006)).

$$C_{3\varepsilon} = \tanh\left|\frac{v}{u}\right| \tag{3.21}$$

$$G_k = -\rho\overline{u_i' u_j'}\frac{\partial u_j}{\partial x_i} \tag{3.22}$$

where $-\rho\overline{u_i' u_j'}$ are Reynolds stresses.

## 3.7 Discrete Phase Model

### 3.7.1 Particle Force Balance

Particles trajectories are predicted by integrating the force balance on the particle, which is written in the Lagrangian reference frame.

$$\frac{du_p}{dt} = F_D(u_f - u_p) + g_x\frac{\rho_p - \rho}{\rho_p} + F_x \tag{3.23}$$

where

$u_f$ = fluid phase velocity (m/s)

$u_p$ = particle velocity (m/s)

$\mu$ = molecular viscosity of the fluid ($m^2$/s)

$\rho$ = fluid density (kg/m$^3$)

$\rho_p$ = density of the particle (kg/m$^3$)

$d_p$ = particle diameter (m)

$F_x$ = additional acceleration (force/unit particle mass) term (m/s$^2$)

The term $g_x(\rho_p - \rho)/\rho_p$ is the gravity force per unit mass and $F_D(u_f-u_p)$ is the drag force per unit particle mass where $F_D$ is as defined below.

$$F_D = \frac{18\mu}{\rho_p d_p{}^2} \times \frac{C_D \,\mathrm{Re}}{24} \tag{3.24}$$

$C_D$ = drag coefficient.

For spherical particles,

$$C_D = a_1 + \frac{a_2}{\mathrm{Re}} + \frac{a_3}{\mathrm{Re}^2} \text{ (Morsi et al in Fluent (2006))} \tag{3.25}$$

where $a_1$, $a_2$ and $a_3$ are constants.

For non-spherical particles,

$$C_D = \frac{24}{\mathrm{Re}_{sph}}\left(1 + b_1 \,\mathrm{Re}_{sph}{}^{b2}\right) + \frac{b_3 \,\mathrm{Re}_{sph}}{b_4 + \mathrm{Re}_{sph}} \quad \text{(Haider et al, 1989).} \tag{3.26}$$

where

$b_1$ = exp(2.3288 - 6.4581$\Phi$ + 2.4486$\Phi^2$)

$b_2$ = 0.0964 + 0.5565$\Phi$

$b_3$ = exp(4.905 - 13.8944$\Phi$ + 18.4222$\Phi^2$ – 10.2599$\Phi^3$)

$b_4$ = exp(1.4681 + 12.2584$\Phi$ – 20.7322$\Phi^2$ +15.8855$\Phi^3$)

$\Phi$ = s/S is the shape factor (3.27)

where

s = surface area of the sphere having the same volume as the particle (m$^2$).

S = actual surface area of the particle ($m^2$).

The Reynolds number $Re_{sph}$ is computed with the diameter of a sphere having the same volume as the particle.

### 3.7.2 Stochastic Tracking – Discrete Random Walk Model

The Stochastic tracking approach predicts the turbulent dispersion of particles by integrating the trajectory equation (equ. 3.23) for the individual particles using the instantaneous fluid velocity $u = \bar{u} + u'(t)$, along the particle path during the integration. By computing the trajectory in this manner for the sufficient number of representative particles called the "number of tries", the random effects of turbulence on the particle dispersion may be accounted for.

Fluent uses random walk model to determine the instantaneous fluid velocity. In the discrete random walk (DRW) model, the fluctuating velocity components are discrete piecewise constant functions of time. Their random value is kept constant over an interval of time given by the characteristic lifetime of the eddies. Each eddy is characterized by:

1. a Gaussian distributed random velocity fluctuation, $u'$, such that $u' = \zeta\sqrt{\overline{u'^2}}$ where $\zeta$ is a normally distributed random number and the remainder of the right-hand side is the local RMS value of the velocity fluctuations.

2. a lifetime, $\tau_e = -T_L \log(r)$

where r is random number between 0 and 1 and the Lagrangian integral time $T_L$ is given by

$$T_L = 0.15\frac{k}{\varepsilon} \qquad (3.28)$$

for k-ε model.

## 3.8 Setting up Discrete Phase Model

### 3.8.1 Particle Tracking and Dragging Parameters

Fig. 3.1 shows the main panel for setting up the Discrete Phase Model. Note that **Interaction with Continuous Phase** option is checked. This means that the two-way coupling between the discrete phase and the continuous phase has been enabled. The discrete phase is updated after every 20 iterations of the continuous phase. There are no rules for choosing the **Number of Continuous Phase Iteration per DPM Iteration**. Too high or too low numbers may delay solution convergence. To find the suitable number is a matter of trial and error. A figure of 20 (shown in Fig. 3.1) has been decided upon through trial and error.

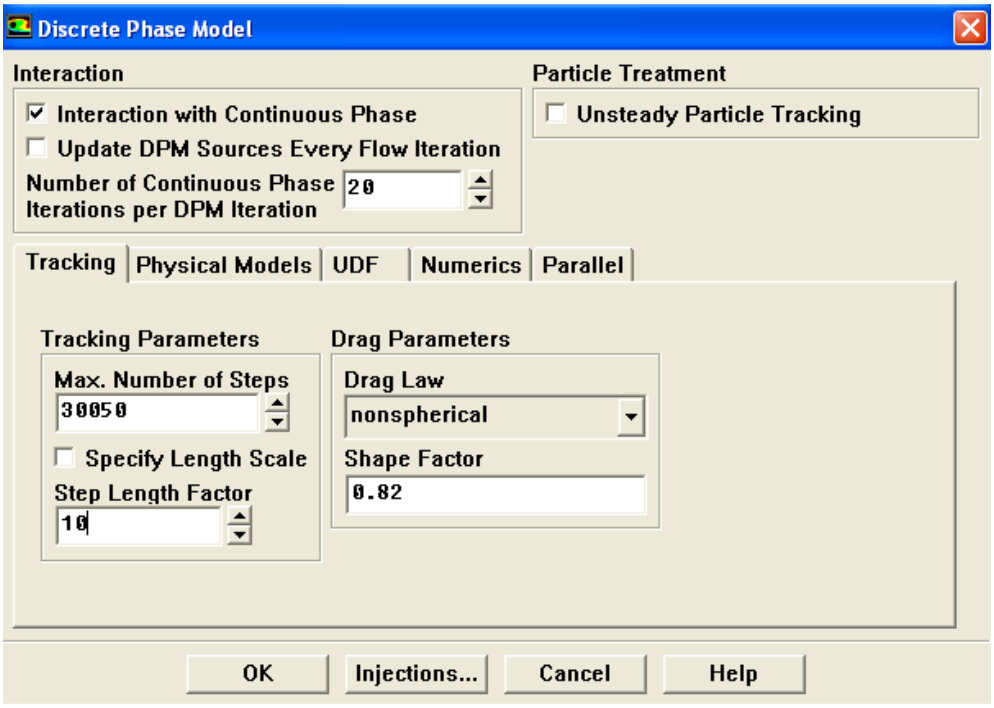


Figure 3.1 The Discrete Phase Model data entry panel.

During tracking some of the particles may be trapped in the recirculating region of the continuous flow field causing Fluent to track them infinitely.

To safeguard against this problem, a figure called Maximum Number of Steps must be specified. **Max. Number of Steps** option specifies the maximum number of time steps used to compute a single particle trajectory via integration of equation 3.23. If the maximum number of steps is exceeded, the trajectory calculation for the current particle injection is abandoned. The **Step Length Factor** λ controls the time step size used to integrate the equations of motion for the particle. The integration time Δt is computed by Fluent based on the characteristic time $\Delta t_{ch}$ required for the particle to traverse a computational cell.

$$\Delta t = \frac{\Delta t_{ch}}{\lambda} \tag{3.29}$$

A rule of thumb to follow (Fluent, 2006) when setting parameters in the panel is that if particles have to advance through N number of cells in the domain, then maximum number of steps is λN. For instance if step length factor is 10, then maximum number of tries for a domain with 3005 cells is 10 x 3005 = 30 050.

Shape factor is as defined in Eqns (3.26) and (3.27). Since the shape factor in Fluent cannot be set separately for coal and biomass streams, a mass weighted average shape factor (Eqn (3.30)) was used based on shape factors for coal and biomass. Ma et.al. (2007) suggests shape factor of 0.25 for biomass. Coal particles are usually assumed spherical in which case shape factor is one. The mass weighted shape factors calculated form equation 3.30 and the mass flow rates are shown in Table 3.1.

$$Mass\ weighted\ shape\ factor\ \phi_{mw} = \frac{m_B\phi_B + m_C\phi_C}{m_B + m_C} \tag{3.30}$$

where

$m_B$ = mass flow rate of biomass (sawdust or grass) (kg/hr).

$m_C$ = mass flow rate of coal (kg/hr).

$\phi_B$ = shape factor of biomass (0.25)

$\phi_C$ = shape factor of coal (1)

Table 3.1 Flow rates and mass weighted shape factors for different co-firing ratios

| Co-firing ratio | Biomass flow rate(kg/hr) | Coal flow rate (kg/hr) | Mass weighted shape factor $\phi_{mw}$ |
|---|---|---|---|
| 100% Coal | 0.00 | 169.00 | 1.00 |
| 10% Sawdust | 20.29 | 152.47 | 0.91 |
| 15% Sawdust | 30.44 | 144.00 | 0.87 |
| 20% Sawdust | 40.58 | 135.53 | 0.83 |
| 10% Grass | 21.61 | 152.47 | 0.91 |
| 15% Grass | 32.42 | 144.00 | 0.86 |
| 20% Grass | 43.22 | 135.53 | 0.82 |

### 3.8.2 Defining Injections

Injections define properties of fuel such as fuel type (liquid or solid), material, diameter size distribution, position at which the fuel is introduced into the furnace and the total fuel flow rate in kg/s. Fig. 3.2 shows the **Injections** data entry panel where these parameters were actually entered. Fuel flow rates were obtained from Table 3.1 and the other parameters are as show in Table 3.2. Two injections for coal were defined because coal flows through an annular section, one to the left of biomass circular inlet and the other to the right as shown in Fig. 4.4.

For simulations of co-firing tests, the particle size distribution data in Table 3.3 was obtained from Rosin-Rammler distribution. For this type of distribution, the mass fraction of particles with a mass fraction greater than diameter d is given by:

$$Y_d = e^{-\left(\frac{d}{\bar{d}}\right)^n} \qquad 3.31$$

where
$\bar{d}$ = mean diameter
n = spread factor.

$\bar{d}$ and n are user specified constants and are obtained from fuel size grading. For example take sawdust size grading (Table 4.3). First, the data

is recast into Rosin-Rammler format as shown in Table 3.2. When $Y_d$ is plotted against d, a graph in Fig 3.3 is obtained. From this graph $\bar{d}$ can be estimated from the fact that when $d = \bar{d},\ Y_d = e^{-1} = 0.368$. For sawdust mean diameter was estimated as $\bar{d}$ = 0.0051m (see figure 3.4).

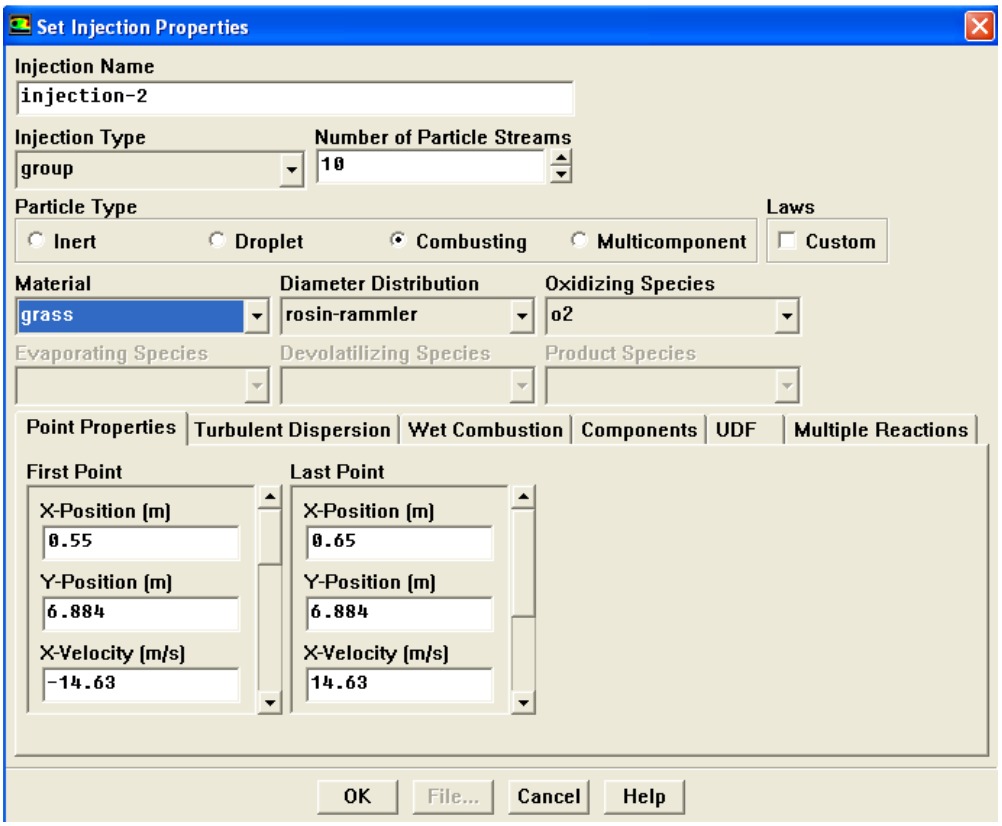

Figure 3.2 Discrete Phase Injections data input panel

Table 3.2 Sawdust size grading presented in Rosin-Rammler format

| Diameter d | Mass Fraction with diameter greater than d, Yd |
|---|---|
| 75 | 0.951 |
| 106 | 0.920 |
| 212 | 0.776 |
| 500 | 0.402 |
| 1000 | 0.146 |
| 3000 | 0.000 |
| 4750 | 0.000 |
| 6000 | 0.000 |

Table 3.3 Discrete phase parameters entered in the injections panel

| | | Coal | | | | Sawdust | | Grass | |
|---|---|---|---|---|---|---|---|---|---|
| | | Injection 1(left) | | Injection 2 (right) | | | | | |
| | | First Point | Last Point | First Point | Last Point | First Point | Last Point | First Point | Last Point |
| **Point properties** | **x-position (m)** | 0.5505 | 0.5690 | 0.6303 | 0.6490 | 0.5750 | 0.6250 | 0.5750 | 0.6250 |
| | **y-position (m)** | 6.8840 | 6.8840 | 6.8840 | 6.8840 | 6.8840 | 6.8840 | 6.8840 | 6.8840 |
| | **x-velocity (m/s)** | -14.63 | 14.63 | -14.63 | 14.63 | -14.63 | 14.63 | -14.63 | 14.63 |
| | **y-velocity (m/s)** | -20.9 | -20.9 | -20.9 | -20.9 | -20.9 | -20.9 | -20.9 | -20.9 |
| **Temperature (K)** | | 368 | | | | 368 | | 368 | |
| **Particle distribution** | **Minimum diameter (m)** | $3 \times 10^{-5}$ | | | | $7.5 \times 10^{-5}$ | | $7.5 \times 10^{-5}$ | |
| | **Maximum diameter (m)** | $1.2 \times 10^{-4}$ | | | | 0.003 | | 0.003 | |
| | **Mean diameter (m)** | $6.5 \times 10^{-5}$ | | | | 0.0051 | | 0.0047 | |
| | **Spread parameter** | 2.96 | | | | 2.08 | | 1.01 | |

Table 3.4 Properties of coal used for the simulation of tests run at the Pilot Scale Combustion Test Facility (PSCTF)

| **Property** | **Coal** | **Used in eqn.** | **Acquired from** |
|---|---|---|---|
| Combustible fraction (%) | 49.8 | 3.7 | Chemical analysis |
| Density (kg/$m^3$) | 1300 | 3.23 | Measured |
| Specific Heat (J/kg K) | 1380 | 3.1 | Engineeringtoolbox |
| Latent heat (J/kg) | $9.4 \times 10^6$ | 3.5 | Ma et al (2009) |
| Vaporization Temp. (K) | 500 | 3.1 | Ma et al (2009) |
| Volatile Component Fraction (%) | 20.7 | 3.2 and 3.4 | Chemical analysis |
| Binary Diffusivity ($m^2$/s) | 0.0005 | 3.9 and 3.10 | Fluent (2006) |
| Particle Emissivity | 0.9 | 3.1 and 3.5 | Fluent (2006) |
| Particle Scattering factor | 0.6 | 3.12 | Fluent (2006) |
| Swelling Coefficient | 1 | 3.4 | No swelling |
| Burnout Stoichiometric ratio | 2.67 | 3.8 | 12kgC +32kg$O_2$→44kg$CO_2$ (32/12) |
| **Single rate devolatilisation model** | | | |
| Pre-exponential factor ($s^{-1}$) | $4.2 \times 10^{14}$ | 3.3 | Ma et al (2009) |
| Activation energy (J/kg-mol) | $2.3 \times 10^5$ | 3.3 | Ma et al (2009) |
| **Kinetics/Diffusion-Limited Combustion Model** | | | |
| Mass diffusion-limited rate constant ($s^{-1}$) | 5e-12 | 3.10 | Fluent |
| Kinetics-limited rate pre-exponential factor (kg/$m^2$s Pa) | $7.225 \times 10^{-3}$ | 3.11 | DTF |
| Kinetics-limited rate activation energy (J/kg-mol) | 72951.00 | 3.11 | DTF |

Table 3.5 Properties of sawdust used for the simulation of tests run at Pilot Scale Combustion Test Facility (PSCTF)

| **Property** | | **Sawdust** | **Used in eqn.** | **Acquired from** |
|---|---|---|---|---|
| Combustible fraction (%) | | 19.0 | 3.7 | Chemical analysis |
| Density (kg/m$^3$) | | 400 | 3.23 | Measured |
| Specific Heat (J/kg K) | | 2500 | 3.1 | Engineeringtoolbox |
| Latent heat (J/kg) | | 9.4 x 10$^6$ | 3.5 | Ma et al (2009) |
| Vaporization Temp. (K) | | 473 | 3.1 | Ma et al (2007) |
| Volatile Component Fraction (%) | | 79.5 | 3.2 and 3.4 | Chemical analysis |
| Binary Diffusivity (m$^2$/s) | | 0.0005 | 3.9 and 3.10 | Fluent (2006) |
| Particle Emissivity | | 0.75 | 3.1 and 3.5 | Engineeringtoolbox |
| Particle Scattering factor | | 0.6 | 3.12 | Ma et al (2009) |
| Swelling Coefficient | | 1 | 3.4 | No swelling |
| Burnout Stoichiometric ratio | | 2.67 | 3.8 | 12kgC +32kg$O_2$→44kg$CO_2$ (32/12) |
| **Single rate devolatilisation model** | | | | |
| Pre-exponential factor (s$^{-1}$) | | 6 x 10$^{13}$ | 3.3 | Ma et al (2009) |
| Activation energy (J/kg-mol) | | 2.5 x 10$^8$ | 3.3 | Ma et al (2009) |
| **Kinetics/Diffusion-Limited Combustion Model** | | | | |
| Mass diffusion-limited rate constant (s$^{-1}$) | | 5e-12 | 3.10 | Fluent (2006) |
| Kinetics-limited rate pre-exponential factor (kg/m$^2$s Pa) | 10% | 3.588 x 10$^{-3}$ | 3.11 | DTF |
| | 15% | 3.380 x 10$^{-3}$ | | |
| | 20% | 4.921 x 10$^{-3}$ | | |
| Kinetics-limited rate activation energy (J/kg-mol) | 10% | 66 777.07 | 3.11 | DTF |
| | 15% | 65 690.08 | | |
| | 20% | 72 680.33 | | |

Table 3.6 Properties of grass used for the simulation of tests run at Pilot Scale Combustion Test Facility (PSCTF)

| **Property** | | **Grass** | **Used in eqn.** | **Acquired from** |
|---|---|---|---|---|
| Combustible fraction (%) | | 15.8 | 3.7 | Chemical analysis |
| Density (kg/m$^3$) | | 350 | 3.23 | Measured |
| Specific Heat (J/kg K) | | 0.714 | 3.1 | Fluent (2006) |
| Latent heat (J/kg) | | 9.4 x 10$^6$ | 3.5 | Ma et al (2009) |
| Vaporization Temp. (K) | | 473 | 3.1 | Ma et al (2007) |
| Volatile Component Fraction (%) | | 77.3 | 3.2 and 3.4 | Chemical analysis |
| Binary Diffusivity (m$^2$/s) | | 0.0005 | 3.9 and 3.10 | Fluent (2006) |
| Particle Emissivity | | 0.9 | 3.1 and 3.5 | Ma et al (2009) |
| Particle Scattering factor | | 0.6 | 3.12 | Ma et al (2009) |
| Swelling Coefficient | | 1 | 3.4 | No swelling |
| Burnout Stoichiometric ratio | | 2.67 | 3.8 | 12kgC +32kg$O_2$→44kg$CO_2$ (32/12) |
| **Single rate devolatilisation model** | | | | |
| Pre-exponential factor (s$^{-1}$) | | 6 x 10$^{13}$ | 3.3 | Ma et al (2009) |
| Activation energy (J/kg-mol) | | 2.5 x 10$^8$ | 3.3 | Ma et al (2009) |
| **Kinetics/Diffusion-Limited Combustion Model** | | | | |
| Mass diffusion-limited rate constant (s$^{-1}$) | | 5e-12 | 3.10 | Fluent (2006) |
| Kinetics-limited rate pre-exponential factor (kg/m$^2$s Pa) | 10% | 5.211 x 10$^{-3}$ | 3.11 | DTF |
| | 15% | 6.663 x 10$^{-3}$ | | |
| | 20% | 4.085 x 10$^{-3}$ | | |
| Kinetics-limited rate activation energy (J/kg-mol) | 10% | 69 037.01 | 3.11 | DTF |
| | 15% | 70 174.36 | | |
| | 20% | 62 484.56 | | |

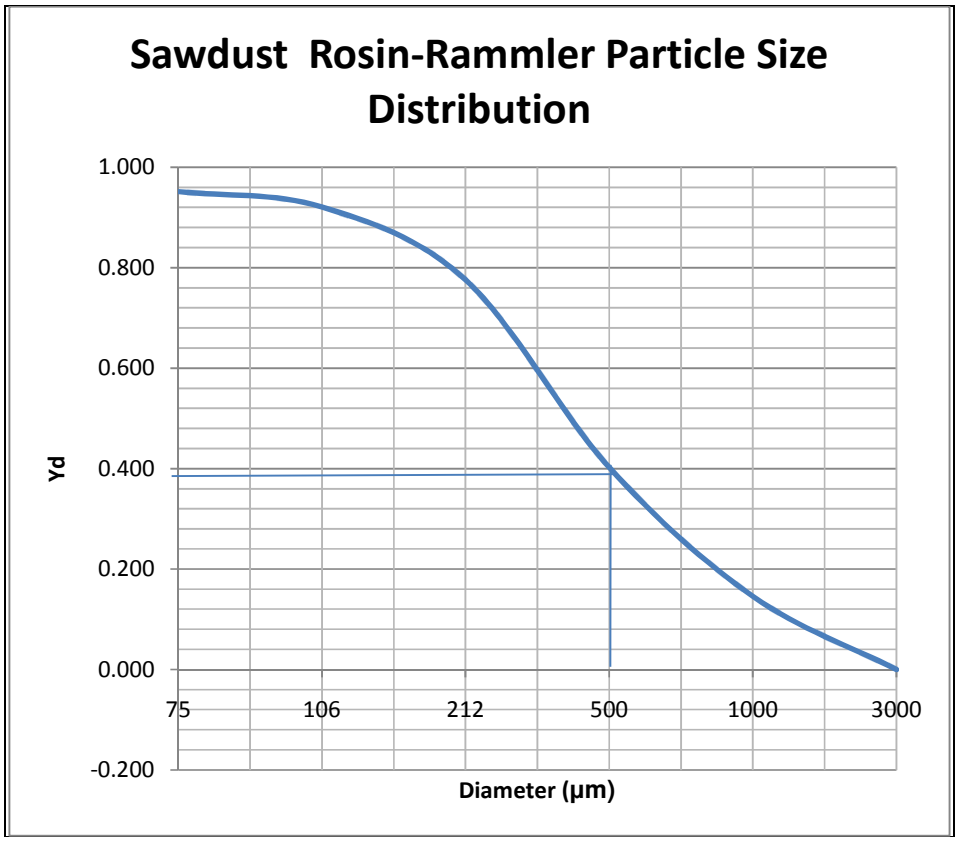


Figure 3.3 Rosin-Rammler particle size distribution for sawdust.

The value of spread parameter can be calculated from the average of values of n (using eqn (3.32)) for each of the diameters in Table 3.2. The spread parameter was calculated as 2.08.

$$n = \frac{\ln\left(ln\, Y_d\right)}{ln\left(-\frac{d}{\bar{d}}\right)} \qquad (3.32)$$

## 3.9 Modelling $NO_X$ Formation

### 3.9.1 Distribution of Nitrogen in Fuel Between Volatiles and Char

The $NO_X$ formation model includes fuel, thermal and prompt $NO_X$ formation sub-models. Fuel $NO_X$ model assumes that the fuel nitrogen in the solid fuel is distributed (not necessarily equally) between volatiles and char. The mass fraction of nitrogen in volatiles and char, can be determined from the following equations (Fluent, 2006):

$$F_{vol} + F_{char} = 1 \tag{3.33}$$

$$\frac{P_{Nv}}{P_{Nc}} = N_{split} \tag{3.34}$$

$$(F_{vol} \times P_{Nv}) + (F_{char} \times P_{Nc}) = TN_{fuel} \tag{3.35}$$

$$P_{Nc} = \frac{TN_{fuel}}{F_{vol} \times N_{split} + F_{char}} \tag{3.36}$$

where

$P_{Nv}$ = percentage by mass of nitrogen in volatiles (Volatile-N)

$P_{Nc}$ = percentage by mass of nitrogen in char (Char-N)

$TN_{fuel}$ = percentage by mass of nitrogen in fuel (daf)

$N_{split}$ = split of nitrogen between volatiles and char

$F_{vol}$ = mass fraction of volatiles in fuel (daf)

$F_{char}$ = mass fraction of char in fuel (daf)

$TN_{fuel}$, $F_{vol}$, and $F_{char}$ for coal and sawdust/grass were obtained from the fuel chemical analysis (Table 5.1) and converted to dry ash free (daf) basis. $N_{split}$ was chosen as 0.4 (see section 3.9.2). From these data the values of $P_{Xv}$ and $P_{Nc}$ were calculated using eqns (3.34) and (3.36), and tabulated in Tables 3.7 and 3.8 for all the tests simulated. $TN_{fuel}$, $F_{vol}$, and $F_{char}$, for 10%, 15% and 20% sawdust/grass were obtained from Table 5.8 and converted to dry ash free basis.

The conversion of fuel nitrogen can happen via two mechanisms. The first mechanism assumes that all the fuel nitrogen first gets converted to a number of intermediate species which then get partially converted to NO through oxidation process. If the reducing conditions prevail instead, then the existing NO will react with the intermediates to form nitrogen ($N_2$). In other words the oxidising conditions favour $NO_X$ formation while the reducing conditions inhibit it. The second mechanism assumes that all fuel nitrogen in the char gets converted directly to NO. The two mechanisms are shown diagrammatically on Fig. 3.4 and 3.5. The important intermediate species in this process are ammonia ($NH_3$) and hydrogen cyanide (HCN).

Table 3.7 Fuel-N Parameters for Simulation of Sawdust-based Co-firing

| **Fuel N Parameters** | **Coal A** | **10% Sawdust** | **15% Sawdust** | **20% Sawdust** |
|---|---|---|---|---|
| $T_{Nfuel}$ | 2.016 | 2.072 | 2.112 | 2.132 |
| $F_{vol}$ | 29.36 | 37.027 | 41.655 | 44.534 |
| $F_{char}$ | 70.64 | 62.973 | 58.345 | 55.466 |
| $N_{split}$ | 0.4 | 0.4 | 0.4 | 0.4 |
| $P_{Nc}$ | 0.0245 | 0.02664 | 0.02816 | 0.02909 |
| $P_{Nv}$ | 0.0098 | 0.01066 | 0.01126 | 0.01164 |

Table 3.8 Fuel-N Parameters for Simulation of Grass-based Co-firing

| **Fuel N Parameters** | **Coal A** | **10% Grass** | **15% Grass** | **20% Grass** |
|---|---|---|---|---|
| $T_{Nfuel}$ | 2.016 | 1.927 | 2.072 | 2.082 |
| $F_{vol}$ | 29.36 | 43.644 | 36.791 | 46.049 |
| $F_{char}$ | 70.64 | 56.356 | 63.209 | 53.951 |
| $N_{split}$ | 0.4 | 0.4 | 0.4 | 0.4 |
| $P_{Nc}$ | 0.0245 | 0.02611 | 0.02659 | 0.02877 |
| $P_{Nv}$ | 0.0098 | 0.01044 | 0.01064 | 0.01151 |

For solid fuels such as coal and biomass, both HCN and $NH_3$ can be generated as intermediates. For example coal tends to favour more production of HCN than that of $NH_3$ for higher ranking coals and vice-versa for lower-ranking coals (Winter et. al in Fluent (2006). Biomass fuels on the other hand produce predominantly more $NH_3$ than HCN (Liu and Gibbs in Fluent (2006).

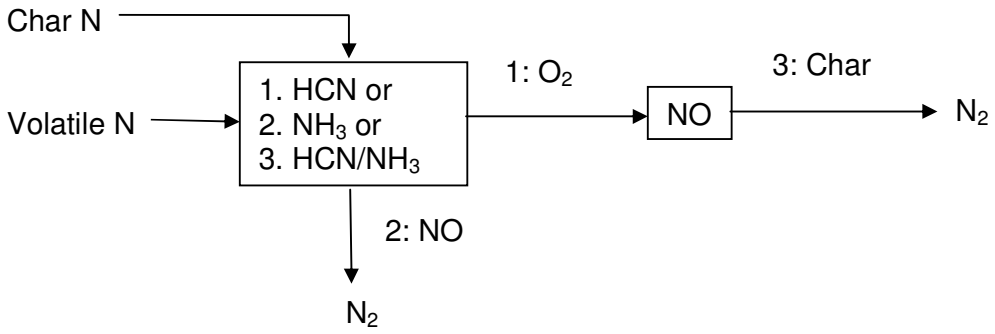


Figure 3.4 First mechanism: $NO_X$ formation all char N converts to the intermediate species (adapted from Fluent (2006)

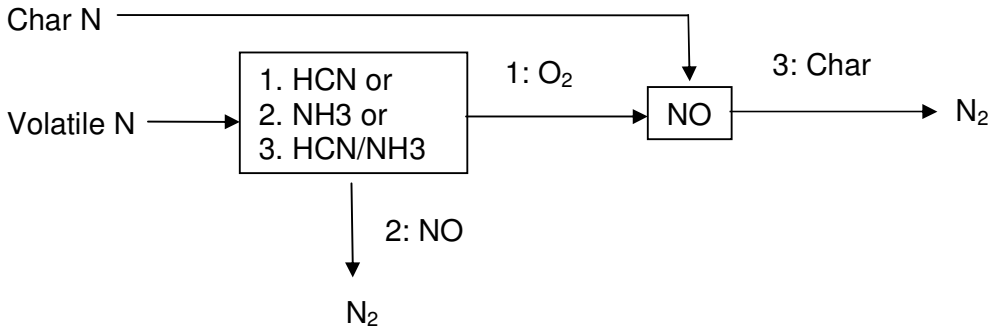


Figure 3.5 Second mechanism 2: $NO_X$ formation all char N converts NO directly (adapted from Fluent (2006)

### 3.9.2 Partitioning of Volatile-N and Char-N into HCN and $NH_3$

During solid fuel pyrolysis fuel-N divides into volatile-N and char-N, each of which can yield HCN and $NH_3$. The yield of HCN from fast coal pyrolysis (above 1100℃) is 10 - 20 times more than that during the slow pyrolysis, whereas NH3 is dominating during the slower pyrolysis (Tsubouchi et al, 2007). This suggests that the volatile N can be expected to contain a higher percentage of HCN than that of NH3.

Table 3.9 Partition of HCN and NH3 in Volatile-N and Char-N

| Co-firing Ratio | Partition of Intermediates in Volatiles | | Partition of Intermediates in Char | |
|---|---|---|---|---|
| | HCN | $NH_3$ | HCN | $NH_3$ |
| 100% Coal | 0.8 | 0.2 | 0.1 | 0.9 |
| 10% Sawdust | 0.5 | 0.5 | 0.1 | 0.9 |
| 15% Sawdust | 0.5 | 0.5 | 0.1 | 0.9 |
| 20% Sawdust | 0.5 | 0.5 | 0.1 | 0.9 |
| 10% Grass | 0.7 | 0.3 | 0.1 | 0.9 |
| 15% Grass | 0.7 | 0.3 | 0.1 | 0.9 |
| 20% Grass | 0.7 | 0.3 | 0.1 | 0.9 |

A value of 80% HCN and 20% was used for coal (see Table 3.8). Heterogeneous char is relatively a slower process than pyrolysis in which case the char-N can be expected to convert mostly to NH3. Values of 10% HCN and 90% NH3 were used for coal char-N partitioning (see Table 3.8). Because of low co-firing ratios, the partition of NH3 and HCN is largely dictated by coal to a larger extend on char-N than on volatile-N. Since most of biomass composition is volatiles, the NH3 produced from it will offset the ratio of HCN/NH3 in the gas phase. The figures of 70% HCN

and 30% NH3 were used for grass volatile-N because of low fuel-N content while 50% HCN and 50% NH3 were used for sawdust volatile-N due to its high fuel-N content (see Table 5.1).

The yields of volatile-N was found to range from 19 – 44% in the temperature range of 350 ℃ to 500 ℃ (Tsubouchi et al, 2007). Using this as a guideline and taking the mid-range value of 30 will give a volatile-N to char-N ratio of 0.4. This value was used to define Nsplit in equation 3.32.

## 3.10 $SO_2$ Formation

Similarlarly to the fuel $NO_X$ model, the $SO_X$ model assumes that the fuel sulphur is converted into a number of intermediate species which are eventually converted to $SO_2$.

$SO_X$ model assumes that the sulphur in the fuel is distributed between volatiles and char. The model requires the total mass fraction of sulphur in the fuel and the mass fraction of sulphur in volatiles and char, which can be determined from eqn (3.33) and the following equations:

$$\frac{P_{Sv}}{P_{Sc}} = S_{split} \tag{3.37}$$

$$(F_{vol} \times P_{Sv}) + (F_{char} \times P_{Sc}) = TS_{fuel} \tag{3.38}$$

$$P_{Sc} = \frac{TS_{fuel}}{F_{vol} \times S_{split} + F_{char}} \tag{3.39}$$

where

$P_{Sv}$ = percentage by mass of sulphur in volatiles (Volatile-S)

$P_{Sc}$ = percentage by mass of sulphur in char (Char-S)

$TS_{fuel}$ = percentage by mass of sulphur in fuel (daf)

$S_{split}$ = split of sulphur between volatiles and char

$F_{vol}$ = mass fraction of volatiles in fuel (daf)

$F_{char}$ = mass fraction of char in fuel (daf)

$TS_{uel}$, $F_{vol}$, and $F_{char}$ for coal and sawdust/grass were obtained from the fuel chemical analysis (Table 5.1) and converted to dry ash free (daf) basis. $S_{split}$ was chosen as 0.7 derived from data in Khan, (1989). From these data the values of $P_{Sv}$ and $P_{Sc}$ were calculated using eqns (3.37) and (3.39), and tabulated in Tables 3.10 and 3.11 for all the tests simulated. $TS_{fuel}$, $F_{vol}$, and $F_{char}$, for 10%, 15% and 20% sawdust/grass were obtained form Table 5.8 and converted to dry-ash-free basis.

Table 3.10 Fuel-S Parameters for Simulation of Sawdust-based Co-firing

| **Fuel S Parameters** | **Coal A** | **10% Sawdust** | **15% Sawdust** | **20% Sawdust** |
|---|---|---|---|---|
| $T_{Sfuel}$ | 2.642 | 1.868 | 1.769 | 1.647 |
| $F_{vol}$ | 29.36 | 37.027 | 41.655 | 44.534 |
| $F_{char}$ | 70.64 | 62.973 | 58.345 | 55.466 |
| $S_{split}$ | 0.7 | 0.7 | 0.7 | 0.7 |
| $P_{Sc}$ | 0.02897 | 0.02101 | 0.02022 | 0.01900 |
| $P_{Sv}$ | 0.02028 | 0.01471 | 0.01415 | 0.01330 |

Table 3.11 Fuel-S Parameters for Simulation of Grass-based Co-firing

| **Fuel S Parameters** | **Coal A** | **10% Grass** | **15% Grass** | **20% Grass** |
|---|---|---|---|---|
| $T_{Sfuel}$ | 2.642 | 1.813 | 1.868 | 1.646 |
| $F_{vol}$ | 29.36 | 43.644 | 36.791 | 46.049 |
| $F_{char}$ | 70.64 | 56.356 | 63.209 | 53.951 |
| $S_{split}$ | 0.7 | 0.7 | 0.7 | 0.7 |
| $P_{Sc}$ | 0.02897 | 0.02086 | 0.02100 | 0.01910 |
| $P_{Sv}$ | 0.02028 | 0.01460 | 0.01470 | 0.01337 |

# 4 EXPERIMENTAL PROCEDURE AND APPARATUS

## 4.1 Fuel Preparation and Sampling

### 4.1.1 Fuel Sourcing and Preparation

Biomass can be divided into two major types, namely ligneous and herbaceous. Due to limitations in the budget, only two biomass types representing each of the categories were used. Sawdust (ligneous) and grass (herbaceous) types of biomass were selected for co-firing experiments with one source of coal, which was selected to be an average representative of coals fired at various Eskom power stations.

Wood was initially considered for ligneous biomass type but milling equipment for wood was not available at the PSCTF. Wood milling equipment was expensive for this project's budget and its purchase could not be justified for just once-off use. Sawdust was therefore chosen because it did not require milling. It was obtained from Timber City, one of the major timber manufactures in South Africa. Research (see section 2.6.3) shows that particle top size for both biomass fuels may be chosen as 4 mm. Because of the high aspect ratio, a 2 mm-sieve was used to sieve sawdust to ensure that particle size was below 4 mm. About three and half drums (200 litres) of sawdust were prepared.

Long grass along roadways is usually cut down to improve visibility. Grass was chosen because the grass from the road side cutting was free and regarded as a waste. Since the time slot allocated for the tests (nos. 11 – 18, Table 5.2) on the PSCTF was out of season for collection of grass, it was purchased from the company which had collected it previously. Although grass required milling, unlike in the case for wood the equipment that could be used to mill grass was available at PSCTF. The first size reduction for grass (with longest pieces about 10 cm) was achieved

through the use of a hammer mill. For the second size reduction, a swing mill was used to achieve grass fuel with the size grading as indicated by Table 4.1.

A swing mill pot was held tightly against the bed by a pneumatically inflated rubber clamp (Fig. 4.1). The inflated rubber clamp allowed the pot to move with the bed along a circular path in the horizontal plane, when the bed was exited by eccentrically mounted rotor beneath the bed. A sliding grinder (Fig. 4.2) had an eccentric recess which caused it to move within the pot under the influence of centrifugal force as the pot rocked. As the grinder moved, it crushed grass particles that were trapped between the pot and the grinder. After about 3 minutes the swing mill could be stopped and the ground grass taken out. Milled grass was then sieved through a 2 mm-sieve and the oversized particles were taken back to the swing mill to be re-milled. This process was very slow due to the low output of the swing mill. It took about 3 days to fill a 200-litre drum. Eventually four 200-litre drums of grass were available.

Only one type of coal was used because of the limited number of tests (Table 5.2) carried out. The coal that was to be chosen was to be representative of coals burned in Eskom coal-fired power stations, based on the average calorific values. The average value of the calorific values of Eskom coals was found to be 19.64 MJ/kg as indicated in Table 4.1. Apart from the calorific value, the coal had to have poor ignition properties in order to amplify the effect, if any, that biomass would have on ignition. It also had to be a coal which was less likely to foul and slag. A choice was made between five selected possible coals whose properties are indicated in Table 4.2. Coal 1 was chosen for the tests because it met the conditions above better than the other coals. Considering the calorific values in Table 4.2, the closest values to the average 19.64 (Table 4.1) in order are: 19.64 MJ/kg for coal 4, 21.18 MJ/kg for coal 2, 21.25 MJ/kg for coal 3, 22.00

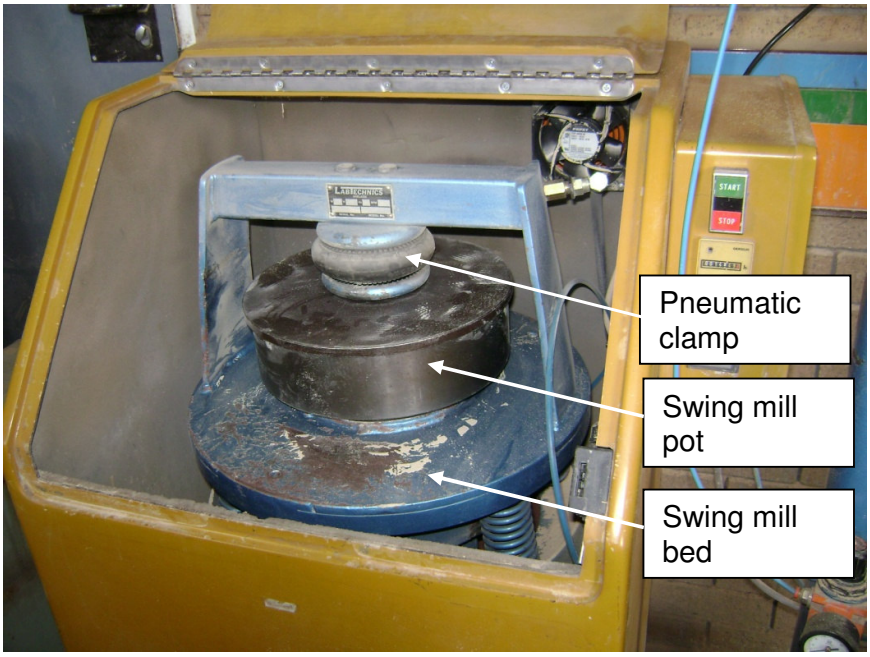


**Figure 4.1 Swing mill pot is held in position by pneumatically inflated rubber clamp during operation.**




**Figure 4.2 Swing mill pot opened to show the sliding grinder**

**Table 4.1 Calorific values of coals from various Eskom power stations**

| Power Station | Calorific Value (MJ/kg) |
|---|---|
| Arnot | 21.81 |
| Camden | 20.03 |
| Duvha | 20.87 |
| Hendrina | 20.79 |
| Kendal | 18.58 |
| Kriel | 20.98 |
| Lethabo | 14.22 |
| Majuba | 20.56 |
| Matimba | 18.74 |
| Matla | 19.05 |
| Tutuka | 20.46 |
| | |
| **Total/Average** | **19.64** |

MJ/kg for coal 5 and 25.34 MJ/kg for coal 3. Coal 4 and 2 although closest in terms of calorific value, they were not selected because of good ignition properties they both might have had, so 1 was selected as it had poor ignition, no fouling and medium slagging (its dolomite ratio (Van Dyk et al, 2005) ranks 4 in ascending order (see Table 4.2)). Ignition assessment is based on fuel ratio (fixed carbon to volatile matter). When fuel ratio is greater than 2.3 ignition is poor. If fuel ratio is below 1.7, ignition is very good but slagging propensity is increased due to high heat release rate. A comfort zone is between 1.7 and 2.3 where there is good ignition but no slagging tendency (Tarr et al, 2006).

### 4.1.2 Preparing a Representative Sample

The splitter was used to mix samples or split them evenly. It consists of a rotating drum (15 rev/min) with ten removable bins (Figure 4.3). As the drum rotates, the vibratory feeder attached to the big hopper feeds fuel at

a uniform rate into each of the ten bins to ensure even distribution of this fuel into the bins.

Table 4.2 Properties of selected possible coals

| TESTS | | COAL 1 | COAL 2 | COAL 3 | COAL 4 | COAL 5 |
|---|---|---|---|---|---|---|
| | | | | | | |
| Proximate Analyses | | | | | | |
| | | | | | | |
| Moisture | % | 2.4 | 6.6 | 3.4 | 3.5 | 3.3 |
| Volatiles | % | 20.2 | 22.4 | 22.2 | 20.4 | 21 |
| Ash | % | 28.8 | 20.8 | 18.1 | 32.2 | 26.3 |
| FC | % | 48.6 | 50.2 | 56.3 | 43.9 | 49.4 |
| | | | | | | |
| Total | % | 100 | 100 | 100 | 100 | 100 |
| | | | | | | |
| Ultimate Analyses | | | | | | |
| | | | | | | |
| C | % | 55.28 | 57.08 | 64.59 | 51.77 | 58.2 |
| H | % | 2.65 | 2.18 | 3.04 | 2.5 | 3.24 |
| O | % | 4.49 | 10.56 | 8.28 | 6.31 | 6.29 |
| N | % | 1.32 | 1.37 | 1.6 | 1.18 | 1.34 |
| S | % | 1.73 | 1.22 | 0.74 | 0.78 | 0.92 |
| CO3 | % | 3.33 | 0.19 | 0.25 | 1.76 | 0.41 |
| Moisture | % | 2.4 | 6.6 | 3.4 | 3.5 | 3.3 |
| Ash | % | 28.8 | 20.8 | 18.1 | 32.2 | 26.3 |
| | | | | | | |
| Total | % | 100 | 100 | 100 | 100 | 100 |
| | | | | | | |
| Calorific Value [MJ/kg] | | 21.25 | 21.18 | 25.34 | 19.64 | 22.00 |
| | | | | | | |
| | | | | | | |
| Ash Elementals XRF % Composition | | | | | | |
| | | | | | | |
| Ti02 | % | 1.4 | 1.7 | 1.8 | 1.6 | 1.6 |
| Al2O3 | % | 24.3 | 30 | 40.3 | 30.5 | 28.7 |
| SiO2 | % | 44.8 | 41.2 | 46.9 | 50.1 | 47.7 |
| Fe2O3 | % | 10.6 | 11.8 | 5.5 | 4 | 4.3 |
| CaO | % | 11.8 | 5.5 | 0.9 | 8.1 | 8.7 |
| MgO | % | 2.4 | 0.2 | 0.2 | 1.4 | 1.6 |
| Na20 | % | 0.01 | 0.01 | 0.01 | 0.01 | 0.01 |
| K20 | % | 0.3 | 0.4 | 0.7 | 0.6 | 0.5 |
| SO3 | % | 3.5 | 8.2 | 0.6 | 3.3 | 4.6 |
| MnO | % | 0.06 | 0.03 | 0.01 | 0.07 | 0.06 |
| | | | | | | |
| Total | % | 99.17 | 99.04 | 96.92 | 99.68 | 97.77 |
| | | | | | | |
| Dolomite Ratio | | 0.56551 | 0.31826 | 0.15048 | 0.67328 | 0.68167 |
| Fixed carbon/Volatile ratio | | 2.40594 | 2.24107 | 2.53604 | 2.15196 | 2.35238 |
| Ignition Assessment | | Poor Ign. | Good Ign. No slag | Poor Ign. | Good Ign. No slag | Poor Ign. |
| Fouling Index | | 0.110412766 | 0.100728395 | 0.05831573 | 0.104709246 | 0.098796154 |
| Fouling Assessment | | No Foul. | No Foul. | No Foul. | No Foul. | No Foul. |

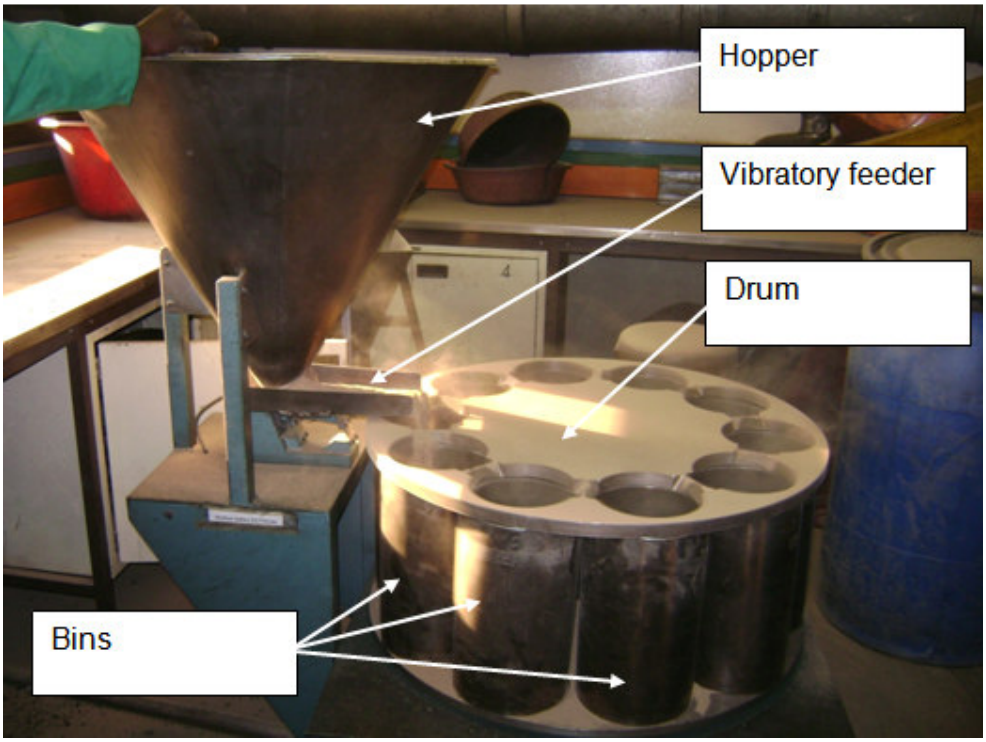


**Figure 4.3 The splitter used to mix or subdivide samples**

The procedure to split a fuel is as follows, a drum would be emptied into the hopper and the splitter would be allowed to run until the bins were full.

The fuel from five alternate bins would be emptied into one empty drum while the rest of the bins would be emptied into another drum. The splitter would be started again and the process of filling and emptying the bins would be repeated until all the fuel in the hopper is finished. At this stage the drum would have been split into two parts.

To mix two fuel samples, both samples would be emptied into the hopper and the splitter would be started. The splitter would be stopped at intervals to empty the bins. When the hopper became empty, the fuel which would have been collected from the bins would be put back into the hopper to repeat the mixing process. The fuel might be put back into the hopper two to three times to ensure thorough mixing.

To take a representative sample of the three drums of grass, the three drums had to be evenly mixed. This was done in three stages. Firstly, each drum was split into two parts. Secondly, the first three halves were mixed together (using the mixing procedure above) and the other three halves were also mixed together. Eventually the two parts (first halves and second halves) were mixed together. Three passes of the fuel through the splitter ensured that it was thoroughly mixed. During the last pass of the fuel, two diametrically opposite (to make the sample as representative as possible) bins were emptied in a plastic bag every time the bins filled. When all the grass fuel had gone through the last pass, the plastic bag contained a representative sample. A representative sample for sawdust was prepared in the same manner. When changing the fuel the splitter was thoroughly cleaned using compressed air and wiping the surfaces with acetone to avoid contamination.

Size grading was then carried out (section 4.1.3) on a representative sample of each biomass type and it was then milled to -212 µm (as required by Eskom coal laboratory) and split into two portions, one which was used for chemical analyses and the other for DTF tests. The DTF portion was further milled to -150 µm and dried at 60 ℃ in the vacuum oven. Coal was also milled to -150 µm and dried in a vacuum oven at 105 ℃ (as required by Eskom coal laboratory). Each of the biomass types was then mixed with coal in a batch process in order to prepare blended samples (about 500g) for the DTF according to the co-firing ratios indicated by Table 5.6.

### 4.1.3 Size Grading

Size grading was done by putting sieves of sizes 6mm, 4.75mm, 3mm, 1mm and 0.5 mm one on top of each other with the smallest at the bottom. A pan was placed at the bottom to collect the finest particles that would pass through all the sieves. About 5 kg of Sawdust or grass was

then placed in the top sieve. Top sieve was closed and the whole column of sieves was put into a mechanical shaker for about 30 minutes. The sample collected in each of the sieves was carefully collected and weighed. The sample collected in the 6mm sieve was recorded as having a diameter range of +6mm (see first column Table 4.3) which means it contained particles bigger than 6mm. The sample collected in the 4.75 mm sieve were recorded as having a diameter range of 4.75mm – 6mm because the sample had particles that were able to pass through a 6 mm sieve but could not pass through a 4.75 mm sieve. The diameter range of the sample collected in the rest of the sieves was recorded similarly.

Sieves 212 µm, 106 µm and 75 µm were also stacked together with the smallest sieve at the bottom. The sample that went through all the first 5 sieves (6mm-0.5mm) was placed in the top sieve (212 µm). The top sieve was closed and the stack of sieves were placed on a mechanical shaker for 45 minutes (more time was required as the sieve size decreases).

Table 4.3 Biomass size grading

| | SAWDUST | GRASS |
|---|---|---|
| Diameter Range | Mass Fraction in Range | Mass Fraction in Range |
| | | |
| +6 mm | 0.0 | 0.0 |
| 4.75 mm - 6 mm | 0.0 | 0.0 |
| 3 mm - 4.75 mm | 0.0 | 0.5 |
| 1 mm - 3 mm | 14.6 | 14.7 |
| 0.5 mm - 1 mm | 25.7 | 21.0 |
| 212 µm - 0.5 mm | 37.3 | 39.3 |
| 106 µm - 212 µm | 14.5 | 8.8 |
| 75 µm - 106 µm | 3.1 | 5.9 |
| -75 µm | 4.5 | 9.3 |
| | | |
| Total | 99.6 | 99.5 |

The sample collected in each of the sieves was weighed and recorded in Table 4.3 as already explained. The diameter range of particles that went through the last sieve (75 μm) was recorded as -75 μm. The two sets of sieves could not be stacked together all at once because their diameters were not equal.

## 4.2 Setting up the Pilot Scale Combustion Test Facility for Tests

### 4.2.1 Description of the Pilot Scale Combustion Test Facility

The Eskom Pilot Scale Combustion Test Facility (PSCTF) located at Rosherville in Johannesburg, consists of 1.2 x 1.2 x 6.7 m vertical radiative section (Figs. 4.5 and 4.7), 1.21 x 0.75 x 7.5 m horizontal water cooled convective section, and other support systems such as fuel preparation and handling system, air control system, cooling water system and ash removal system. PSCTF is a 1 $MW_{th}$ plant with down fired single low-$NO_X$ burner. The combustion test facility has been designed for three seconds residence time in the radiative section and five seconds in the convective section. It has multiple access ports for flame viewing, pyrometer measurements, fly ash sampling, slagging measurement and flue gas sampling. The PSCTF operates at 1200 ℃ – 1500 ℃ in the radiative section and 150 ℃ in the convective section. Gas species analysis include $O_2$, $CO_2$, CO, $SO_2$, NO, $N_2O$ and $NO_x$ (Reaction Engineering International, 1999).

The PSCTF burner consists of three concentric annular areas for passage of fuel and air into the furnace Fig. 4.6. The burner has a 50 mm central pipe around which there is an annular hollow section in which flows coal and primary air ushered in by the slanting pipe. The central pipe accommodates a diesel lance which is used for heating the furnace during start-up. The diesel lance is used to control the rate of heating (35℃ per

hour) to avoid the cracking of the ceramic material lining the furnace and also provides a pilot flame when coal is introduced into the furnace. Secondary air is channelled through guide vanes in order to have a swirling motion as it enters the annular area around the coal pipe (Fig. 4.6). Optional tertiary air can be supplied through tertiary pipe as shown in Fig 4.6. Tertiary air was not supplied for all the tests (11 – 18 and 1-4 Table 5.2) as secondary air was sufficient for air staging.

When the furnace is warm enough (815℃ or higher), coal is slowly introduced to the furnace until the full flow rate of coal is reached (Reaction Engineering International, 1999). At this stage the diesel lance in no longer required and the diesel flow can be stopped.

When co-firing tests were conducted, the diesel lance was removed to provide room for biomass feeding as shown in Figs. 4.4 and 4.5. Feeding

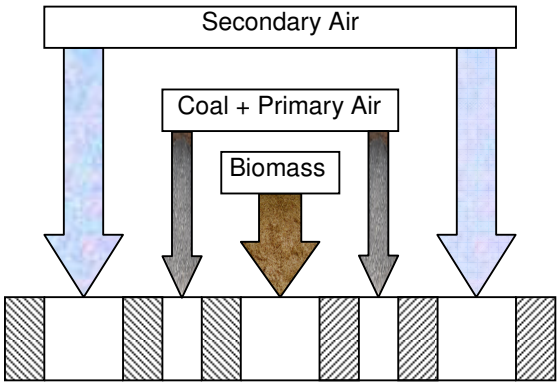


Figure 4.4 Fuel and air flows through the PSCTF low-NOX burner

biomass through the diesel lance pipe raised concerns about the flash-back due to its high reactivity. If the feeding velocity of biomass is lower than its burning velocity, flash-back would occur. To avoid this problem the furnace suction pressure was increased to a value that would be just enough to avoid flash-back because too much air entering through this

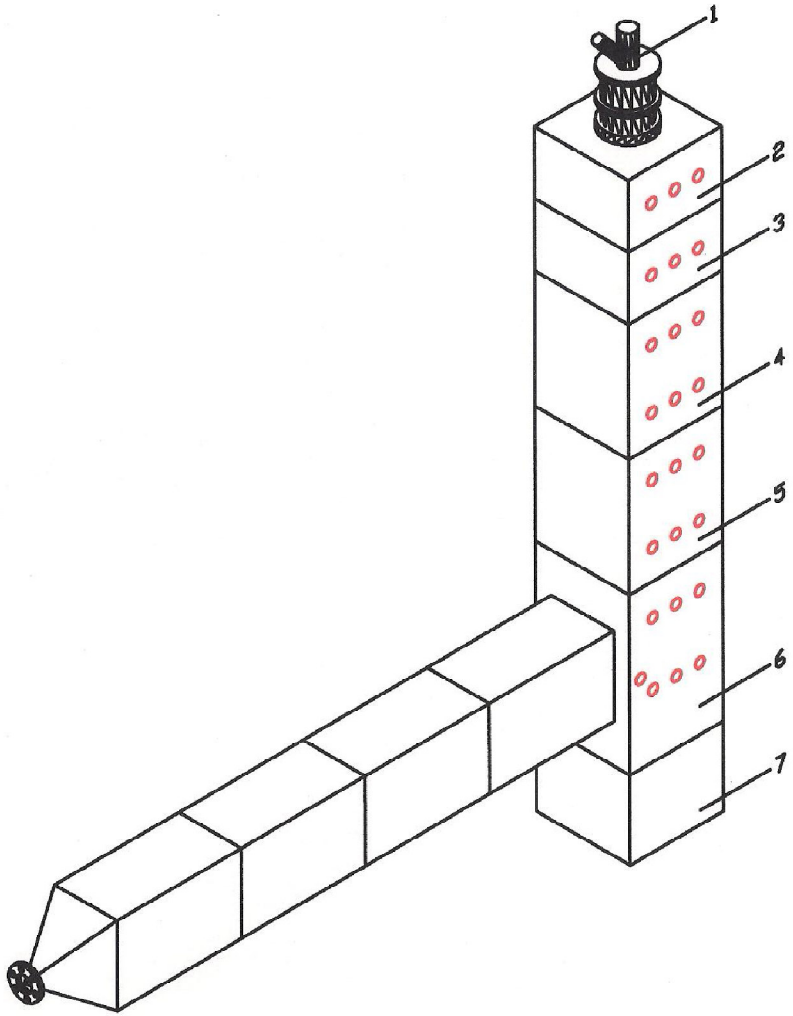


Figure 4.5 Eskom Pilot Scale Combustion Test Facility

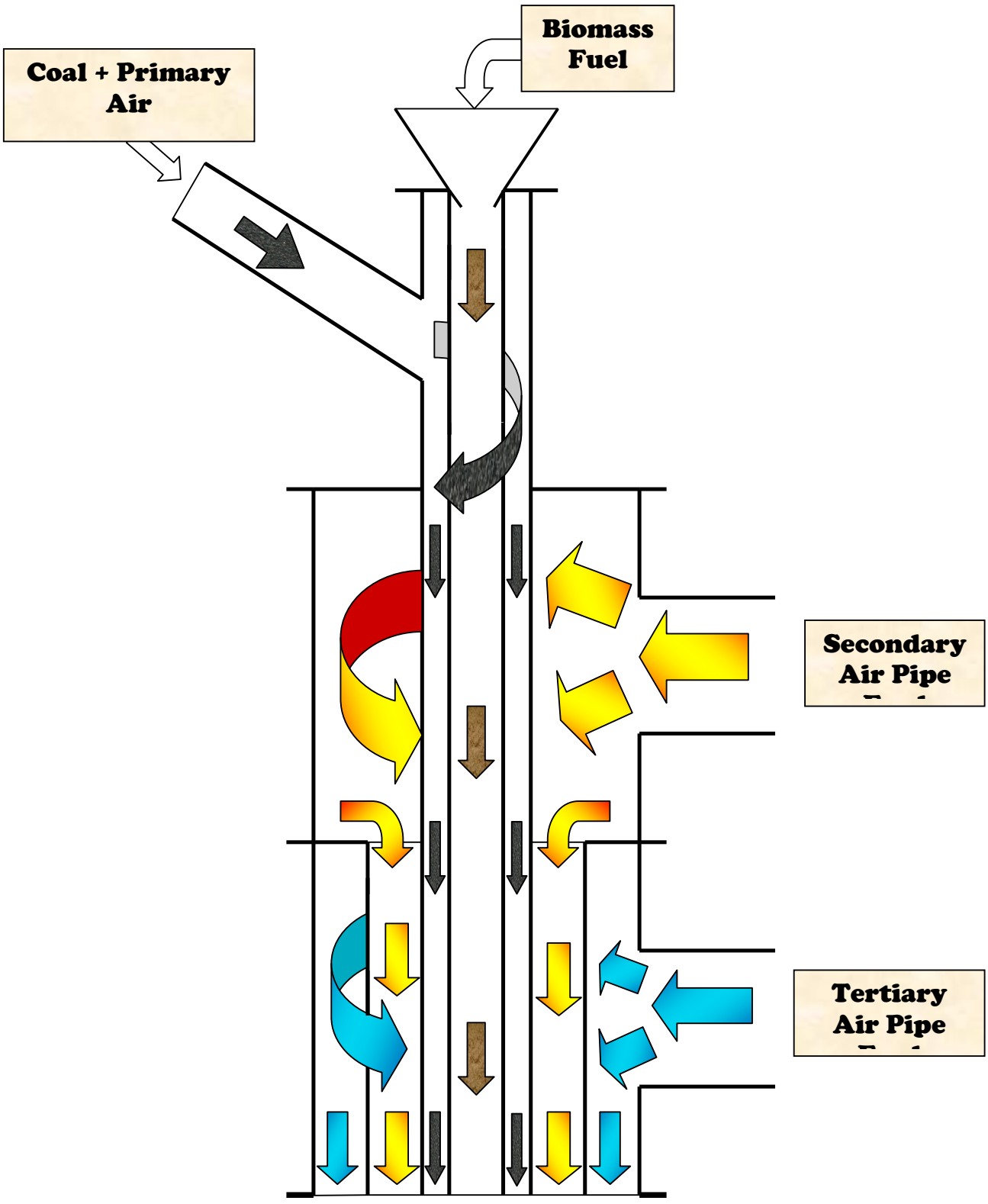


Figure 4.6 A Diagrammatic representation of the PSCTF burner

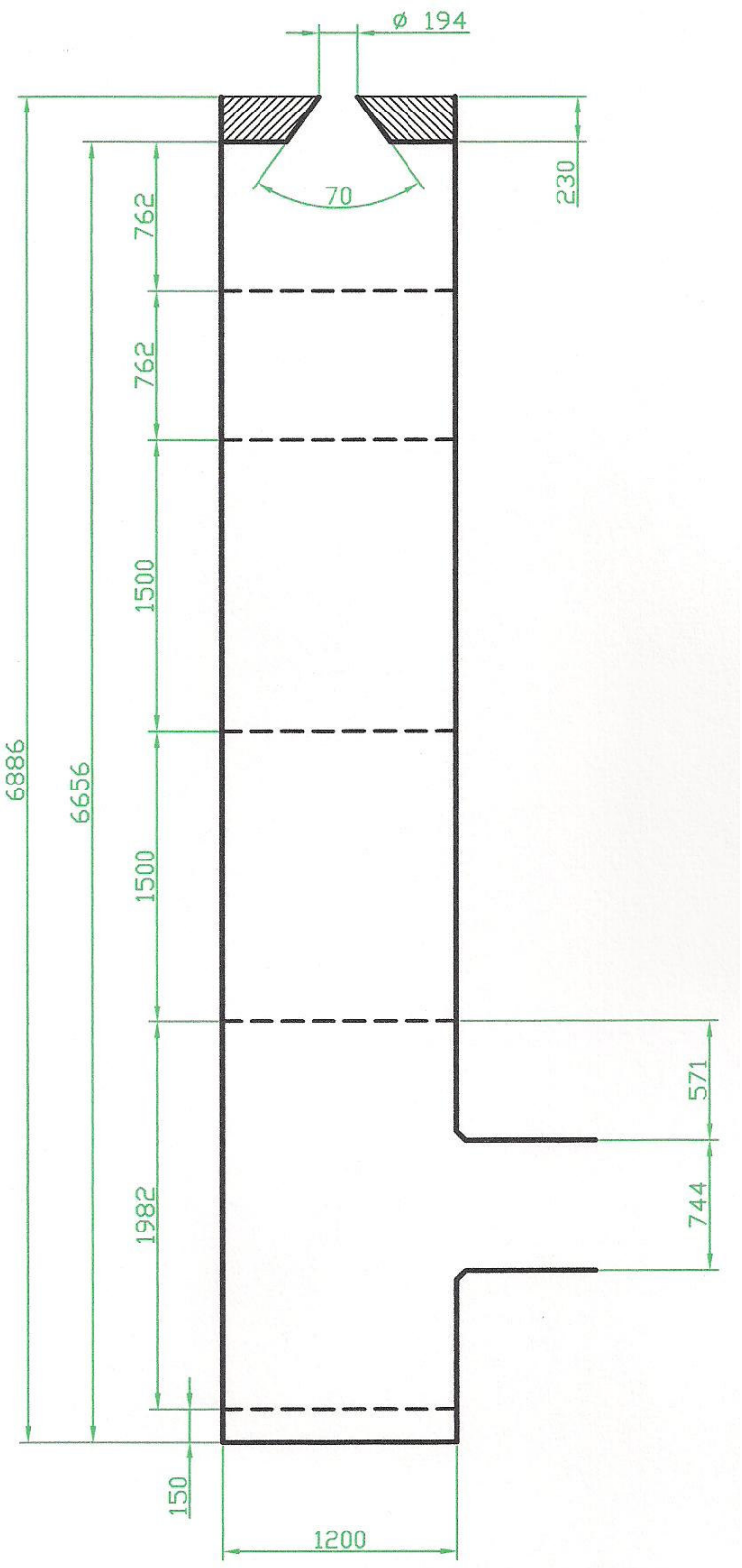


**Figure 4.7 Dimensions of the Eskom Pilot Scale Combustion Test Facility**

duct would disturb the air staging. Actually the biomass did flash back during the first co-firing test and the pressure was adjusted just enough to stop it. As the flow rate of biomass was increased for higher co-firing ratios, the furnace suction pressure was also increased. To make the conditions for testing uniform for all the tests, even the baseline test was done with the diesel lance removed.

### 4.2.2 Biomass Vibratory Feeder

The vibratory feeder used to feed biomass into the burner was purchased from Eriez Magnetics (S.A) company in Johannesburg. It consisted of Eriez Model 15 A vibratory feeder drive fitted and tuned to stainless steel feeder tray 400 mm long x 75 mm wide and controlled by a manually operated variable speed controller Model R5FC. Fig. 4.8 shows the vibratory feeder mounted on top of the PSCTF burner feeding biomass into the funnel fitted in the hole for diesel lance (removed). The funnel was made at the Lerotholi Polytechnic in Maseru, Lesotho.

This feeder was custom built for feeding milled sawdust and grass given the range of their bulk density (370 - 420 kg/m$^3$), moisture content (8-9% air-dried-basis), feed rate (20 – 50 kg/hr), particle size (150 μm) and the fact that it was not free flowing. Before running the tests, the vibratory feeder was calibrated for feeding grass and sawdust. This calibration was done by filling the hopper with 1.92 kg mass of sawdust or grass. The vibrator was then started and the fuel fed from its tray was collected and weighed. The stop watch was used to record the time it would take to empty the hopper. It was realised that if the same fuel sample was used over and over again its flow properties changed, so each sample was used once. Using the fuel sample once, would represent the actual feeding conditions in which the fuel flows continuously with one pass into the furnace.

A mass of 1.92 kg would take 5.7 minutes if it was flowing at 20.3 kg/hr (sawdust flow rate at 10% co-firing ratio). The setting on the vibrator was varied until it gave this value as nearly as possible. Once the setting was found, it was marked. Settings for 15% sawdust, 20% sawdust, 10% grass, 15% grass and 20% grass were similarly marked. For each of the marked settings, a number of tests were run to test the accuracy of the settings. The tests were carried out in the laboratory at University of the Witwatersrand and on top of the PSCTF when it was running other Eskom tests. It was found that the settings for grass were on the target value within 2%, 5% and 1% for the co-firing ratios of 10%, 15% and 20% respectively, while those of sawdust were within 5%, 4% and 4% for the co-firing ratios of 10%, 15% and 20% respectively. These tolerances were comparable to those of a coal weigh feeder which were 2%, 3%, 3%, 2%, 2%, 1%, 1% for test nos. 11,13 -18 (from average values of second and third column of Appendix A).

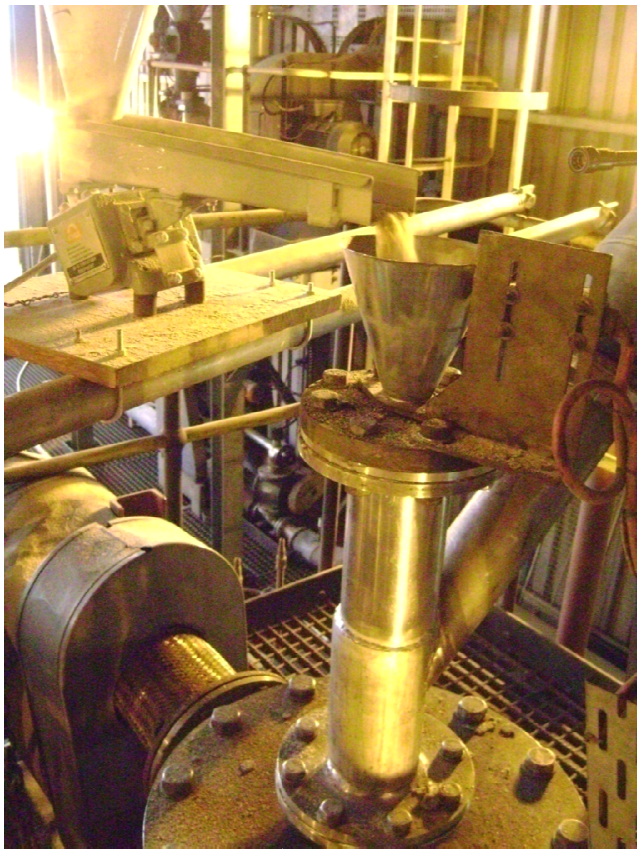

Figure 4.8 Feeding of biomass into the PSCTF burner using a vibratory feeder

### 4.2.3 Chemical and Physical Analyses

To set up a test on the Pilot Scale Combustion Test Facility, the fuel(s) to be tested were sent to the Eskom Coal Laboratory for chemical analyses. The report from the laboratory contained calorific value (CV), proximate analysis , ultimate analysis and ash elemental analysis (on air-dried basis) (Table 5.1).

Proximate analysis was done according to AMST 5142 Method. In this method, moisture, volatile matter and ash are determined sequentially in a single instrumental procedure by establishing the loss in mass of the analysis specimen when heated under rigidly controlled conditions of temperature, time, atmosphere and specimen mass. Ultimate analysis

(CHN only) was done according to AMST D5373 in which case carbon, hydrogen, and nitrogen were determined concurrently in a single instrumental procedure; while the ultimate analysis (Sulphur) was done according to ASTM 4239. In this method a test specimen is heated in a tube furnace in a stream of oxygen to oxidize the sulphur to sulphur dioxide. The gas stream containing the sulphur dioxide passes through a cell where it is measured at a precise wavelength by an infrared absorption detector. The ash elemental analysis was done using X–ray fluorescence technique.

The stoichiometric air to fuel ratio (kg of air per kg of fuel) was used together with calorific value and rated power of the plant (1 $MW_{th}$) to determine the stoichiometric air flow rate in kg/hr. The following sample calculation demonstrates the procedure followed to calculate stoichiometric air to fuel ratio and hence air flow requirements.

### 4.2.4 Sample Calculation of Air Flow requirements for Test 13 (Table 5.2)

The following combustion equations are used to determine the stoichiometric mass of oxygen required to burn carbon, hydrogen and sulphur.

$$C + O_2 \rightarrow CO_2 \qquad (4.1)$$

$\Rightarrow$ 12 kg of C react with 32 kg of $O_2$ to produce 44 kg of $CO_2$

$\Rightarrow$ 1 kg of C reacts with 2.67 of $O_2$ to produce 3.67 kg of $CO_2$

$$H_2 + 0.5O_2 \rightarrow H_2O \qquad (4.2)$$

$\Rightarrow$ 2 kg of $H_2$ react with 16 kg of $O_2$ to produce 18 kg of $H_2O$

$\Rightarrow$ 1 kg of $H_2$ reacts with 8 kg of $O_2$ to produce 9 kg of $H_2O$

$S + O_2 \rightarrow SO_2$ (4.3)

$\Rightarrow$ 32 kg of S reacts with 32 kg of $O_2$ to produce 64 kg of $SO_2$

$\Rightarrow$ 1 kg of S reacts with 1 kg of $O_2$ to produce 2 kg of $SO_2$

(Molecular masses of C = 12 kg/kmol, $O_2$ = 32 kg/kmol, $H_2$ = 2 kg/kmol and S = 32 kg/kmol, $CO_2$ = 44 kg/kmol, $H_2O$ = 18 kg/kmol, $SO_2$ = 64 kg/kmol).

To calculate the mass of air required to completely burn 1 kg of sawdust, the proximate and ultimate analyses are required. It is convenient to tabulate the figures (Table 4.4). Figures in column two are from the proximate and ultimate analysis of sawdust from Table 5.1. The last column of Table 4.4 calculates the amount of oxygen required to burn reactive constituents in the fuel using equations 4.1 – 4.3. The value corresponding to oxygen in the fuel has negative sign because it offsets the amount of total oxygen that would be required from air.

Table 4.4 Sample calculation for stoichiometric mass of air required to burn sawdust.

| Constituent | Mass of constituent in fuel (kg/kg fuel) | $O_2$ required to burn constituent (kg/kg fuel) |
|---|---|---|
| Carbon (C) | 0.4613 | 2.67 x 0.4613 = 1.2301 |
| Hydrogen ($H_2$) | 0.0449 | 8.0 x 0.0449 = 0.3592 |
| Oxygen ($O_2$) | 0.3561 | -0.3561 |
| Nitrogen ($N_2$) | 0.0309 | - |
| Sulphur (S) | 0.0004 | 1 x 0.004 = 0.004 |
| Carbonate ($CO_3$) | 0.0024 | - |
| Moisture | 0.0905 | - |
| Ash | 0.0135 | - |
| Total | 1 kg | 1.2372 |

Since air consists of 23.2% $O_2$ by mass, the stoichiometric air required is 1.2372/0.232 = 5.3 kg/kg fuel.

Mass flow rate of fuel is determined from thermal rating of the plant and the calorific value. For 10% sawdust co-firing ratio (energy basis), mass flow rate of sawdust alone such that it contributes to 10% of energy output is:

$$\dot{m}_{Sawdust} = \frac{(0.1) \times 1\ MW}{17.7\ MJ/kg} \times 3600 = 20\ kg/hr$$

$$Stoichiometric\ air\ flow\ rate\ (kg/hr) = (Fuel\ mass\ flow\ rate\ (kg\ /\ hr) \times stoichiometric\ air\ ratio\ (kg\ air/kg\ fuel)$$
$$= 20 \times 5.3 = 106\ kg/hr$$

A similar calculation is also required for coal. As previously done, chemical analysis of coal from Table 5.1 is entered into Table 4.5 to calculate the stoichiometric mass of air required to burn coal.

Table 4.5 Sample calculation for stoichiometric mass of air required to burn coal A.

| Constituent | Mass of constituent in fuel (kg/kg fuel) | $O_2$ required to burn constituent (kg/kg fuel) |
|---|---|---|
| Carbon (C) | 0.5528 | 2.67 x 0.5528 = 1.4741 |
| Hydrogen ($H_2$) | 0.0265 | 8.0 x 0.0265 = 0.2120 |
| Oxygen ($O_2$) | 0.0449 | -0.0449 |
| Nitrogen ($N_2$) | 0.0132 | - |
| Sulphur (S) | 0.0173 | 1 x 0.0173 = 0.0173 |
| Carbonate ($CO_3$) | 0.0333 | - |
| Moisture | 0.024 | - |
| Ash | 0.288 | - |
| Total | 1 kg | 1.6585 |

Since air consists of 23.2% $O_2$ by mass, the stoichiometric air required is 1.6585/0.232 = 7.1 kg/kg fuel.

Mass flow rate of fuel is determined from thermal rating of the plant and the calorific value. For 10% sawdust co-firing ratio (energy basis), mass flow rate of coal alone such that it contributes to 90% of energy output is:

$$\dot{m}_{coal\ A} = \frac{(0.9) \times 1\ MW}{21.25\ MJ/kg} \times 3600 = 152.5\ kg/hr$$

$$Stoichiometric\ air\ flow\ rate\ (kg/hr) = (Fuel\ mass\ flow\ rate\ (kg\ /\ hr) \times stoichiometric\ air\ ratio\ (kg\ air/kg\ fuel)$$

$$= 152.5 \times 7.1 = 1082.75\ kg/hr$$

Total stoichiometric air flow rate $= \dot{m}_{Sawdust} + \dot{m}_{coal\ A}$

= 106 + 1082.75 = 1188.75 kg/hr

Total air required for complete combustion = Total stoichiometric air flow rate x (1+%Excess air (see section 4.2.5)).

Total air required = 1188.75 x 1.4 = 1664 kg/hr.

Total air should be split between primary air and secondary air (low-NOX burners' principle) such that,

Total air = Primary air + Secondary air (4.4)

According to the design requirements of the PSCTF the ratio of primary air should lie between 2 and 3. A figure of 2.95 was chosen based on Eskom operators' experience:

$$\frac{Secondary\ air}{Primary} = 2.95 \quad (4.5)$$

Combining equation 4.4 and 4.5

Total air = Primary air (1+2.95)

$$Primary\ air = \frac{Total\ air}{3.95} = \frac{1543}{3.95} = 390.7\ kg/h$$

Secondary air = Total air – Primary = 1543 – 390.7 = 1152 kg/hr

The mass flow rate of Coal A, the primary and secondary air values were then entered on the PSCTF controller computer to control air flow into the furnace. The flow rate for biomass was controlled separately using a vibratory feeder (see section 4.2.2).

### 4.2.5 Excess Air

In practice, stoichiometric air to fuel ratio does not result in complete combustion due to fluctuations in fuel flow and lack of perfect mixing between fuel and air in the combustion zone, such that extra air called excess air is required to achieve complete combustion of the fuel. Whenever there is excess air there will be oxygen in the flue gas. Excess air itself cannot be measured directly but can be calculated (using equation 4.6) from the % oxygen (dry basis) in flue gas.

$$\%Excess\ Air\ = \frac{\%O_{dry}}{2.94 - \%O_{dry}} \qquad (4.6)$$

From the past experience by the Eskom operators, it has been established that the PSCTF correlated better with the commercial power stations when it is running at about 6% excess oxygen in the flue gas which from equation 4.6 above gives about 40% excess air.

### 4.2.6 Data Recording and Sampling

As the tests were running, the data about temperatures, and gaseous emissions were logged on the computer and could be later retrieved on a spreadsheet for analysis. Such spreadsheets are in Appendices A and E.

The operator also records on a sheet of paper for each test, the start and finish time and the relevant data for the purpose of extracting only the relevant data from the downloaded log sheet and also to counter-check the values. Appendices D and H contain such handwritten sheets that were filled in when the tests in this project were conducted.

Table 4.6 Sampling ports used, their distance from the burner mouth and the quantities sampled

| Sampling Port | Distance from the Burner Mouth [m] | Quantity Sampled |
|---|---|---|
| Port 4 | 0.40 | Gas temperature |
| Port 7 | 1.15 | Slag deposit |
| Port 9 | 1.15 | Fly ash |
| Port 10 | 1.15 | Gas temperature |
| Port D | 1.80 | Gas temperature |
| Port 15 | 2.65 | Fly ash |
| Port 21 | 3.45 | Fly ash |
| Port 27 | 4.90 | Gas temperature |

The PSCTF has a number of sampling ports throughout the length of the radiative and convective sections. For instance in Fig. 4.5, component nos. 2 and 3 each has 3 sampling ports while component nos. 4 and 5 each has 6 ports. Component 6 has 7 ports. Port 9 is at the centre of component no.3 and it is 1.15 m below the burner mouth. Table 4.6 shows the ports used to measure gas temperature and sample fly ash. The distance of each port from the burner mouth and what it was used for, are also shown. Fig. 4.9 shows a water cooled sampling probe for fly ash at port 9 and the slagging probe just before being inserted into the furnace through port 7.

Apart from the logged data, samples of fly ash were sampled at port 9, 15 and 21 and were sent to the Eskom Coal Laboratory for analysis of

combustible matter. The results from the laboratory were used for determining the combustion efficiency using equation 2.1. Data that are obtained from these ports appear in Appendices B and F.



Figure 4.9 Fly ash sampling at port 9 and slagging probe on the floor. The Slagging probe was used to take slag samples which were sent to Van Alphen Consultancy for detailed analysis.

## 4.3 Conducting Tests in the Drop Tube Furnace (DTF)

### 4.3.1 Description of the Drop Tube Furnace

The Eskom DTF has a heated area of Φ 70mm x 1320, heating rate of $10^5$ ℃/sec and a maximum residence time of 4 sec. The schematic of Eskom DTF is shown in Fig. 11 and its full scale photograph in Figs. 10 and 11. Raw fuel or char is fed through water cooled injection probe (Fig. 10) into the combustion chamber and the partially reacted sample is collected on

the water cooled sampling probe (Fig. 12). The main purpose of using the DTF was to determine the reaction kinetics of coal and its biomass blends for the seven tests that were conducted in the DTF (Table 5.6). These kinetics were used when running computer simulations of the tests conducted on the PSCTF.

### 4.3.2 Procedure for running tests in the DTF

Reaction kinetics is a measure of char reactivity. Before running tests that would determine reaction kinetics, char samples have to be prepared from the raw fuels. When preparing char, a fuel (150 µm top size) is fed through a 2-mm diameter injection probe into the electrically heated combustion chamber maintained at the temperature of about 1400℃. In the combustion chamber, the feed fuel is subjected to pyrolysis under nitrogen atmosphere for about 1.8 seconds to produce char.

When running combustion tests to determine reaction kinetics, char samples from the same blend are fed through a 1-mm diameter injection probe into the combustion chamber maintained in turn at 1000 ℃, 1200 ℃ and 1400 ℃. At each temperature setting, there are predefined positions at which the sampling probe can be positioned in order to capture the char reaction history for that temperature as the particles pass through the combustion chamber. For 1000℃, position P1 and P3 are used and at the temperatures of 1200 ℃ and 1400 ℃ positions P1, P3 and P5 (see Fig. 4.13) are used. Since reaction is expected to be faster as temperature increases, there are more positions at 1200 ℃ and 1400 ℃ than at 1000 ℃. For each position at different temperatures, samples of combustible residue is collected and analysed for unburned carbon.

For the tests conducted at the DTF, each sample was around 500g. About 200 g of char was prepared by feeding each of the samples at about 1g per minute at the temperature of 1400 ℃. The collected char as well as raw fuels were sent to the Eskom Coal Laboratory for proximate, ultimate

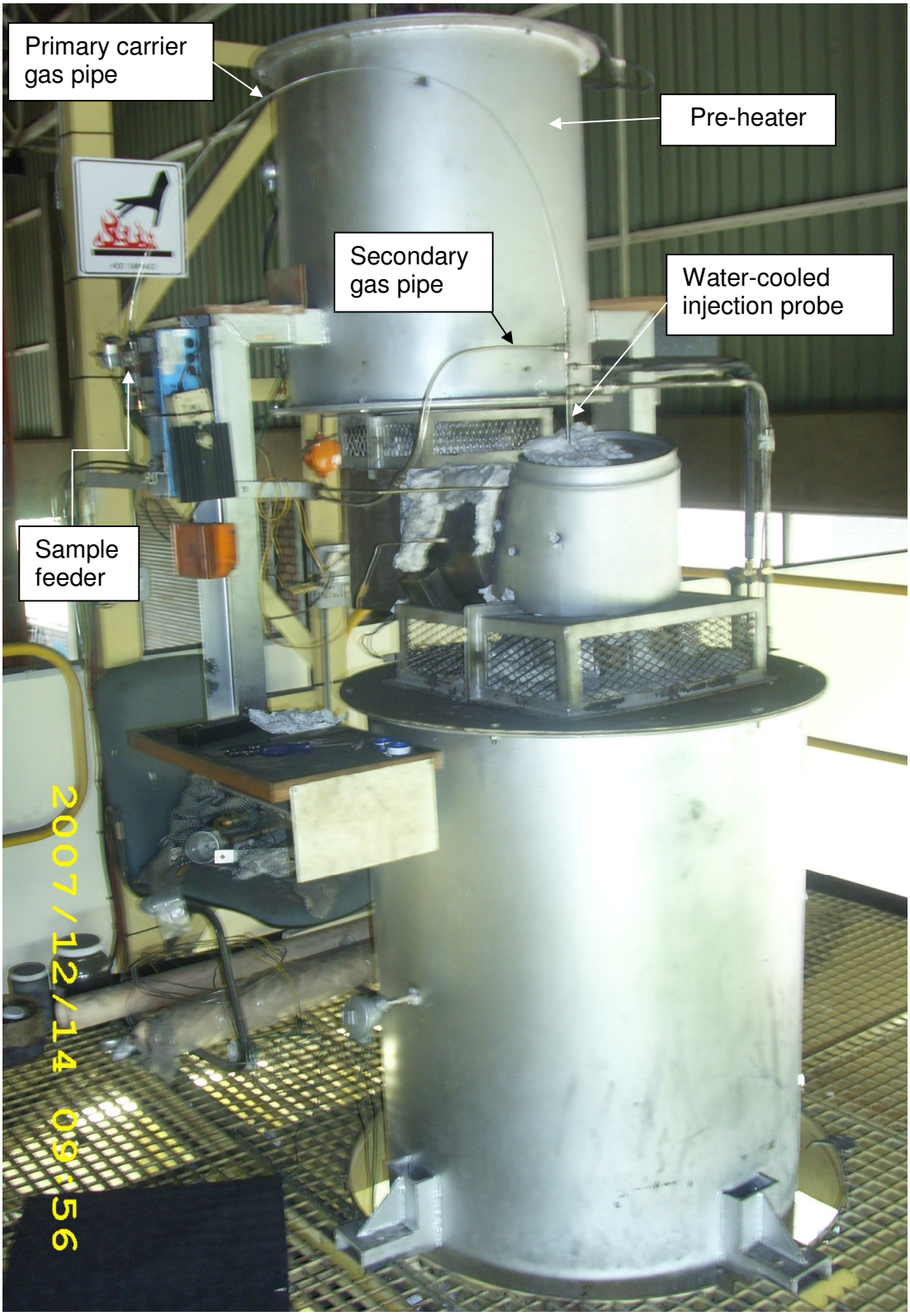


Figure 4.10 Eskom DTF top half showing pre-heater and water cooled injection probe.

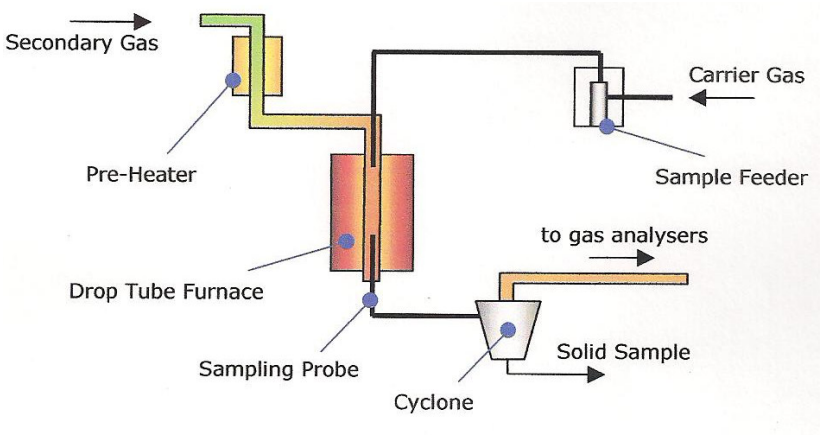


Figure 4.11 Eskom Drop Tube Furnace Schematic (source: Eskom Fuel and Combustion Technology Brochure, 2005)




Figure 4.12 Eskom DTF Showing bottom-half with water cooled sampling probe

and calorific value analyses. Char samples were also analysed for density measurement and average particle diameter (Table 5.12).

Each of the chars were burned in turn at the rate of 0.1 g/min and the combustible residue was collected for each position of the sampling probe. The samples were sent Eskom Coal Laboratory for analysis of the unburned carbon in the residue. These results together with char ash content (from char proximate analysis Table 5.9) were used to calculate combustion efficiency using the modified ash tracer method (see section 4.3.5).

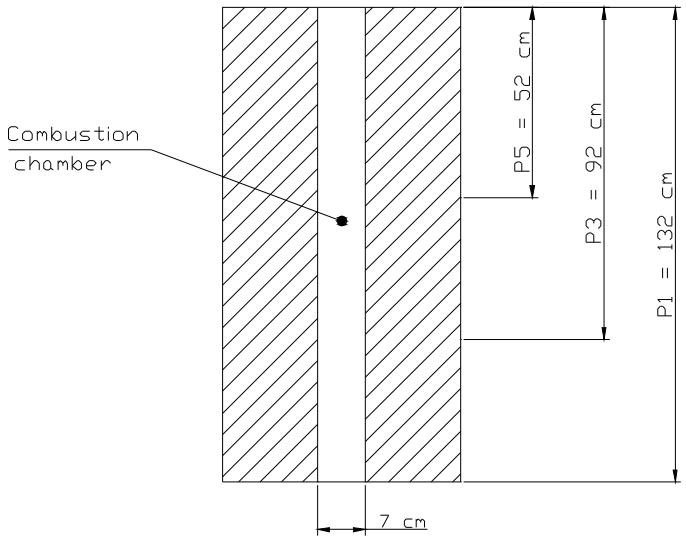


Figure 4.13 Sampling probe positions from the DTF combustion chamber entry.

Before doing experiments calibration data (Table 4.7) for gas temperatures and wall temperatures must be available. They are required as input data into the DTF program. This program was written by Mark Van der Riet and Mike Smoog for Eskom in 1990. The Drop Tube Furnace (DTF) kinetic theory on which the program is based was compiled by Mark Van der Riet.

Table 4.7 Gas temperature and wall temperature calibration data for DTF

| Set Temp. / Probe Position | 1000 °C | 1200 °C | 1400 °C |
|---|---|---|---|
| | Gas Temperature Profile [°C] | | |
| P1 | 876 | 1095 | 1303 |
| P3 | 976 | 1186 | 1399 |
| P5 | 982 | 1183 | 1397 |
| | DTF Wall Temperature Profile [°C] | | |
| P1 | 902 | 1114 | 1314 |
| P3 | 1005 | 1201 | 1411 |
| P5 | 1011 | 1203 | 1409 |

When all the data are available, they are fed into the DTF program especially written for calculating the activation energy [kJ/mol] and the pre-exponential factor [kg/m$^2$/s/atm] to determine the reaction kinetics. The printout of that program for the seven tests conducted is shown in Appendix I. It was discovered by the author that the program is giving incorrect calculations. The program source code was then requested, so that the error could be traced and corrected. It was then found out that there were two errors in the code that were responsible for the incorrect calculations. The calculation for **Surface Area,** was written as $6/X\rho_c$ instead of $6(1-B)/X\rho_c$ (Field, 1970) where X is particle diameter and $\rho_c$ is the char density (DAF). In the calculation for **Diffusional Reaction Rate Coefficient** also, the value of universal gas constant had been entered incorrectly, it appears as 585 instead of 5.85 x $10^5$. The program was then implemented using the spreadsheet (Appendix J) with corrections effected and different kinetics were obtained (Appendix J). See sample calculation in section 4.3.4. This spreadsheet was shared with Eskom as the first step towards solving this problem.

The reaction kinetics were determined from a log-log plot of particle temperature $T_p$ and surface reaction rate $K_s$ which gave a linear relationship. Activation energy E = slope of the line x universal gas constant (R) and the pre-exponential factor A = exp(y-intercept of the line).

### 4.3.3 Determination of Reaction Kinetics

The rate of char reaction can be expressed in terms of Arrhenius equation

$$K_s = Ae^{\left(\frac{-E}{RT_P}\right)} \quad (4.7)$$

where $K_s$ = surface reaction rate coefficient ($kg.m^{-2}.s^{-1}.atm^{-1}$)

A = frequency factor ($kg.m^{-2}.s^{-1}.atm^{-1}$)

E = activation energy ($J\ mol^{-1}$)

R = universal gas constant ($8.31441\ J.mol^{-1}.K^{-1}$)

$T_p$ = particle temperature (K).

Taking natural logarithm on both sides of equation 4.7 we get

$$ln\ K_s = -\left(\frac{E}{R}\right) \times \frac{1}{T_p} + \ln(A) \quad (4.8)$$

It can be seen from Equation 4.8 that a plot of ln $K_s$ vs $1/T_P$ will be a straight line whose slope is E/R and the y-intercept is ln A. Activation energy E = slope of the line x universal gas constant (R) and the pre-exponential factor A = exp(y-intercept of the line).

To plot this graph, $K_s$ and $T_p$ values need to be calculated for each of the sampling probe positions P5, P3 and P1 at each temperature settings.

Particle diameter (X) and particle density ($\rho_c$) are used to calculate initial surface of reaction $S_0 = 6(1-B)/X\rho_c$ (Field et al, 1970). This surface area can then be used to calculate rate of carbon removal per unit surface area q using $q = 3(1-U^{0.33})/S_0t$ (Field et al, 1970). Value of q is used to calculate

overall reaction rate coefficient $K_o = q/P_g$ from which $K_s$ can be calculated using $K_s = K_o K_{diff}/(K_{diff} - K_o)$ (Field et al, 1970).

Note that q is undefined when B = 1. The corrected ash tracer method (eqn (4.10)) sometimes gives values greater or equal to hundred. To avoid this problem, whenever the corrected efficiency is hundred or more, the ash tracer method without correction (eqn (2.7)) is used.

Particle temperature is found by considering equilibrium heat balance i.e. heat gained by the particle = heat lost by the particle. Heat gained by the combusting particle $H_g$ = 9791 000 q, where q is the rate of carbon removal per unit surface area which would have been already found above. The sum of Heat lost by radiation $H_r = \varepsilon\sigma(T_P^4 - T_w^4)$ and by conduction $H_c = 2\lambda(T_p - T_g)/X$ is equal to heat gained such that :

$$9791000\ q - \frac{2\lambda(T_P - T_g)}{X} - \varepsilon\sigma(T_p^4 - T_w^4) = 0 \qquad (4.9)$$

$T_p$ can be found from this equation through an iterative solution.

Once all the eight pairs of data are calculated per test, regression analysis is applied to ln $K_s$ and $1/T_p$ to find activation energy and the pre-exponential factor A (See Summary of the Kinetic Reactions Data, Appendix J, pageJ-15).

### 4.3.4 Sample Calculation of Kinetics for 15% Grass (See Appendix J, page L-14 for comparison).

Appendix J contains information and results of calculations used to determine reaction kinetics for all the seven tests carried out at the DTF. A sample calculation is given in this section to show how those figures were arrived at.

**Calculation of the Surface Reaction Rate Coefficient ($K_s$)**

| | |
|---|---|
| Gas temperature set point | 1000 K |
| Actual gas temperature | 976 ℃ (Table 4.7) |
| Probe position | 0.92 m |
| Char ash (dry basis) | 42.07 % |
| Particle density ($\rho_c$) | 1720 kg/m$^3$ |
| Particle diameter (X) | 2.67 x 10$^{-5}$ m |
| Nitrogen flow rate | 0.02001 m$^3$/s |
| Universal gas constant (R) | 8.20562 x 10$^{-5}$ m$^3$.atm/mol K |

Combustion efficiency = 78.766 % From Table 5.11

B = combustion efficiency (%)/100 = 0.78766

Initial surface area $S_0 = \frac{6(1-B)}{X\rho_c}(Field, 1970)$

$$= \frac{6(1-0.78766)}{2.67\times10^{-5}(1720)} = 27.74\ m^2/kg$$

Rate of carbon removal $q = \frac{3(1-U^{0.3333})}{S_0 t}$

U = 1-B = 1- 0.78766 = 0.21234

t = residence time = 2.247 (see **Calculation of Residence Time** below)

$$\therefore q = \frac{3(1-U^{0.33})}{S_0 t} = \frac{3(1-0.21234^{0.0333}}{27.74(2.247)} = 0.01942\ kg/m^2.s$$

Overall reaction coefficient $K_o = \frac{q}{P_g}$

$P_g$ = partial pressure of oxygen in the gas

= (%vol. /100) x atmospheric pressure (atm)

= 0.03 x 1 = 0.03 atm

$$\therefore K_o = \frac{q}{P_g} = \frac{0.01942}{0.03} = 0.6473\ \ kg/m^2.s.atm$$

Surface reaction rate coefficient $K_s = \frac{K_o K_{diff}}{K_{diff} - K_o}$

Diffusional reaction rate coefficient $K_{diff} = \frac{24\phi D}{XRT_g}$

$T_g$ = gas temperature = 976+273.2 = 1249.2 K (see Table 4.7)

$\phi$ = stoichiometric ratio of carbon to oxygen = 2

D = Diffussion coefficient = $D(T_0,P_0).(T_g/T_0)^{1.75}.(P_0/P)$ (Van der Riet, 1998)

$= 2.17 \times 10^{-4}(1200^{-1.75})( 1249.2)^{1.75}$ (1/1)

$= 2.32825 \times 10^{-4}$ $m^2/s$

$$\therefore K_{diff} = \frac{24\phi D}{XRT_g} = \frac{24(2)(2.32825 \times 10^{-4})}{2.67 \times 10^{-5}(8.20562 \times 10^{-5})(1249.2)}$$

$$= 4083.3\ kg/m^2\ .s.atm$$

$$\therefore K_s = \frac{K_o K_{diff}}{K_{diff} - K_o} = \frac{(0.6471)(4083.3)}{(4083.3 - 0.6471)} = 0.6472\ kg/m^2\ .s.atm$$

**Calculating particle temperature $T_P$**

Heat gain by combusting particle is given by

$H_g$ = 9791000 x q = 9791000 x 0.01942 = 190141.22 J/m.s

Heat loss by conduction

$$H_c = \frac{2\ \lambda\ (T_P - T_g)}{X} = \frac{2(0.078755)(T_P - 1249.2)}{2.67 \times 10^{-5}}$$

$$= 5899.3T_p - 7.37 \times 10^6$$

Heat loss by radiation

$H_r = \varepsilon\sigma(T_P^4 - T_W^4)$

Emissivity of surface ε =0.9 (see Table 3.4),

Stefan-Boltzman constant σ = 5.67 x $10^{-8}$ $J/m^2.s.K^4$

Local DTF temperature $T_w$ = 1005+273.2 = 1278.2 K

$$H_r = (0.9)(5.67 \times 10^{-8})(T_P^4 - 1278.2^4) = 5.103 \times 10^{-8} T_P^4 - 1.362 \times 10^5$$

From equation 4.9

$$190\,141.22 - 5.103 \times 10^{-8} T_P^4 + 1.362 \times 10^5 - 5899.3 T_p + 7.37 \times 10^6 = 0$$

$$-5.67 \times 10^{-8} T_P^4 - 5899.3 T_p + 7.71 \times 10^6 = 0$$

Table 4.8 Temperature and surface reaction rate coefficient values for 15% grass

| Temperature[K] | $K_s$[kg/m$^2$s atm] | ln($K_s$) | ln(1/T) |
|---|---|---|---|
| 1281.20 | 0.64721 | -0.4350915 | 7.81E-04 |
| 1235.75 | 1.70308 | 0.5324387 | 8.09E-04 |
| 1531.63 | 1.83965 | 0.6095768 | 6.53E-04 |
| 2100.87 | 17.17977 | 2.8437324 | 4.76E-04 |
| 2924.60 | 46.11105 | 3.8310525 | 3.42E-04 |
| 1759.24 | 2.51822 | 0.9235531 | 5.68E-04 |
| 1974.32 | 8.87896 | 2.1836850 | 5.07E-04 |
| 2106.56 | 15.14088 | 2.7173982 | 4.75E-04 |

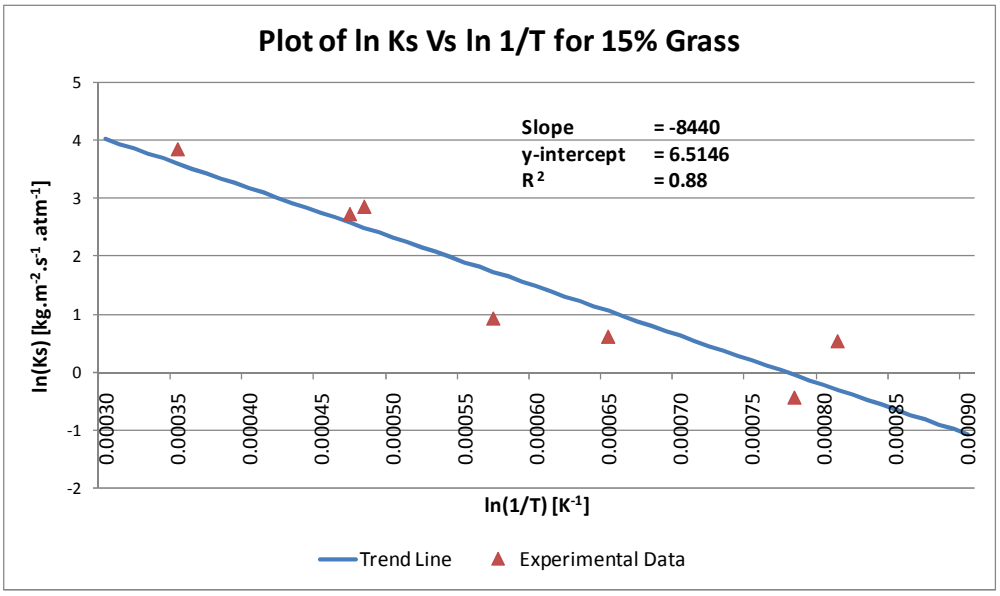


Figure 4.14 Best fitting line drawn through DTF experimentally derived data points.

What-if-analysis tool (Goal Seek) from "Data" menu of Microsoft Excel 2007 was used to get the solution to eqn (4.9) and the answer was 1281 K. Therefore for 15% grass $K_s$ = 0.6472 kg/m$^2$ s atm and T = 1281 K. A similar set of results can be found for the rest of probe positions for 15% grass. Such values are reproduced in Table 4.8 form Appendix J for ease of reference.

When ln($K_s$) is plotted against ln(1/T) and the best line is fitted through the data, the slope and y-intercept can be found (Fig.4.14). Activation energy E = slope x universal gas constant = -(-8440) x 8.31441 = 70 174 J/mol and the pre-exponential factor A = exp(y-intercept) = exp(6.514604) = 694.93 kg/m$^2$ s atm.

**Calculating Residence Time** (Van der Riet, 1998)

$$t = \sum_{i=1}^{n} \frac{L_i}{v_g + v_p}$$

where $L_i$ = length of slice (i)

n = number of slices

$v_g$ = linear velocity of gas (m/s)

$v_p$ = free fall velocity in gas (m/s)

The combustion chamber has been divided into slices because the velocities are not constant throughout. It has been divided into 3 slices which conveniently coincide with the probe positions since gas temperatures at these positions are known from the calibration values (see Table 4.7). These gas temperature values are used to calculate $v_p$ and $v_g$.

For example the residence time for:

15% grass at 1000 ℃ is

$$t_{at\ P3} = \frac{0.92}{0.3963 + 0.01316} = 2.2469\ s$$

$$t_{at\ P1} = \frac{0.92}{0.3963 + 0.01316} + \frac{1.32 - 0.92}{0.3645 + 0.01398} = 3.304\ s.$$

For 15% grass at 1200 ℃, the residence time is

$$t_{at\ P1} = \frac{0.52}{0.4619 + 0.01177} + \frac{0.92 - 0.52}{0.4629 + 0.01175} + \frac{1.32 - 0.92}{0.4340 + 0.01231}$$

$$= \frac{0.52}{0.4619 + 0.01177} + \frac{0.4}{0.4629 + 0.01175} + \frac{0.4}{0.4340 + 0.01231}$$

$$= 2.837\ s$$

This is how the residence times in Appendix J were calculated.

### 4.3.5 Calculation of Combustion Efficiency

The combustion efficiencies were calculated using the corrected ash tracer method as shown below:

$$\eta_c = \left[1 - \frac{A_0}{100 - A_0} \times \frac{100 - A_i}{A_i}\right] \times 100 \times 1.031 + 1.7 \qquad (4.10)$$

Where $A_0$ = ash content of the feed fuel (char) on dry basis and

$A_i$ = ash content of combustible residue on dry basis.

The factors 1.031 and 1.7 were empirically derived by Scaroni et al, (1981) and were intended to account for ash changes during combustion. If the corrected combustion efficiency exceeds 100%, it is capped at 100%.

**Sample Calculation for coal A at 1000 ℃ and P1**

Ash content char $A_0$ = 42.4/(100-0.2) = 42.5%

Note 0.2 is the moisture content of coal A from Table 5.9.

Ash content of combustible matter $A_i$ = 100 – U = 100 – 15.4

= 84.6 % (U is from Table 5.10).

Using eqn (4.10), combustion efficiency is therefore

$$\eta_c = \left[1 - \frac{42.5}{100 - 42.5} \times \frac{100 - 84.6}{84.6}\right] \times 100 \times 1.031 + 1.7 = 90.9\%$$

# 5 RESULTS

## 5.1 Chemical Analysis Results

Table 5.1 Chemical and Physical Properties of Fuels and Ashes (Air-dried basis)

| PROXIMATE ANALYSES | | COAL A | COAL B | SAWDUST | GRASS |
|---|---|---|---|---|---|
| Volatile Matter | % | 20.2 | 19.6 | 72.3 | 71.2 |
| Fixed Carbon | % | 48.6 | 47.5 | 17.3 | 14.55 |
| Ash | % | 28.8 | 30.3 | 1.35 | 6.35 |
| Moisture | % | 2.4 | 2.6 | 9.05 | 7.9 |
| ULTIMATE ANALYSES | | | | | |
| Carbon | % | 55.28 | 55.91 | 46.13 | 43.73 |
| Hydrogen | % | 2.65 | 2.73 | 4.49 | 4.27 |
| Oxygen | % | 4.49 | 5.44 | 35.61 | 37.07 |
| Nitrogen | % | 1.32 | 1.16 | 3.09 | 0.35 |
| Sulphur | % | 1.73 | 0.88 | 0.04 | 0.09 |
| Carbonates | % | 3.33 | 0.98 | 0.24 | 0.24 |
| GROSS CALORIFIC VALUE | MJ/kg | 21.25 | 21.7 | 17.7 | 16.7 |
| NET CALORIFIC VALUE | MJ/kg | 20.61 | 20.61 | 16.5 | 15.5 |
| BULK DENSITY | kg/m3 | 1300 | 1300 | 400 | 350 |
| ASH ANALYSES | | | | | |
| Ti02 | % | 1.40 | 1.80 | 39.60 | 0.02 |
| Al2O3 | % | 24.30 | 26.00 | 4.40 | 0.70 |
| SiO2 | % | 44.80 | 60.80 | 15.20 | 81.70 |
| Fe2O3 | % | 10.60 | 3.40 | 8.20 | 0.84 |
| CaO | % | 11.80 | 1.40 | 19.20 | 3.51 |
| MgO | % | 2.40 | 0.70 | 0.62 | 2.10 |
| Na20 | % | 0.01 | 0.10 | 1.10 | 0.10 |
| K20 | % | 0.30 | 0.20 | 4.50 | 6.87 |
| SO3 | % | 3.50 | 1.70 | 2.97 | 1.21 |
| MnO | % | 0.06 | 0.70 | 1.27 | 0.13 |
| P2O5 | % | 0.83 | 0.08 | 1.58 | 1.19 |
| Cl | % | - | - | 0.03 | <0.01 |
| Fuel Ratio (FC/VM) | | 2.410 | 2.42 | 0.25 | 0.20 |
| Molar Ratio H/C | | 0.580 | 0.59 | 1.43 | 1.41 |
| Iron and Calcium | | 22.40 | 4.800 | 27.40 | 4.35 |
| Fouling Index | | 0.110 | 0.020 | 3.18 | 1.135 |
| ASH FUSION TEMPERATURES | | | | | |
| Deformation Temperature | ˚C | 1310 | 1550 | 1250 | 1380 |
| Softening Temperature | ˚C | 1320 | 1550 | 1280 | 1390 |
| Hemisphere Temperature | ˚C | 1330 | 1550 | 1300 | 1410 |
| Flow Temperature | ˚C | 1340 | 1550 | 1330 | 1430 |

A representative sample (see section 4.12) of each of the fuels was sent to Eskom Coal Laboratory at Rosherville for chemical and physical analyses (see section 4.2.3). Data in Table 5.1 were used to calculate air and fuel flow requirements for the tests on the Pilot Scale Combustion Test Facility (PSCTF). Sample calculation for air flow rates is given in section 4.2.3. The data were also used in the simulation of the combustion process (Section 3.9.1 and 3.10). Coal A and B are two different samples of the same coal (see section 5.2 for details).

## 5.2 Results From The Pilot Scale Combustion Test Facility

Table 5.2 Co-firing tests done on the PSCTF

| Test (Eskom No.) | Date | Fuel blend | Biomass to Coal Ratio (on Energy Basis) |
|---|---|---|---|
| 11 | 26/09/2007 | Coal alone (baseline coal A) | 0%:100% |
| 13 | 26/09/2007 | Sawdust and coal | 10%:90% |
| 14 | 26/09/2007 | Sawdust and coal | 15%:85% |
| 15 | 26/09/2007 | Sawdust and coal | 20%:80% |
| 16 | 26/09/2007 | Grass and coal | 10%:90% |
| 17 | 26/09/2007 | Grass and coal | 15%:85% |
| 18 | 26/09/2007 | Grass and coal | 20%:80% |
| Repeat tests | | | |
| 1 | 08/08/2008 | Coal alone (baseline coal B) | 0%:100% |
| 2 | 08/08/2008 | Sawdust and coal | 10%:90% |
| 3 | 08/08/2008 | Sawdust and coal | 15%:85% |
| 4 | 08/08/2008 | Sawdust and coal | 20%:80% |

The first seven tests (nos. 11-18) in Table 5.2 were carried out on the Pilot Scale Combustion Test Facility (PSCTF) (The ratio of biomass to coal is written throughout this report in short for better presentation. For example 10% biomass is short for 10% Biomass:90% Coal). These tests were all carried out as planned, but the results obtained from the PSCTF tests (Table 5.3) using mixtures of sawdust with coal (nos. 13 - 15 above) appeared to be questionable (see section 6.1.3). It was agreed that these

three sawdust tests should be repeated using the PSCTF. A difficulty in doing so was that the original coal had been used up and so a new batch of coal had to be used. This necessitated a new coal-alone (baseline) test, as well as the necessary coal analysis and preparation, and so four new tests (Table 5.2 test nos. 1 – 4) were carried out, results of which are shown in Table 5.4.

Unfortunately the results from these additional tests are not comparable with those of the original tests because the air-flow operating conditions were different. In the original tests the primary and secondary air flows were adjusted for each test, according to calculations, to account for extra air admission. This was done in accordance with the principle of operation of the low-$NO_x$ burner, with a rich fuel zone in the primary combustion flame area. In the additional tests the Eskom operator instead attempted to maintain an excess oxygen figure of 6% in the flue gas (in fact the excess oxygen decreased as the co-firing ratio was increased, Table 5.4). This in turn gave rise to increasing gas temperatures, resulting in progressive increases in the gaseous emissions from test to test (rather than the temperature and emission reductions as observed in the original tests). For this reason, the results from the additional tests can not be used to check the original tests as the tests were not run under the same conditions. Since these additional tests were not comparable, the conclusions drawn in this thesis with respect to sawdust are based largely on the original tests, nos. 13 - 15.

Table 5.3 Summary of the data obtained from the Pilot Scale Combustion Test Facility using the original coal sample (coal A).

| Measured Quantities | Residence Time to Reach Port [s] | Units | Test 11 Baseline | Test 13 10% Sawdust | Test 14 15% Sawdust | Test 15 20% Sawdust | Test 16 10% Grass | Test 17 15% Grass | Test 18 20% Grass |
|---|---|---|---|---|---|---|---|---|---|
| Furnace Pressure | | Pa | -77 | -94 | -130 | -307 | -349 | -381 | -289 |
| Gas Temp Port 4 | 0.254 | K | 1604 | 1563 | 1585 | 1279 | 1429 | 1397 | 1383 |
| Gas Temp Port 10 | 0.730 | K | 1648 | 1608 | 1646 | 1345 | 1592 | 1585 | 1570 |
| Gas Temp Port D | 1.142 | K | 1548 | 1504 | 1524 | 1226 | 1444 | 1440 | 1438 |
| Gas Temp Port 28 | 3.109 | K | 1387 | 1349 | 1382 | 1094 | 1345 | 1349 | 1339 |
| Average gas Temperature | | K | 1547 | 1506 | 1534 | 1236 | 1453 | 1443 | 1433 |
| Average Wall Temperature | | K | 1329 | 1330 | 1328 | 1049 | 1310 | 1301 | 1298 |
| Covective Exit Temperature | | K | 475 | 484 | 496 | 240 | 516 | 522 | 518 |
| Oxygen (Ziconia) wet basis | | % | 5.29 | 7.06 | 5.10 | 7.44 | 8.06 | 8.71 | 9.18 |
| Oxygen (dry basis) | | % | 4.80 | 6.61 | 5.06 | 7.27 | 7.49 | 8.13 | 8.35 |
| Carbon Monoxide | | ppm | 82 | 33 | 44 | 38 | 41 | 32 | 25 |
| CO2 | | % | 14.23 | 12.48 | 14.01 | 11.85 | 11.67 | 11.04 | 10.91 |
| SO2 | | ppm | 628 | 729 | 721 | 581 | 497 | 445 | 453 |
| NO | | ppm | 1210 | 1059 | 1063 | 929 | 734 | 682 | 616 |
| NOx | | ppm | 1470 | 1286 | 1283 | 1134 | 901 | 823 | 744 |
| NO2 | | ppm | 260 | 227 | 220 | 206 | 167 | 141 | 128 |
| N2O | | ppm | -4 | -3 | -3 | -4 | -3 | -3 | -3 |
| Combustion Efficiency RTD Port 9 | 0.730 | % | 95.96 | 97.82 | 96.40 | 97.20 | 97.24 | 97.76 | 97.70 |
| Combustion Efficiency RTD Port 15 | 1.682 | % | 98.72 | 99.52 | 98.61 | 99.22 | 97.46 | 99.20 | 99.09 |
| Combustion Efficiency RTD Port 21 | 2.189 | % | 98.94 | 99.71 | 99.08 | 99.31 | 98.30 | 99.48 | 99.55 |
| Rate of Slag Formation | | g/hr | NM | NM | 17.5 | 13.9 | 31.3 | 32.4 | 19.2 |

Table 5.4 Summary of the data obtained from the PSCTF for the additional tests using the second coal sample (coal B)

| **Measured Quantities** | **Time to reach port [s]** | **Units** | **Baseline Coal B (Test 1)** | **10% Sawdust (Test 2)** | **15% Sawdust (Test 3)** | **20% Sawdust (Test 4)** |
|---|---|---|---|---|---|---|
| Furnace Pressure | | Pa | -208.15 | -184.24 | -168.33 | -183.76 |
| Gas Temp Port 4 | 0.286 | K | 1237.97 | 1254.19 | 1268.05 | 1283.05 |
| Gas Temp Port 10 | 0.822 | K | 1346.36 | 1367.71 | 1381.14 | 1400.29 |
| Gas Temp Port D | 1.287 | K | 1216.79 | 1241.67 | 1252.76 | 1269.00 |
| Gas Temp Port 28 | 3.504 | K | 932.39 | 961.29 | 974.33 | 995.29 |
| Average gas Temperature | | K | 1183.38 | 1206.21 | 1219.07 | 1236.90 |
| Average wall Temperature | | K | 980.88 | 981.39 | 982.49 | 984.87 |
| Convective exit Temperature | | K | 170.48 | 177.81 | 180.86 | 187.86 |
| Oxygen (Zirconia) wet basis | | % | NM | NM | NM | NM |
| Oxygen (dry basis) | | % | 6.12 | 5.52 | 4.76 | 4.38 |
| Carbon Monoxide | | ppm | 23.69 | 31.38 | 29.94 | 30.78 |
| CO2 | | % | 12.84 | 13.43 | 14.08 | 14.50 |
| SO2 | | ppm | 477.09 | 441.52 | 431.52 | 405.25 |
| NO | | ppm | 1302.45 | 1446.17 | 1527.38 | 1526.92 |
| $NO_X$ | | ppm | 1486.89 | 1642.56 | 1729.64 | 1732.59 |
| NO2 | | ppm | 184.44 | 196.38 | 202.26 | 205.68 |
| N2O | | ppm | 0.04 | 0.08 | 0.11 | 0.27 |
| Combustion Efficiency RTD Port 9 | 0.822 | % | 90.80 | 90.29 | 90.31 | 93.63 |
| Combustion Efficiency RTD Port 15 | 1.895 | % | 98.43 | 98.40 | 98.27 | 97.82 |
| Combustion Efficiency RTD Port 21 | 2.467 | % | 98.76 | 98.96 | 98.67 | 98.49 |
| Rate of Slag Formation | | g/hr | 74.82 | NM | NM | NM |

Table 5.3 gives the summary of the data obtained from the initial set of tests. The gaseous emission values in ppm have been corrected to 6% excess oxygen using equation 5.1 below. This was done to ensure that the readings are measured from the same reference.

$$Normalised\ Reading = \left(\frac{6 - \%O_2}{20.9 - 6} + 1\right) \times Reading\ to\ be\ normalised \quad (5.1)$$

The data from the PSCTF were logged in a file every minute and an average value of the measured quantity were then taken for each test. Each test took about 30 minutes. This time was necessary to obtain time-averaged value for each of the measured quantities in order to iron out inherent minor fluctuations in the system such as those due to the on/off controller on the coal weigh feeder. The values given in Table 5.3 and 5.4 are such averaged values. To feed the biomass into the furnace, a diesel lance which runs through the centre of the burner was removed to make room for the biomass vibratory feeder. The furnace pressure had to be decreased to prevent biomass blowout through its feeding pipe.

When running tests at the PSCTF more than one person is required for sampling (fly ash, slags ), monitoring the instruments and in our case of co-firing , to monitor the biomass fuel flow rate. Since biomass co-firing was done for the first time, my major concern was the safety and to ensure that the feeding rate of biomass was steady. For the first two tests I was on top of the rig where biomass feeding was introduced. Since one cannot be at all places at the same time, the operator at that time was helping us to collect the samples which I had already indicated that fly ash and slag deposits were required. It was thought that since this is one of the routine exercises, it will be easy to handle.

When I was confident that the feeding for biomass was running without problems, I went down to see the samples, that is when I realised slag samples had not been taken. These samples were for the baseline and 10% sawdust. To cut the costs, the baseline test was shared between Eskom and this project. For a block of tests tested that week slag deposits were not being sampled so these tests (11 and13) were inadvertently treated like previous ones despite having been made aware of the type of samples that would be required. It was during Test 13 when it became clear that the slag sample for baseline was not taken. At that time, it was already late to sample slag deposit for Test 13 because slag deposits

need time to form, at least 30 minutes. When the repeat tests were organised it was hoped that the missing data would be filled. The baseline slag deposit was sampled and its value is recorded in Table 5.4. During Test 2, the temperatures in the furnace rose such that when the slagging probe was removed to collect the slag deposit, it was found that the probe had melted. Fouling data could not be collected because the PCSTF was not equipped for collecting fouling samples.

Curve fitting algorithms were used to fit the curves through these combustion efficiency values and gas temperatures for respective tests. It was then possible to draw the curves in Figs. 6.11 – 6.13 from the data in Appendices C and G.

Table 5.5 Percentage unburned carbon for the test done on the PSCTF

| | % Unburned Carbon-in-ash | | | |
|---|---|---|---|---|
| | Port 9 | Port 15 | Port 21 | CO [ppm] |
| Coal A (T11) | 7.2 | 2.4 | 2.0 | 82 |
| 10% SD (T13) | 4.4 | 1.0 | 0.6 | 33 |
| 15% SD (T14) | 7.4 | 3.0 | 2.0 | 44 |
| 20% SD (T15) | 6.2 | 1.8 | 1.6 | 38 |
| 10% GS (T16) | 5.4 | 5.0 | 3.4 | 41 |
| 15% GS (T17) | 4.6 | 1.7 | 1.1 | 32 |
| 20% GS (T18) | 4.9 | 2.0 | 1.0 | 25 |
| Coal B (T1) | 14.9 | 2.9 | 2.3 | 23 |
| 10% SD (T2) | 16.7 | 3.2 | 2.1 | 32 |
| 15% SD (T3) | 17.3 | 3.6 | 2.8 | 32 |
| 20% SD (T4) | 12.6 | 4.7 | 3.3 | 32 |

## 5.3 Drop Tube Furnace (DTF) Results

Table 5.6 Tests that were done at the DTF

| Test (Eskom No.) | Fuel blend | Biomass to Coal Ratio (on Energy Basis) |
|---|---|---|
| 1 | Coal alone (baseline coal A) | 0%:100% |
| 2 | Sawdust and coal | 10%:90% |
| 3 | Sawdust and coal | 15%:85% |
| 4 | Sawdust and coal | 20%:80% |
| 5 | Grass and coal | 10%:90% |
| 6 | Grass and coal | 15%:85% |
| 7 | Grass and coal | 20%:80% |

Table 5.6 indicates the seven tests that were carried out with the DTF. Seven samples of around 500g were prepared for these tests. A sample of 500g was used for the baseline test. Using the mass of the baseline sample as the reference, the blends were prepared on a batch process, from the respective raw fuels as indicated in Table 5.7. One portion of each of the samples was used for DTF tests and the other for chemical analysis. Chemical analysis results of the raw biomass/coal blends are shown in Table 5.8.

Table 5.7 Mass of respective raw fuels required to prepare blends to be co-fired

| Co-firing Ratio | Coal A required [kg] | Sawdust required [kg] | Sawdust/coal blend prepared [kg] | Grass required [kg] | Grass/coal blend prepared [kg] |
|---|---|---|---|---|---|
| 0% | 0.500 | 0.000 | - | 0.000 | - |
| 10% | 0.450 | 0.060 | 0.510 | 0.064 | 0.514 |
| 15% | 0.425 | 0.090 | 0.515 | 0.096 | 0.521 |
| 20% | 0.400 | 0.120 | 0.520 | 0.128 | 0.528 |
| | | | | | |
| Total | 1.775 | 0.270 | 2.045 | 0.287 | 2.062 |

About 300g of char was produced from the DTF at 1400℃ in a 100% nitrogen atmosphere and a flow rate of 1g/min. This char was then sent for chemical analysis (proximate, ultimate and ash analysis), density measurement and average particle size distribution. The results are presented in Tables 5.8 and 5.12. One of the most important reasons for carrying out the DTF tests was to determine the reaction kinetics of the coal and its biomass blends. The values of activation energy and pre-exponential factors are among the kinetic parameters in Table 5.9. These were obtained from a log-log plot of particle temperature and surface reaction rate coefficient $K_s$, refer to section 4.3.4 for sample calculations.

The chars derived from the coal and its biomass blends for co-firing were combusted in turn at 1000 ℃, 1200 ℃ and 1400 ℃ in a 3% oxygen environment. For 1000 ℃ partially reacted char was collected at positions P3 and P1, while for 1200 ℃ and 1400 ℃ it was collected at positions P5, P3 and P1. Distances of each position from the injection probe are P5 = 52cm, P3 = 92 cm and P1 = 132 cm (see section 4.3.2 for details). Carbon burnout is minimum at P5 and maximum at P1.

The samples collected were sent to the Eskom coal laboratory for determining the unburned carbon in the sample and the results are shown in Table 5.10. These results were used together with ash content of char from Table 5.9 (figures had to be converted to dry basis) for each of the tests to calculate respective combustion efficiencies (see section 4.3.5) that are shown in Table 5.11.

The ash content of char was obtained from Table 5.9 and then converted to dry basis. Ash content of combustible residue was calculated from 100-U, where U is %unburned carbon obtained from Table 5.10.

Table 5.8 Raw fuels analysis results

| | | COAL A | 10% Sawdust | 15% Sawdust | 20% Sawdust | 10% Grass | 15% Grass | 20% Grass |
|---|---|---|---|---|---|---|---|---|
| **PROXIMATE ANALYSES** | | | | | | | | |
| Inherent Moisture | % | 2.8 | 3.3 | 3.5 | 3.6 | 3.2 | 3.4 | 3.5 |
| Ash | % | 28.9 | 25.4 | 24.0 | 22.3 | 26.0 | 24.3 | 23.1 |
| Volatile Matter | % | 20.4 | 26.4 | 30.2 | 33.0 | 30.9 | 26.6 | 33.8 |
| Fixed Carbon | % | 47.9 | 44.9 | 42.3 | 41.1 | 39.9 | 45.7 | 39.6 |
| Fuel Ratio (FC/VM) | % | 2.3 | 1.7 | 1.4 | 1.2 | 1.3 | 1.7 | 1.2 |
| **ULTIMATE ANALYSES** | | | | | | | | |
| Carbon | % | 54.75 | 53.81 | 53.45 | 53.26 | 53.53 | 52.69 | 56.41 |
| Hydrogen | % | 2.41 | 2.72 | 2.93 | 2.89 | 2.98 | 2.87 | 2.29 |
| Nitrogen | % | 1.30 | 1.42 | 1.48 | 1.45 | 1.35 | 1.08 | 1.48 |
| Sulphur | % | 1.47 | 1.28 | 1.24 | 1.12 | 1.27 | 1.22 | 1.17 |
| Carbonates | % | 3.96 | 2.77 | 2.42 | 2.53 | 2.60 | 2.61 | 2.31 |
| Oxygen | % | 4.41 | 9.30 | 10.98 | 12.85 | 9.07 | 11.83 | 9.74 |
| **GROSS CALORIFIC VALUE** | MJ /kg | 21.00 | 20.46 | 20.41 | 20.32 | 20.46 | 20.41 | 20.17 |
| **DEFORMATION TEMPERATURES** | | | | | | | | |
| Deformation Tem. | ˚C | 1340 | 1350 | 1350 | 1320 | 1340 | 1320 | 1330 |
| Softening Temp. | ˚C | 1360 | 1360 | 1360 | 1330 | 1360 | 1340 | 1350 |
| Hemisphere Temp. | ˚C | 1380 | 1380 | 1380 | 1350 | 1370 | 1360 | 1360 |
| Flow Temp. | ˚C | 1400 | 1390 | 1390 | 1360 | 1390 | 1380 | 1380 |

Table 5.9 Char analysis results

| | | COAL A | 10% Sawdust | 15% Sawdust | 20% Sawdust | 10% Grass | 15% Grass | 20% Grass |
|---|---|---|---|---|---|---|---|---|
| **PROXIMATE ANALYSES** | | | | | | | | |
| Inherent Moisture | % | 0.2 | 0.4 | 0.2 | 0.4 | 0.2 | 0.4 | 0.2 |
| Ash | % | 42.4 | 43.0 | 42.4 | 40.8 | 42.8 | 41.9 | 42.5 |
| Volatile Matter | % | 0.01 | 0.01 | 0.01 | 0.01 | 0.01 | 0.1 | 0.01 |
| Fixed Carbon | % | 57.4 | 56.6 | 57.4 | 58.8 | 57.0 | 57.6 | 57.3 |
| **GROSS CALORIFIC VALUE** | MJ/kg | 20.5 | 19.36 | 19.66 | 20.22 | 19.13 | 20.01 | 20.04 |
| **KINETIC PARAMETERS** | | | | | | | | |
| Activation Energy, E | kJ/mol | 72.951 | 66.777 | 65.690 | 72.680 | 69.037 | 70.174 | 62.485 |
| Pre-exponential factor | $kg/m^2/s/atm$ | 731.91 | 363.45 | 342.42 | 498.55 | 527.83 | 674.93 | 413.79 |
| Burnout Time | s | 1.1 | 2.6 | 2.5 | 1.5 | 2.5 | 2.4 | 1.7 |
| **ASH ANALYSES** | | | | | | | | |
| Silicon (as SiO2) | % | 44.1 | 44.1 | 44.5 | 43.5 | 45.1 | 45 | 45.9 |
| Aluminium (as Al2O3) | % | 25.4 | 26 | 26.2 | 25.7 | 25.5 | 24.7 | 24.5 |
| Iron (as Fe2O3) | % | 8.4 | 8.3 | 8.5 | 8.3 | 8.1 | 7.8 | 7.8 |
| Titanium (as TiO2 | % | 1.4 | 1.6 | 1.7 | 1.7 | 1.4 | 1.4 | 1.3 |
| Phosphorus (as P2O5) | % | 0.83 | 0.84 | 0.82 | 0.8 | 0.87 | 0.82 | 0.83 |
| Calcium (as CaO) | % | 11.5 | 11.5 | 11.8 | 11.5 | 11.2 | 10.9 | 10.9 |
| Magnesium (as MgO) | % | 2.3 | 2.3 | 2.4 | 2.2 | 2.3 | 2.3 | 2.3 |
| Sodium (as Na2O) | % | 0 | 0 | 0 | 0 | 0 | 0 | 0 |
| Potassium (as K2O) | % | 0.3 | 0.3 | 0.3 | 0.4 | 0.5 | 0.6 | 0.7 |
| Sulphur (as SO3) | % | 5.3 | 5.5 | 4.4 | 4.4 | 5.6 | 4.6 | 4.7 |
| Manganese (as MnO) | % | 0.07 | 0.04 | 0.04 | 0.04 | 0.05 | 0.04 | 0.04 |

.

Table 5.10 Unburned carbon determined from the combustible residue at each testing position.

| Position | Temp [℃] | Unburned Carbon of combustible residue U[%] | | | | | | |
|---|---|---|---|---|---|---|---|---|
| | | Baseline | 10% Sawdust | 15% Sawdust | 20% Sawdust | 10% Grass | 15% Grass | 20% Grass |
| P1 | 1000 | 15.4 | 14.4 | 22.5 | 13.6 | 22.5 | 14.4 | 14.2 |
| P3 | 1000 | 31.8 | 28.1 | 28.3 | 27.6 | 28.7 | 25.8 | 23.8 |
| P1 | 1200 | 7.5 | 6.5 | 7.6 | 6.8 | 11.3 | 6.6 | 8.7 |
| P3 | 1200 | 9.7 | 23.6 | 21.3 | 15.1 | 11.8 | 8.0 | 8.1 |
| P5 | 1200 | 29.4 | 28.4 | 27.1 | 22.9 | 30.0 | 22.5 | 19.8 |
| P1 | 1400 | 3.5 | 10.1 | 10.0 | 7.0 | 8.7 | 7.8 | 3.5 |
| P3 | 1400 | 5.6 | 14.2 | 18.1 | 5.9 | 11.4 | 9.9 | 8.8 |
| P5 | 1400 | 12.7 | 26.6 | 21.2 | 26.4 | 14.7 | 20.8 | 22.2 |

Table 5.11 Combustion efficiency calculated at each testing position.

| Position | Temp [℃] | Combustion Efficiency [%] | | | | | | |
|---|---|---|---|---|---|---|---|---|
| | | Baseline | 10% Sawdust | 15% Sawdust | 20% Sawdust | 10% Grass | 15% Grass | 20% Grass |
| P1 | 1000 | 90.91 | 91.63 | 82.69 | 93.54 | 83.71 | 92.21 | 92.15 |
| P3 | 1000 | 69.22 | 74.19 | 74.75 | 77.53 | 75.56 | 78.77 | 80.92 |
| P1 | 1200 | 98.61 | 99.36 | 98.54 | 99.58 | 95.55 | 99.51 | 97.51 |
| P3 | 1200 | 96.60 | 80.61 | 84.19 | 92.08 | 95.08 | 98.29 | 98.06 |
| P5 | 1200 | 73.03 | 73.74 | 76.49 | 83.56 | 73.67 | 83.06 | 85.92 |
| P1 | 1400 | 100.00 | 96.00 | 96.34 | 99.42 | 97.88 | 98.47 | 100.00 |
| P3 | 1400 | 100.00 | 91.84 | 87.97 | 100.00 | 95.45 | 96.57 | 97.42 |
| P5 | 1400 | 93.70 | 76.42 | 84.31 | 79.14 | 92.28 | 85.14 | 82.98 |

Table 5.12 Char particle diameter and density

| | Density ($kg/m^3$) | Particle Diameter (m) |
|---|---|---|
| Coal A | 1620 | $3.43 \times 10^{-5}$ |
| 10% Sawdust | 1730 | $3.49 \times 10^{-5}$ |
| 15% Sawdust | 1740 | $3.62 \times 10^{-5}$ |
| 20% Sawdust | 1740 | $2.08 \times 10^{-5}$ |
| 10% Grass | 1720 | $3.51 \times 10^{-5}$ |
| 15% Grass | 1720 | $2.67 \times 10^{-5}$ |
| 20% Grass | 1760 | $3.10 \times 10^{-5}$ |

# 6 DISCUSSION OF RESULTS

This chapter discusses the experimental results from the PSCTF and the DTF regarding the emissions, ignition behavior and ash deposition. It further compares the emissions and temperature profiles predicted by computer simulation using Fluent with the experimental results.

## 6.1 Experimental Results – Emissions

### 6.1.1 $NO_X$

The results from the combustion test facility when co-firing coal A with sawdust and grass show that, for both types of biomass there is a clear reduction trend in the $NO_x$ emissions (see Figs 6.1 and 6.2). Grass was able to reduce $NO_x$ emissions by 39%, 44% and 49% at 10%, 15% and 20% co-firing ratios respectively. $NO_x$ emissions for sawdust were reduced by 13%, 13% and 29% at 10%, 15% and 20% co-firing ratios respectively. These results agree with Pederson et al, 1996; Spliethoff et al, 1998; Battista et al, 2000; Boylan et al, 2000; Hus et al, 2000; Tillman, 2000; Annamalai et al, 2003b; Demirbas 2004; Kwong et al, 2007; Narayanan et al, 2007) in that co-firing biomass can reduce $NO_X$ emissions.

$NO_x$ emissions from grass-based co-firing decreases linearly with the increasing co-firing ratio (see Fig 6.2). This trend may be attributed to dilution due to lower nitrogen content in grass than that in coal (Table 5.1) as indicated by earlier studies (Pederson et al, 1996; Boylan et al, 2000; Hus et al, 2000; Demirbas 2004; Kwong et al, 2007) and also due to decreasing peak temperature as co-firing ratio increases (Fig. 6.9). Generally the sawdust $NO_x$ emissions decrease with increasing biomass proportion (see Fig.6.1). Fig. 6.3 shows the emissions profiles from the repeated tests as discussed in section 5.2. Apparently Fig. 6.3 shows a different behavior which will be discussed in detail in section 6.1.2.

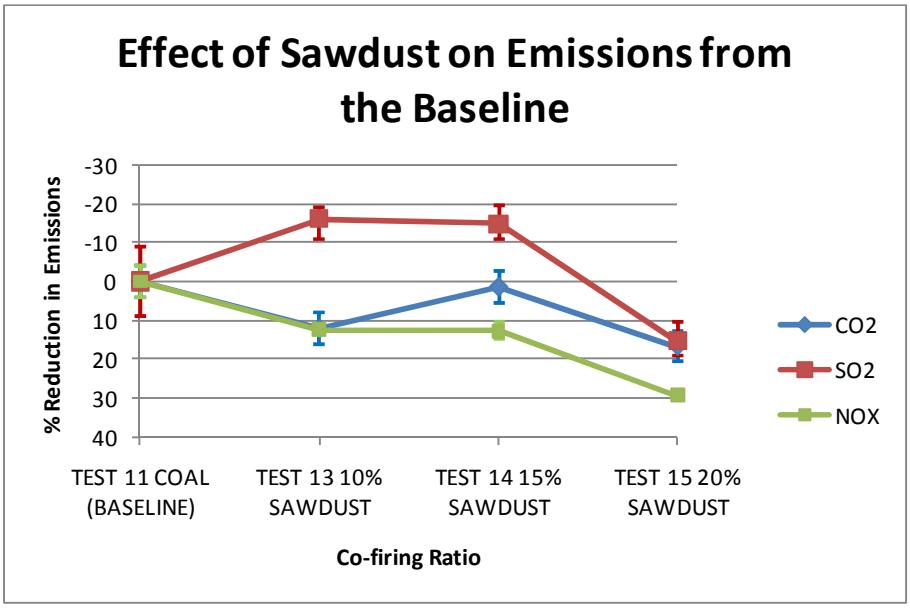


Figure 6.1 Effect of Sawdust on Emissions from the Baseline (Original test nos. 11, 13-15)

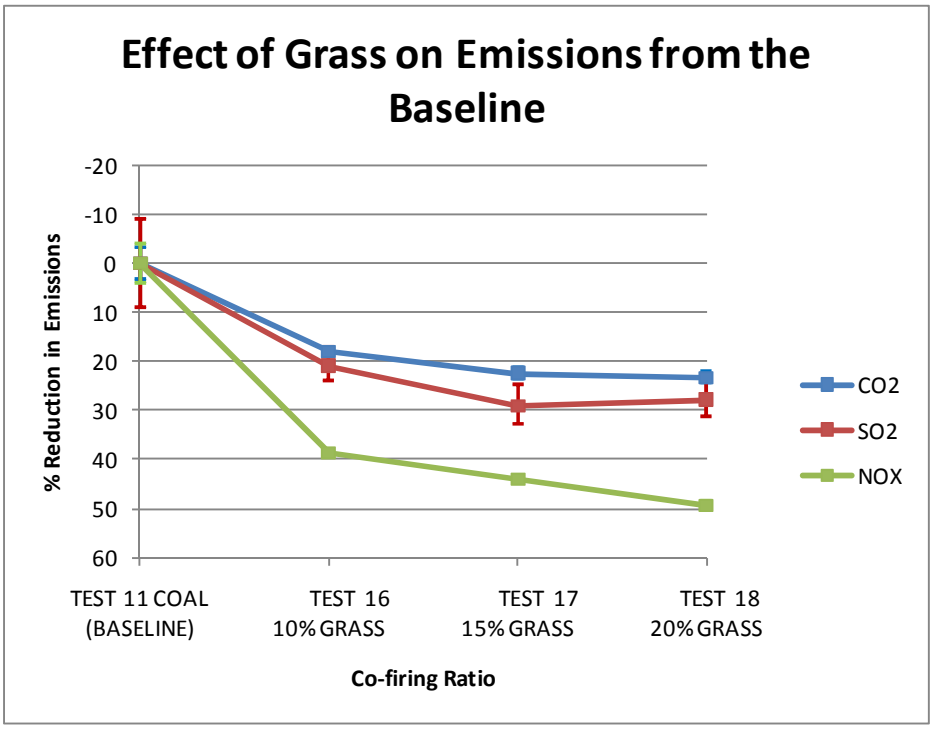


Figure 6.2 The effect of grass on emissions from the baseline (Original test nos. 11, 16-18)

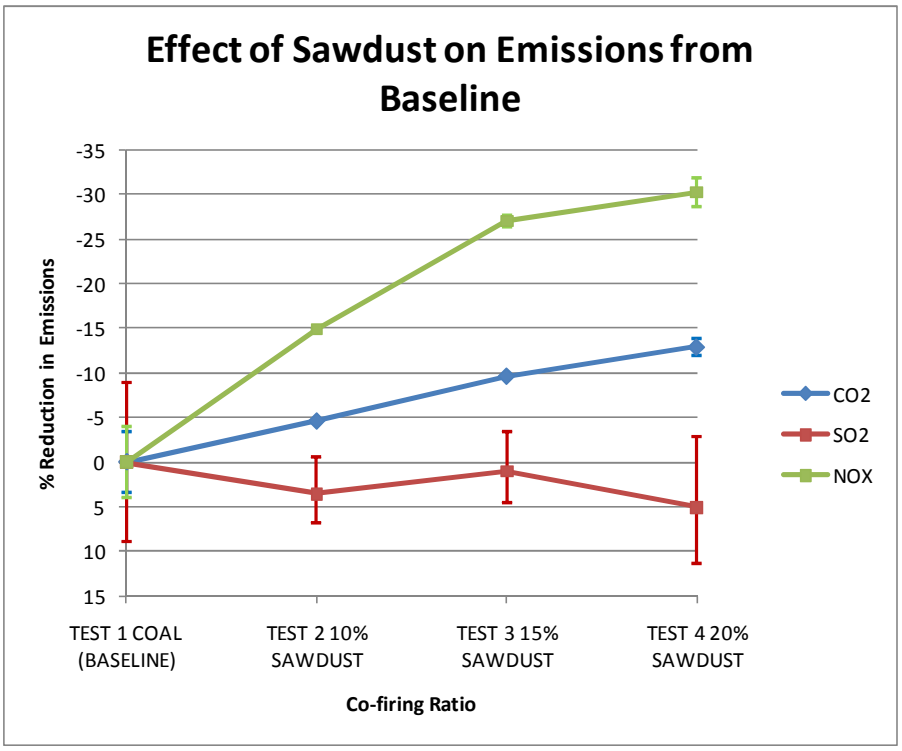


Figure 6.3 The effect of sawdust on emissions from the baseline (Repeated test Nos. 1-4)

The nitrogen content of sawdust is more than double that of coal (see Table 5.1) and yet the reduction in $NO_X$ is observed for all co-firing ratios (Fig. 6.1). This would suggest that fuel nitrogen seems to have little or no influence on production of $NO_x$ as suggested by (Skodras et al, 2002, Gani et al, 2005; Kazagic et al, 2009). It would therefore seem probable that the reduction in $NO_X$ emissions for grass were also not primarily due to low fuel-N in grass but due to reduction in peak temperature.

Figs. 6.11 - 6.13 show graphs of flue gas temperature and combustion efficiency against time for tests that were run on the PSCTF. The drop in peak temperature observed in Figs. 6.11 and 6.13 reduces thermal $NO_x$ which appears to be the dominant contributor to overall $NO_x$ (Beér et al, 1995). This will explain why there is still a reduction in $NO_x$ for sawdust

even though it had higher nitrogen content than coal. There is more temperature drop associated with grass based co-firing than that of sawdust, hence more reduction in $NO_x$ is observed for grass. The peak temperatures were strongly affected by excess air more than moisture content of the biomass because sawdust with higher moisture content than grass, did not result in bigger drop in temperatures than grass. This may be acceptable because moisture content below 10% as is the case here, does not heavily impact temperatures (Maciejewska 2006). Fig.6.4 shows that excess air is inversely proportional to temperature and by extension to thermal $NO_x$ (Fig. 6.5) for values of excess air between 26% and 67%. Figs. 6.4 and 6.5 have been produced from figures in Table 6.1. Excess air seems to have a stronger influence on $NO_X$ formation than fuel N (Kazagic et al, (2009). Khang et al, (2009) also confirm that NOx emissions are a strong function of operating temperature and excess air level.

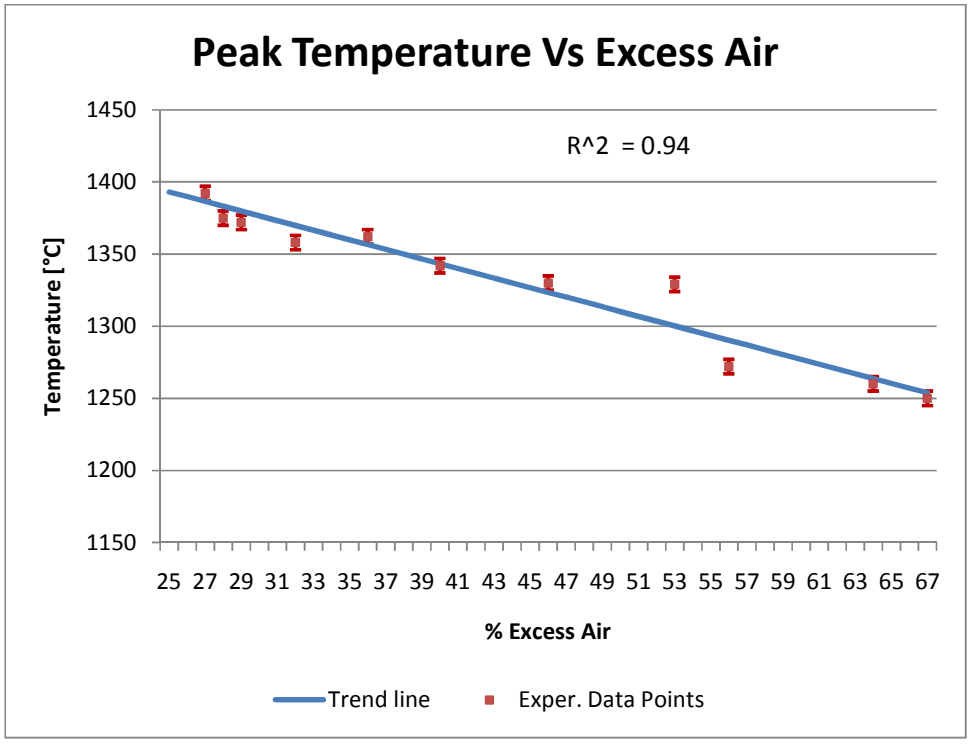


Figure 6.4 Correlation of peak flue gas temperature and excess air for tests nos. 11, 13-18 and 1-4.

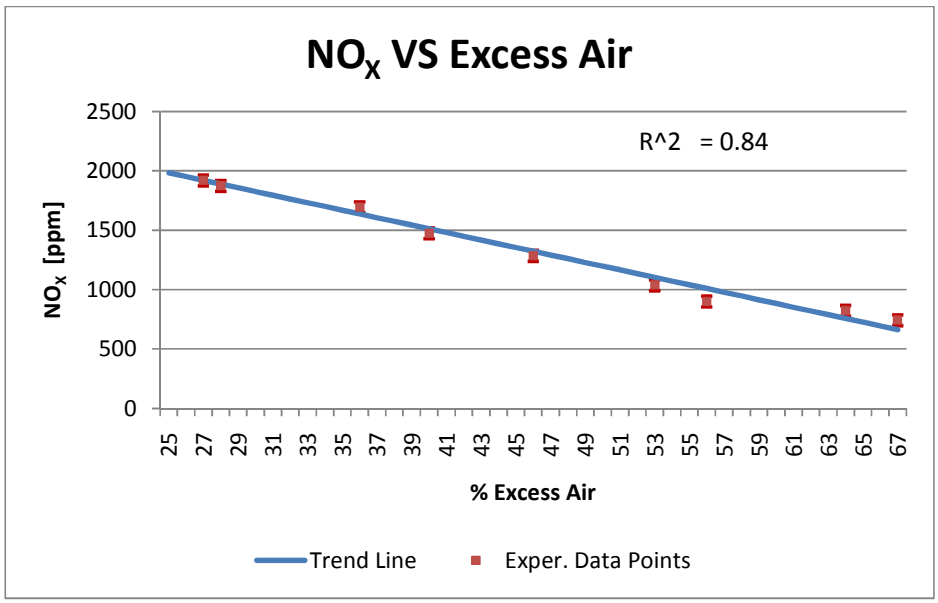


Figure 6.5 Correlation of $NO_x$ emissions and excess air for tests nos. 11, 13-18 and 1-4

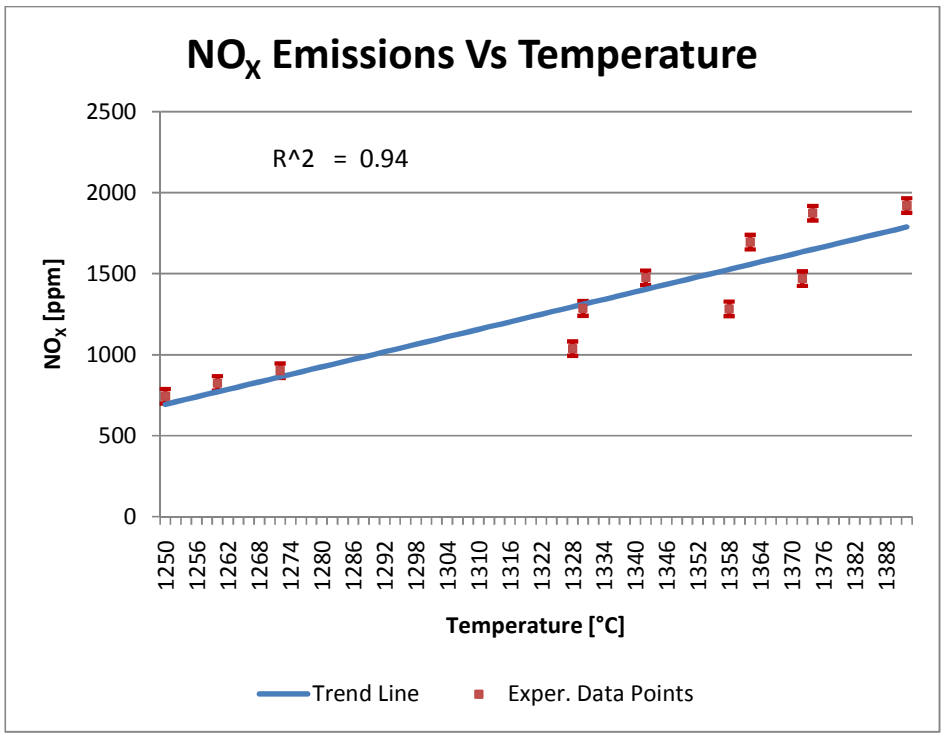


Figure 6.6 Correlation of $NO_x$ emissions and peak flue gas temperature and excess air for tests nos. 11, 13-18 and 1-4

A graph of $NO_x$ vs excess air in (Kazagic et al, 2009) for % excess air between 0 and 20, shows that $NO_x$ increased with increasing excess air but showed a flattening behaviour towards 20% excess value. The $NO_x$ behaviour in Fig. 6.5, showing a decreasing trend as excess air increases, and that in Kazagic et al, (2009) would suggest that there is a turning point (van Loo et al, 2002) somewhere between 20% and 26% excess air. This is confirmed by earlier research that low excess air promotes $NO_x$ production (Abbas et al, 1994) and high excess air discourages it (Gungor 2009). In fact a plot of $NO_x$ emissions in Gungor (2008) between 12% and 24% excess air indicates a turning point around 22 %. The reduction in $NO_x$ in this case can be attributed primarily to reduction in thermal $NO_X$ due to cooling from excess air.

Table 6.1 Excess air, peak flue gas temperature and $NO_X$ for all tests run on PSCTF

| **Original Tests** | Test 11 Coal A | Test 13 10% SD | Test 14 15% SD | Test 15 20% SD | Test 16 10% GS | Test 17 15% GS | Test 18 20% GS |
|---|---|---|---|---|---|---|---|
| Excess air (%) | 29.83 | 46.23 | 31.95 | 53.30 | 55.87 | 63.65 | 66.55 |
| Peak Temp.(K) | 1372 | 1330 | 1358 | 1329 | 1272 | 1260 | 1250 |
| NOX (ppm) | 1470 | 1286 | 1283 | 1038 | 901 | 823 | 744 |
| | | | | | | | |
| **Repeated Tests** | Test 1 Coal A | Test 2 10% SD | Test 3 15% SD | Test 4 20% SD | | | |
| Excess air (%) | 41.41 | 35.89 | 29.47 | 26.52 | | | |
| Peak Temp.(K) | 1342 | 1362 | 1375 | 1392 | | | |
| NOX (ppm) | 1475 | 1695 | 1874 | 1921 | | | |

Note: SD = Sawdust and GS = Grass

### 6.1.2 Repeat Tests (Coal B and Sawdust only)

The increasing trend of $NO_X$ from the repeated sawdust-based co-firing (Fig. 6.3) can be attributed to the relatively low excess air, high flame temperature and small residence time due to the high induction draft fan setting (see section 5.2 and Table 6.2 second last row). The contribution of excess air to $NO_X$ formation is multifaceted. First, excess air is the amount of air required above the stoichiometric quantity to ensure complete combustion and hence better combustion efficiency. Excess air should be as small as possible to avoid significant reduction in thermal efficiency through thermal stack losses. The penalty that comes with a low amount of excess air, however, is that it increases the amount of oxygen in the reaction zone at high temperature and these conditions favour $NO_X$ formation by thermal $NO_X$ mechanism (Bebar et al, 2002; Baukal 2001). The fuel $NO_X$ formation rate is also high as temperature increases. Although more excess air would avail more oxygen for reaction with nitrogen, beyond some optimum point its effect in lowering the flame temperature (Van Loo et al, 2002) by absorbing the heat outperforms its contribution towards $NO_X$ formation by fixation (Baukal, 2001). Even though the heat absorbed by excess air lowers the flame temperature and by extension lowers the $NO_X$ formation, it does so at the cost of lowering thermal efficiency through stack losses. The relatively low amount of excess air used in the repeat tests actually promoted the high peak flame temperature (Fig. 6.9) and hence higher $NO_X$ emissions through thermal and fuel $NO_X$ mechanisms.

Fuel $NO_X$ was also encouraged by the role played by the major $NO_X$ precursors in the flame zone. $NO_X$ formation from biomass is a complex process which not only depends on fuel parameters but is also sensitive to the operating conditions. Under certain conditions biomass can reduce $NO_X$ emissions while on the other hand it can increase them (Wu et al, 2007;Van Loo et al, 2002). $NH_3$ and HCN are considered as the major $NO_X$ precursors in the combustion of coal and biomass. $NO_X$ is generated

predominantly in and around the flame itself and the localised temperature affects it greatly. HCN is the dominating intermediate in the pure coal flame, whereas $NH_3$ is dominant in biomass flames (Wu et al, 2007). These trends are due to largely aromatic forms of nitrogen in coal in comparison to the dominantly amine forms of nitrogen in biomass. In the fuel-rich eddies, in the generally fuel-lean environment, reactions involving $NH_3$ and HCN mainly include thermal decomposition. Below 1800 K, HCN decomposes more readily than $NH_3$ whereas above this temperature both species thermally decompose at increasingly rapid and similar rates (Wu et al 2007). Within the flame front, however, $NH_3$ is more chemically reactive than HCN at short residence times of up to 0.1 ms (Wu et al 2007).

Since biomass predominantly forms $NH_3$ rather than HCN (Phong-Anant et al, 1985; Spliethoff et al, 1998), it is logical to conclude that the gas phase was dominated by $NH_3$ since firstly, the sawdust fuel used has more nitrogen content than coal and secondly, because of the higher volatile yield of sawdust than that of coal. The reaction of $NH_3$ at high temperatures in forming NO is much faster than NO reduction to $N_2$ by thermal decomposition of $NH_3$ in the fuel rich pockets within the flame (Wu et al, 2007; Gani et al, 2005, Li et al, 2000). This results in the positive net increase in $NO_X$ production. The thermal decomposition of HCN mainly produced by coal alone under the same conditions would be faster than that of $NH_3$ (Wu et al 2007; Li et al, 2000) and hence would result in less $NO_X$ produced.

It is therefore conceivable that the relatively slow rate of thermal decomposition of $NH_3$ to $N_2$ in the fuel-rich eddies coupled with relatively faster chemical reaction of $NH_3$ when oxidising to NO may produce higher $NO_X$ than that would be produced by coal at the same conditions if residence time in the flame reaction zone is too short. Longer residence times in the flame zone favours the decomposition of the $NH_3$ and HCN

and brings about drastic reduction in $NO_X$ emissions (Spliethoff et al, 1996). The setting of the induction draft (ID) fan to a higher value (and hence higher pressure gradient) than necessary for this set of experiments might have reduced residence time so that this would happen. The settings of the ID fan for the repeat tests done in August 2008 are higher than those of the original tests done in September 2007, see Table 6.3 last row 'Furnace Pressure' and compare the two sets.

Table 6.3 compares the values of variables in the original and repeated sawdust-based co-firing tests. Table 6.2 shows values that were calculated (see section 4.2.4 for sample calculation) for the tests based on the new coal (coal B) sample. The actual amounts of 'Secondary Air' used for repeated tests indicated in Table 6.3, are lower than those in Table 6.2. The reason for this is that the Eskom operator tried to maintain the oxygen level at 6% percent by varying the secondary air. His argument was that the extra air admitted due to the removed diesel lance actually added some air which needed to be corrected. What he did not realize was that the extra air was part of primary air not secondary air hence the adjustment if at all could have been made on primary air so that there would not have been too much air in the primary zone. The situation was

Table 6.2 Comparison of original sawdust results (Sep 2007) and the results of repeated tests (Aug 2008).

| Mass Flows | | Baseline | 10% Sawdust | 15% Sawdust | 20% Sawdust |
|---|---|---|---|---|---|
| Biomass Flow | kg/hr | 0.00 | 20.24 | 30.36 | 40.49 |
| Stoichiometric (Biomass) | kg/kg | 5.29 | 5.29 | 5.29 | 5.29 |
| Coal Flow | kg/hr | 163 | 147 | 139 | 130 |
| Stoichiometric (Coal) | kg/kg | 6.93 | 6.93 | 6.93 | 6.93 |
| Excess Air | % | 42.681 | 42.681 | 42.681 | 42.681 |
| Air/fuel ratio | | 2.503 | 2.767 | 2.922 | 3.096 |
| CA/PA Ratio | | 2.95 | 2.95 | 2.95 | 2.95 |
| Total Air (Required) | kg/hr | 1612 | 1604 | 1600 | 1595 |
| Primary Air Flow (PA) | kg/hr | 408 | 406 | 405 | 404 |
| Secondary Air Flow (SA) | kg/hr | 1204 | 1198 | 1195 | 1191 |
| Tertiary Air Flow | kg/hr | 0 | 0 | 0 | 0 |

Table 6.3 Comparison of original sawdust results (Sep 2007) and the results of repeated tests (Aug 2008).

| | | | Test 11 | Test 1 | Test 13 | Test 2 | Test 14 | Test 3 | Test 15 | Test 4 |
|---|---|---|---|---|---|---|---|---|---|---|
| | | | | Repeat | | Repeat | | Repeat | | Repeat |
| | | | 100% Coal | 100% Coal | 10% SD | 10% SD | 15% SD | 15% SD | 20% SD | 20% SD |
| **FUEL** | | SI Units | | | | | | | | |
| Coal Flow | | kg/hr | 173 | 165 | 157 | 148 | 149 | 141 | 139 | 131 |
| Biomass Flow | | kg/hr | 0.00 | 0.00 | 20 | 20 | 30 | 30 | 40 | 40 |
| Load | | MW | 1.02 | 1.01 | 1.02 | 1.01 | 1.03 | 1.01 | 1.02 | 1.01 |
| Grind size - passing 75 microns | | % | 77.98 | 76.15 | 78.11 | 76.12 | 84.24 | 77.58 | 85.30 | 78.18 |
| Co-firing ratio (energy basis) | | | | | | | | | | |
| Coal | | % | 100 | 100 | 90 | 90 | 85 | 85 | 80 | 80 |
| Sawdust | | % | 0 | 0 | 10 | 10 | 15 | 15 | 20 | 20 |
| **AIR** | | | | | | | | | | |
| Total Air flow | | kg/hr | 1645 | 1517 | 1637 | 1527 | 1616 | 1550 | 1624 | 1553 |
| Combustion Air / Primary Air | | kg/hr | 2.85 | 2.45 | 2.84 | 2.40 | 2.90 | 2.27 | 2.86 | 2.24 |
| SecondarAir / Tertiary Air | | kg/hr | 0.00 | 0.00 | 0.00 | 0.00 | 0.00 | 0.00 | 0.00 | 0.00 |
| Swirl Number SA | | | 1 | 1 | 1 | 1 | 1 | 1 | 1 | 1 |
| Excess Air | | % | 29.83 | 41.41 | 46.23 | 35.89 | 31.95 | 29.47 | 53.30 | 26.52 |
| Primary Air Flow | | kg/hr | 427 | 397 | 427 | 404 | 415 | 429 | 421 | 433 |
| Primary Air Temperature | | ℃ | 94 | 93 | 94 | 93 | 94 | 93 | 94 | 93 |
| Secondary Air Flow | | kg/hr | 1182 | 971 | 1175 | 970 | 1167 | 972 | 1168 | 970 |
| Secondary Air Temperature | | ℃ | 301 | 301 | 301 | 301 | 297 | 304 | 303 | 301 |
| Tertiary Air Flow | | kg/hr | 0 | 0 | 0 | 0 | 0 | 0 | 0 | 0 |
| Tertiary Air Temperature | | ℃ | 168 | 172 | 182 | 173 | 181 | 173 | 181 | 173 |
| Overfire air Flow | | kg/hr | 36 | 0 | 35 | 0 | 34 | 0 | 35 | 0 |
| Overfire air Temperature | | ℃ | 207 | 195 | 216 | 195 | 215 | 195 | 216 | 195 |
| **FLUE GAS** | | | | | | | | | | |
| Furnace Pressure | | Pa | -77 | -208 | -94 | -184 | -130 | -168 | -307 | -184 |

made worse by setting an unnecessarily big suction pressure which admitted about 38% extra air over and above the primary air, consequently upsetting the air staging of the burner. This extra air appears under “Purge Air” in Appendix E. As already argued more oxygen in the primary zone promotes high heat release rate and by extension high flame temperature, which favours $NO_X$ production.

### 6.1.3 $SO_2$

$SO_2$ emissions profiles for sawdust based co-firing are shown in Fig. 6.1 which shows for the first two co-firing ratios an increase of emissions from the baseline and a reduction of 15% for the last co-firing ratio. This was an unexpected result that could not be explained, as a result the tests for the first two co-firing ratios were taken as possible outliers and the sawdust-based co-firing tests were repeated. The results for $SO_2$ for the repeated tests are shown in Fig. 6.3.

The general expectation is for $SO_2$ to decrease with the co-firing ratio due to the lower sulphur content of biomass compared to coal (Van Loo et al, 2002). The alkaline ash due to biomass is also expected to capture some of the $SO_2$ resulting in further reduction in $SO_2$ emissions (Robinson et al, 2003; Wieck-Hansen et al, 2000). This is not the case for the original tests and the new tests.

The standard deviation is a measure of how widely values are dispersed from the average value (the mean). If a distribution's standard deviation is greater than its mean, the mean is inadequate as a representative measure of central tendency. So the smaller the standard deviation, the better the mean. Standard deviation can be calculated using eqn (6.1).

$$s = \sqrt{\frac{\sum(x - \bar{x})^2}{n - 1}} \qquad (6.1)$$

where

$x$ = single value in the distribution

$\bar{x}$ = mean

$n$ = number of values in the distribution

Table 6.4 shows the standard deviation data computed (using eqn (6.1)) on the logged data for gas temperature and gaseous emissions in Appendices A and E. The data include original tests and the repeated tests. For the original tests of sawdust-based co-firing, in Table 6.4 the values of standard deviation per test for $SO_2$ meter are the highest compared with those of $SO_2$ meter for sawdust (repeats) and grass. This is also reflected by the averages. The averages of standard deviation per test for original sawdust tests, repeated tests and grass are 29.74, 8.27 and 17.58 respectively. These comparatively big deviations for original sawdust results may suggest that the instruments were not working properly when the tests were conducted or the tests were taken before steady state was reached. During the tests temperature was used to decide if steady state had been reached and according to standard deviation for the temperatures there is not much fluctuation. If the $SO_2$ meter had not been working for sawdust, it is likely that it would have shown similar behavior for grass co-firing tests which were done on the same day but after sawdust tests. There is no similar fluctuation in grass $SO_2$ readings. A similar pattern of averages for $NO_X$ meters can be observed. Therefore the possibility of malfunctioning meters is ruled out.

**Table 6.4 Standard deviation of the logged data for original and repeat tests.**

| | | Standard Deviation per Test | | | | | | |
|---|---|---|---|---|---|---|---|---|
| | | Gas Temp. | $SO_2$ | $CO_2$ | NO | $NO_X$ | Coal Flow | SS Error |
| | Coal A | 6.000 | 54.604 | 0.563 | 51.133 | 49.558 | 4.73 | 4.0 |
| | | | | | | | | |
| SAWDUST | 10% SD | 3.000 | 35.112 | 0.602 | 56.212 | 59.232 | 5.381 | 5.0 |
| ORIGINAL | 15% SD | 3.350 | 35.669 | 0.613 | 56.169 | 72.930 | 5.019 | 5.0 |
| TESTS | 20% SD | 9.000 | 18.443 | 0.515 | 43.117 | 41.047 | 4.883 | 3.0 |
| | | | | | | | | |
| | Average | 5.117 | 29.741 | 0.577 | 51.833 | 57.736 | 5.094 | |
| | | | | | | | | |
| | | | | | | | | |
| | | Standard Deviation per Test | | | | | | |
| | | Gas Temp. | $SO_2$ | $CO_2$ | NO | $NO_X$ | Coal Flow | SS Error |
| | Coal B | 1.760 | 11.587 | 0.208 | 29.764 | 27.492 | 2.611 | 2.0 |
| | | | | | | | | |
| SAWDUST | 10% SD | 3.000 | 9.643 | 0.551 | 29.561 | 33.277 | 1.156 | 1.0 |
| REPEAT | 15% SD | 5.000 | 6.848 | 0.573 | 27.423 | 34.321 | 1.021 | 2.0 |
| TESTS | 20% SD | 5.000 | 8.331 | 0.649 | 71.636 | 66.817 | 1.182 | 1.0 |
| | | | | | | | | |
| | Average | 4.333 | 8.274 | 0.591 | 42.873 | 44.805 | 1.120 | |
| | | | | | | | | |
| | | Standard Deviation per Test | | | | | | |
| | | Gas Temp. | $SO_2$ | $CO_2$ | NO | $NO_X$ | Coal Flow | SS Error |
| | | | | | | | | |
| GRASS | 10% GS | 9.000 | 21.529 | 0.373 | 33.049 | 31.176 | 3.375 | 1.0 |
| ORIGINAL | 15% GS | 4.000 | 14.455 | 0.264 | 30.307 | 36.489 | 3.521 | 2.0 |
| TESTS | 20% GS | 3.600 | 16.747 | 0.272 | 26.789 | 36.680 | 3.296 | 1.0 |
| | | | | | | | | |
| | Average | 5.533 | 17.577 | 0.303 | 30.048 | 34.782 | 3.397 | |

The coal flow rate standard deviation per test and the steady state (SS) error (Table 6.4) has the similar pattern as those of $SO_2$ readings. The steady state error found by subtracting the set flow rate from average of actual flow rate (third column average minus first column average in Appendix A) also has a similar pattern. It would therefore be plausible to suspect that the fluctuations seen in $SO_2$ and $NO_x$ meters is caused by fluctuations in the coal flow rate.

Figs. 6.7 and 6.8 show the impact of flow rate fluctuations on the $SO_2$ meter readings obtained for sawdust-based (original tests) and grass-

based co-firing. To compare the trends of coal flow rate standard deviations (Table 6.4) and $SO_2$ meter readings (Table 5.3), were normalized by expressing them as a percentage of the total of coal A readings plus either sawdust or grass readings as shown in Table 6.5.

Table 6.5 Normalized values of coal flow rate standard deviation and $SO_2$ meter readings.

| | Coal Flow Rate Std Deviation | Coal Flow as % of Total. | $SO_2$ meter Readings [ppm] | $SO_2$ as % of Total. |
|---|---|---|---|---|
| | Sawdust-based co-firing | | | |
| Coal A | 4.730 | 23.635 | 628 | 24.061 |
| 10%SD | 5.381 | 26.888 | 729 | 27.931 |
| 15%SD | 5.019 | 25.079 | 721 | 27.625 |
| 20%SD | 4.883 | 24.399 | 532 | 20.383 |
| | | | | |
| Total | 20.013 | 100 | 2610 | 100 |
| | Grass-based co-firing | | | |
| Coal A | 4.730 | 31.698 | 628 | 31.043 |
| 10%GS | 3.375 | 22.618 | 497 | 24.567 |
| 15%GS | 3.521 | 23.596 | 445 | 21.997 |
| 20%GS | 3.296 | 22.088 | 453 | 22.392 |
| | | | | |
| Total | 14.922 | 100 | 2023 | 100 |

$SO_2$ emissions for baseline should have been higher than 10% because of the higher flow rate but this was not the case. This can be attributed to low excess air of 29.83% (Table 6.3) below the target of 42% as well as grind

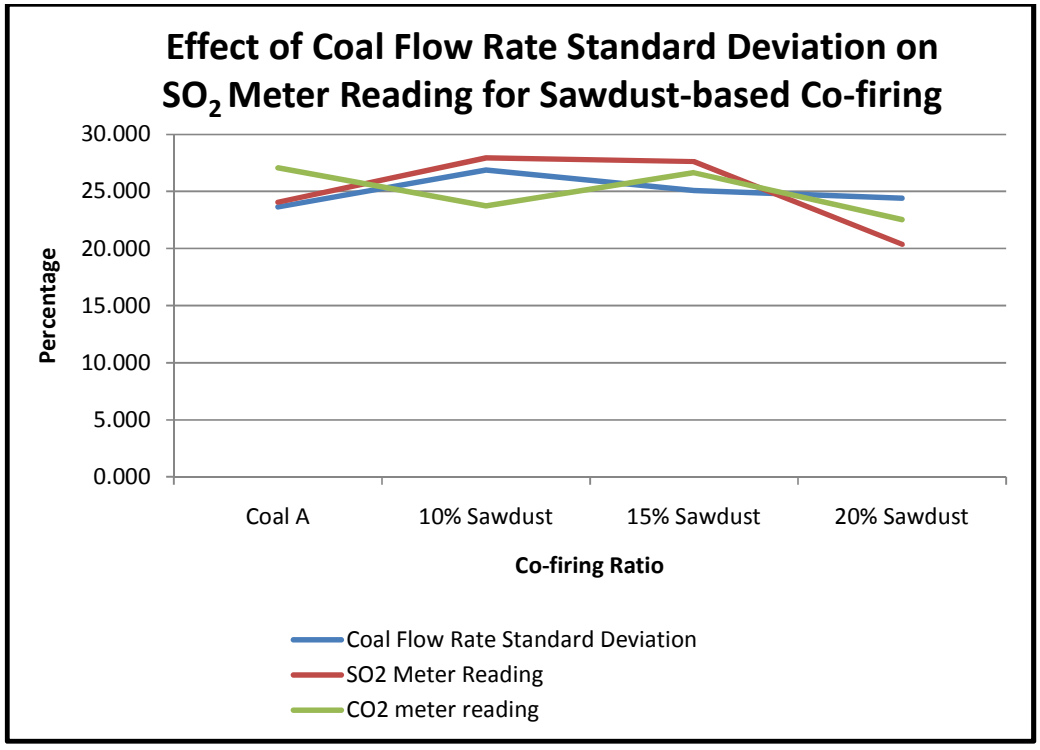


Figure 6.7 Effect of fluctuations in coal flow rate on $SO_2$ emissions for sawdust-based co-firing.

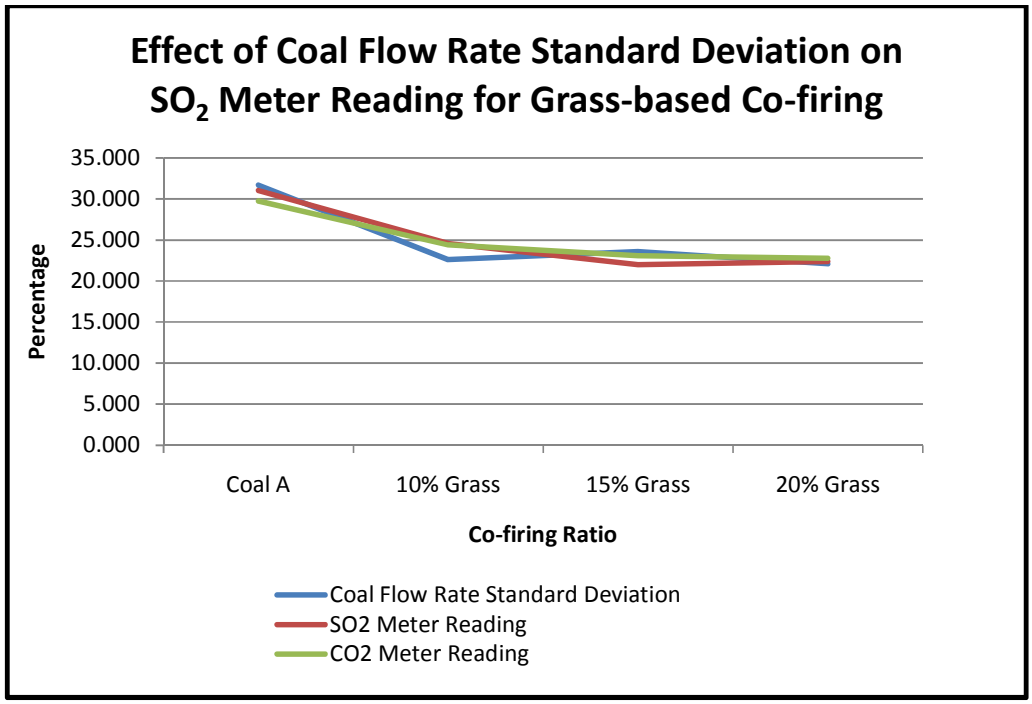


Figure 6.8 Effect of fluctuations in coal flow rate on $SO_2$ emissions for grass-based co-firing.

size. Excess air decreased because more fuel than the target value was supplied. Smaller grind size helps to improve diffusion limited reactivity (Tillman, 2000). The Baseline coal had the highest grind size compared to the other tests (see Appendix B) which could have inhibited the formation of $SO_2$.

At 10% sawdust co-firing ratio in Fig. 6.6, the $SO_2$ increases with coal flow but when coal profile decreases at 15% co-firing ratio, there is only a slight decrease in $SO_2$ emissions. The reason for this is that at 15% co-firing ratio the biomass feed rate, like that of coal, has also been above the set point and therefore producing $SO_2$ emissions which would tend to push the $SO_2$ curve higher. This is confirmed by the fact that the $CO_2$ profile rises at this ratio (Fig. 6.6) despite highest carbon in ash, second highest CO emission (Table 5.5) and low excess air. At 10% co-firing ratio, however biomass flow rate was below the target value such that it tended to negate the over supply of coal. This is so because the $CO_2$ emissions are low and the carbon-in-ash and CO emissions at port 21 (Table 5.5) are also low for this ratio. Although biomass counteracted the over supply of coal as far as $CO_2$ emissions are concerned, it did not do so for the $SO_2$ emissions because firstly, coal A has over 40 times as much sulphur as sawdust (see Table 5.1) and secondly, the co-firing ratio is low. For these two reasons, the steady state error in coal flow rate supply, dominated the fate of $SO_2$ emissions for 10% co-firing ratio. Because of the higher co-firing ratio at 20%, comparatively lower steady state error in coal flow supply, the $SO_2$ emissions were reduced. The conditions at 20% co-firing ratio are acceptable enough not to treat this data as an outlier compared to 10% and 15%.

The repeated sawdust-based co-firing tests indicate modest reduction in $SO_2$ emissions. This is mainly due to surprisingly small sulphur in coal B because re-sampled coal comes from the same mine. Differences like this in a coal do happen and are influenced by the geological setting, and

mining practice. The percentage reductions depend on the difference in sulphur content between the baseline coal and the biomass. The trend of $SO_2$ emissions as co-firing ratio was increased, could not be concluded from the original tests. From the results of repeated tests it can be said that biomass was able to reduce sawdust emissions for all co-firing ratios. These are 4%, 1% and 5% at 10%, 15% and 20% co-firing ratios. The 15% percent ratio resulted in smallest reduction because of the coal flow feeding rate steady state error (Table 6.4) which is higher than the other two co-firing ratios. Although the error is small, it is effective in influencing the trend because the amount of sulphur in both coal and sawdust is very small and therefore results in lower sulphur related emissions. These results can not be used to compare sawdust with grass with regard to the extend of reductions because of substantially different sulphur content of the two baseline coal samples A and B.

The conclusions that are drawn in this project regarding sawdust $SO_2$ emissions are with regard to 20% sawdust (test 15) which gives 15% reduction in $SO_2$ emissions from those of the baseline.

Fig. 6.7 also shows that the low fluctuations in coal flow rate of coal resulted in the low fluctuations in $SO_2$ meter readings for grass-based co-firing. Grass reduces $SO_2$ emissions by about 21% at 10% co-firing ratio and 30% at the co-firing ratio of 15% while at 20% co-firing ratio the reduction was 29% (Fig. 6.2). The reduction in $SO_2$ emissions decrease with increasing co-firing ratio for 10% and 15% co-firing ratio. There is a slight increase however at 20%. This is attributed to slight fluctuation in fuel supply.

### 6.1.4 $CO_2$

$CO_2$ stack emissions when co-firing biomass may actually increase relative to coal (Van Loo et al, 2002) in proportion to the co-firing ratio. The net $CO_2$ reduction is achieved when the rate of biomass consumption is equal or less than the rate at which it is re-grown and not by the change in stack $CO_2$ emissions. The stack $CO_2$ measured may be higher or lower than that of the baseline depending on the biomass fuel used. If stack $CO_2$

Table 6.6 Normalized values of coal flow rate standard deviation, $CO_2$ meter readings and % excess air.

| | Coal Flow Rate Std Deviation | Coal Flow as % of Total. | $CO_2$ meter Readings [ppm] | $CO_2$ as % of Total. | Excess Air | Excess Air as % of Total |
|---|---|---|---|---|---|---|
| | Sawdust-based co-firing | | | | | |
| Coal A | 4.730 | 23.635 | 14.23 | 27.069 | 29.83 | 18.492 |
| 10%SD | 5.381 | 26.887 | 12.48 | 23.740 | 46.23 | 28.659 |
| 15%SD | 5.019 | 25.079 | 14.01 | 26.650 | 31.95 | 19.807 |
| 20%SD | 4.883 | 24.399 | 11.85 | 22.541 | 53.30 | 33.042 |
| | | | | | | |
| Total | 20.013 | 100 | 52.57 | 100 | 161.31 | 100 |
| | Grass-based co-firing | | | | | |
| Coal A | 4.730 | 31.698 | 14.23 | 29.739 | 29.83 | 13.817 |
| 10%GS | 3.375 | 22.618 | 11.67 | 24.389 | 55.87 | 25.878 |
| 15%GS | 3.521 | 23.596 | 11.04 | 23.072 | 63.65 | 29.481 |
| 20%GS | 3.296 | 22.088 | 10.91 | 22.800 | 66.55 | 30.824 |
| | | | | | | |
| Total | 14.922 | 100 | 47.85 | 100 | 215.90 | 100 |

measurements for a co-firing test are lower so much the better, but if they are high it doesn't necessarily indicate a problem. Ideally $CO_2$ emissions

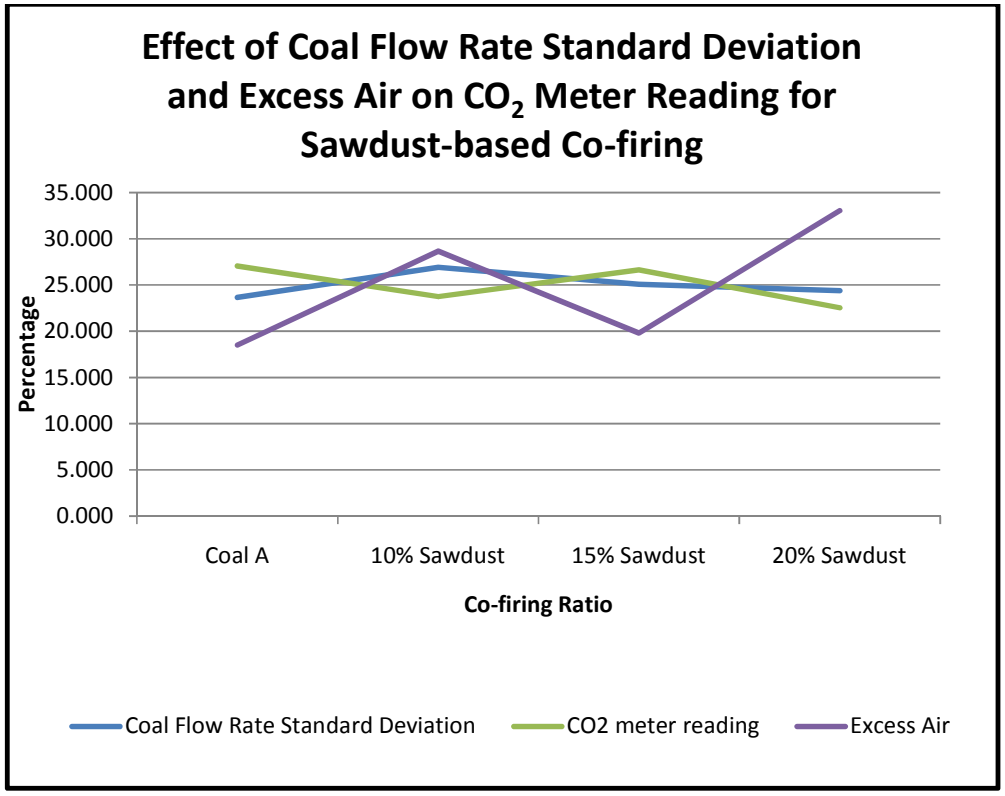


Figure 6.9 Effect of fluctuations in coal flow rate on $CO_2$ emissions and the actual excess air for sawdust-based co-firing.

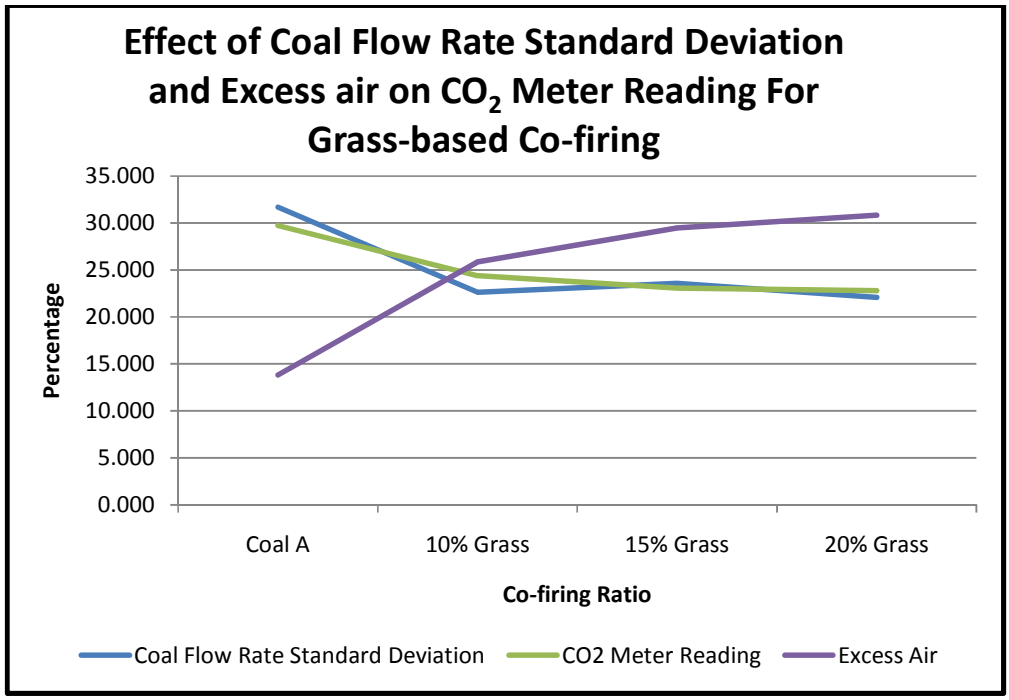


Figure 6.10 Effect of fluctuations in coal flow rate on $CO_2$ emissions and the actual excess air for grass-based co-firing.

would remain constant for a given power rating because most of the energy that results from combustion of fuel comes from the exothermic reaction of carbon and oxygen. In practice however this is not the case because of the changing plant parameters such as load, response time of the fuel feeder controller, combustion behaviour etc. When there is significant distribution of carbon to unburned-carbon-in-ash and CO, the $CO_2$ stack emissions can be below that which would be obtained form complete combustion of carbon. The fluctuations in the fuel supply dictate the profile of $CO_2$ emissions that can be the flue gas.

Fig 6.9 shows the influence of fuel flow fluctuations on $CO_2$ and excess air for sawdust-based co-firing. The fuel fluctuations which have already been discussed in section 6.1.3 have resulted in the profiles shown on Fig. 6.1. The impact is better illustrated by the excess air profile. When trying to operate at constant excess air ratio, the fluctuations in fuel ratio will be reflected by excess air. For instance if excess oxygen is set at 6% ( about 40% excess air) and the fuel supply is above target value, the extra fuel supplied will consume some of the oxygen and reduce the amount of excess oxygen and at the same time produce extra $CO_2$. On the other hand, if fuel supply is below the target, excess oxygen will exceed the set target (6%) because of the oxygen which was not used and $CO_2$ will drop. Since $CO_2$ varies inversely with excess air, the curve of excess air will almost look like a reflection of $CO_2$ profiles as shown in Figs 6.9 and 6.10. So the unexpected behaviour of $CO_2$ levels at 10% and 15% co-firing ratio were due to fluctuations in coal and biomass flow rates. These data were treated as outliers and were disregarded from the conclusions drawn which were based on 20% co-firing ratio only.

The profiles for repeated tests however show an increasing trend and are proportional to the co-firing ratios. This can be expected because the standard deviation of coal supply in Table 6.4 shows little fluctuations. The

upward trend is due to concentrating effect of decreasing trend of excess air which make it appear as if it is increasing.

For the grass-based co-firing there was a steady supply of fuel and the $CO_2$ profiles in Fig. 6.2 show a decreasing trend which is proportional to the co-firing ratio. The reduction in stack $CO_2$ emissions are as follows: 18%, 22% and 23% at 10%, 15% and 20% respectively.

As far as the gaseous emissions are concerned in general, grass seems to perform better than sawdust.

### 6.1.5 Ignition Behaviour Shown by the Results from the ERID/ESKOM Pilot Scale Combustion Test Facility

Figures 6.11 to 6.13 show the flue-gas temperature profiles and the combustion efficiencies of the fuels combusted at the PSCTF. For grass based co-firing, the combustion efficiency of the coal used was improved by 0.55% and 0.62% for 15% and 20% co-firing ratios respectively; whereas that of sawdust was between 0.78% and 0.38% as co-firing ratio was increased from 10% to 20%. Combustion efficiency for 10% grass dropped by 0.65%. The rapid release of volatiles from biomass particles at the early stage of combustion has resulted in the improved ignitability of the coal, which would otherwise take longer to burn. For both biomass types, there is a decrease in gas temperature when co-firing as compared to the baseline.

The temperature profiles of grass-based co-firing (Fig. 6.6) indicate a decrease in flame temperature as the co-firing ratio is increased. The decrease of gas temperature as a function of co-firing ratio for sawdust is not as clear as that of grass (Fig. 6.4). The decrease in gas temperature is due to excess air and the moisture content of the biomass.

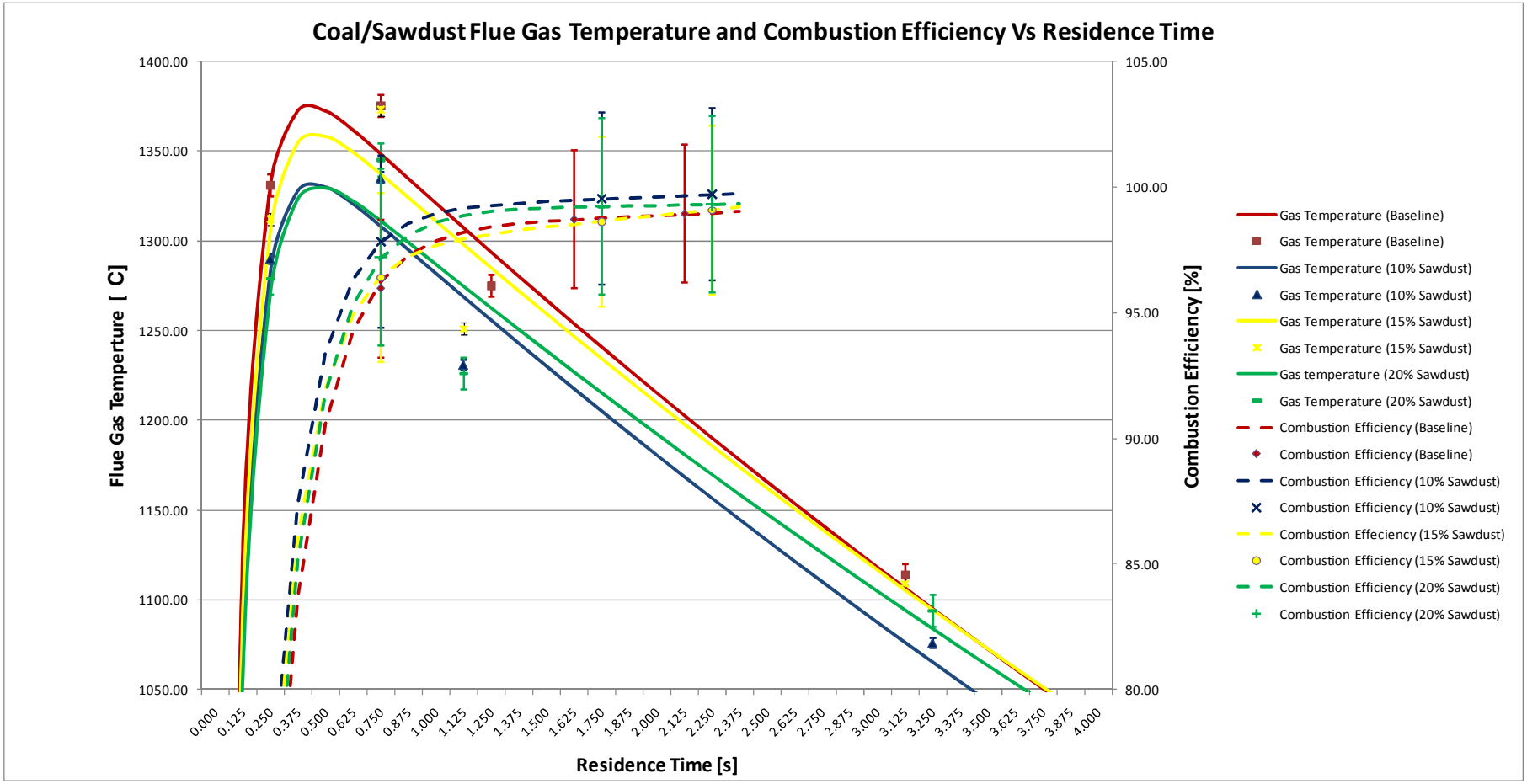


**Figure 6.11** Effect of sawdust on flue gas temperature profiles and combustion efficiency (Original Test nos. 11, 13-15)

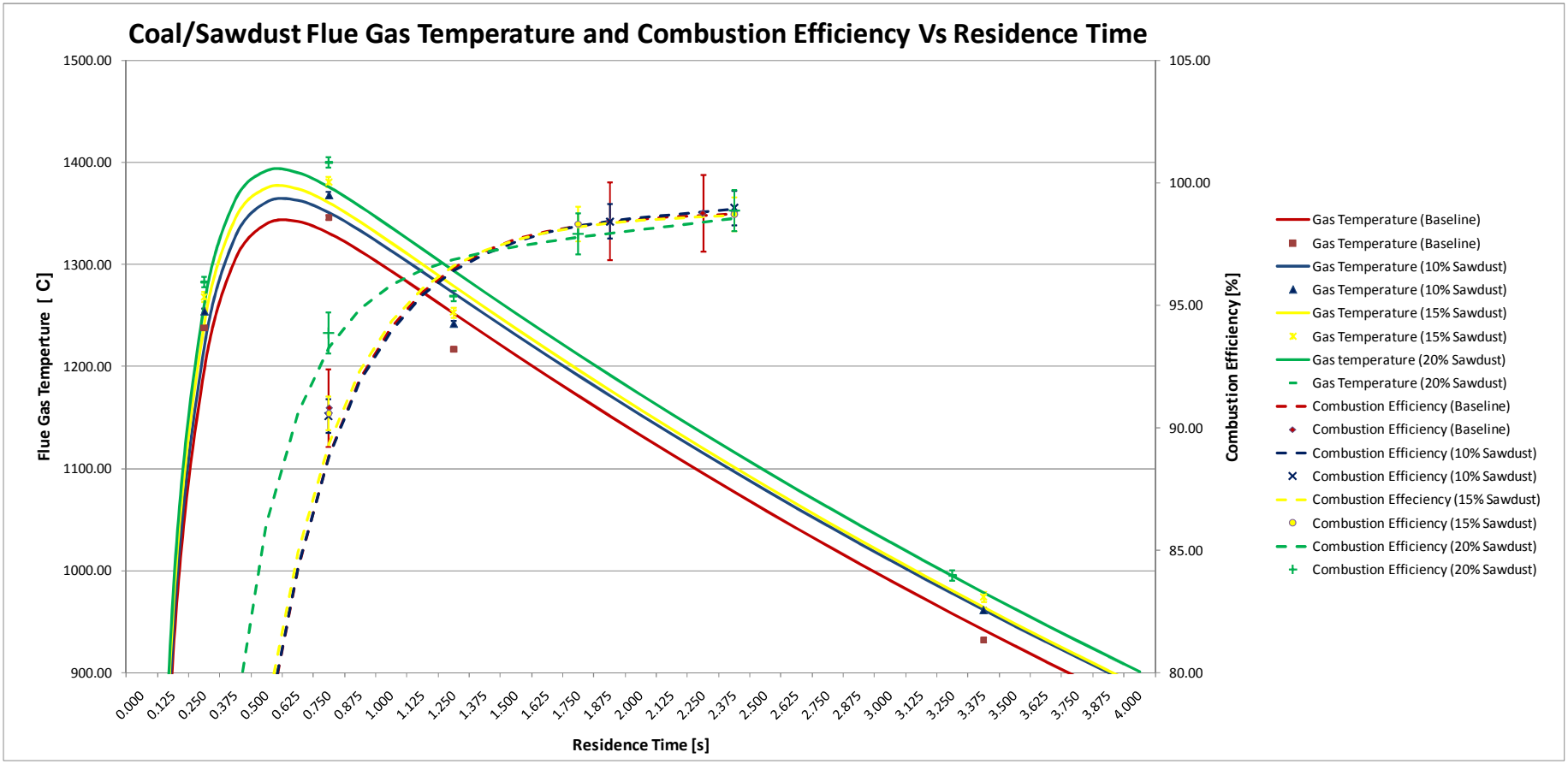


**Figure 6.12** Effect of sawdust on flue gas temperature profiles and combustion efficiency (Repeated Test nos. 1-4)

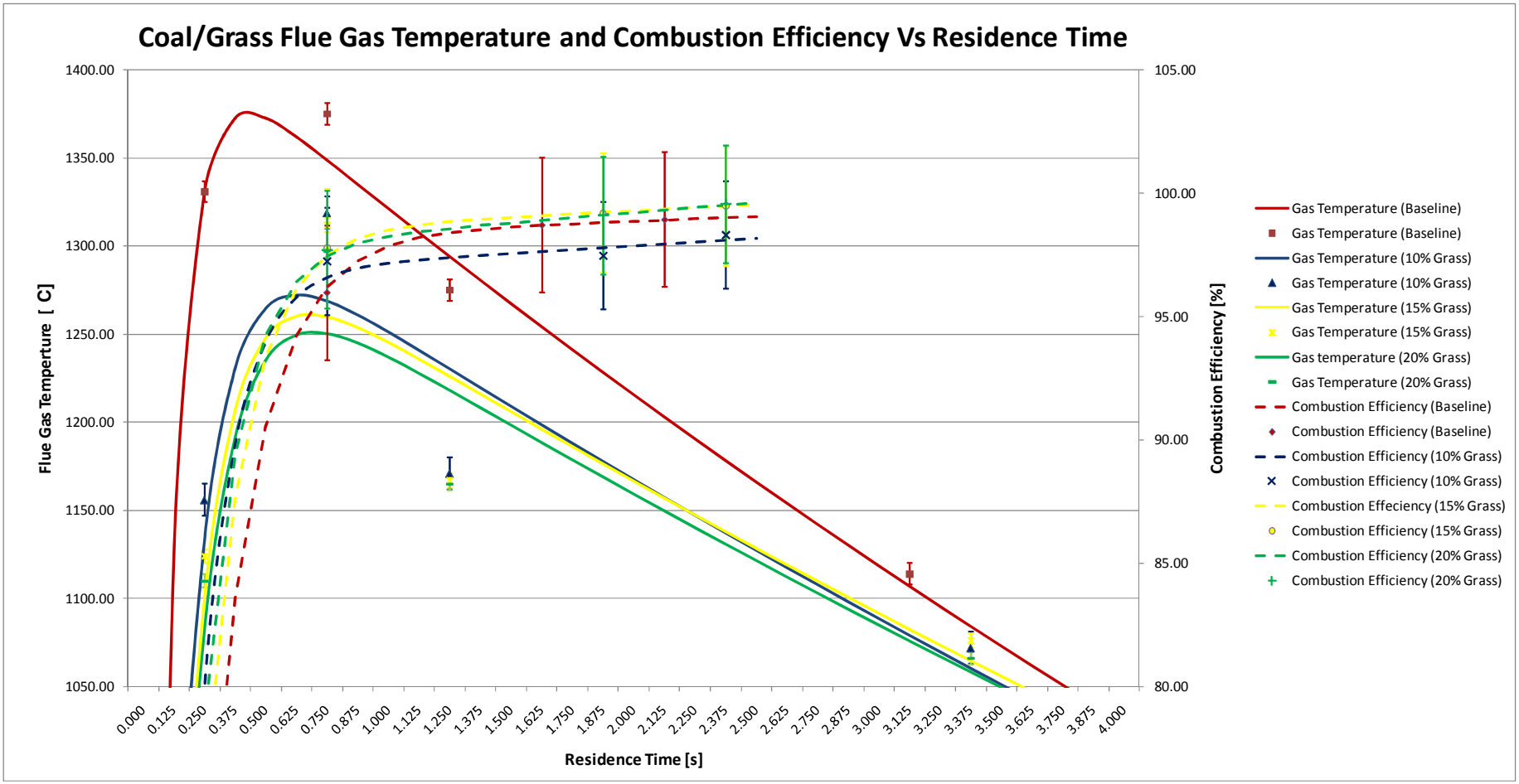


**Figure 6.13** Effect of grass on flue gas temperature profiles and combustion efficiency (Original test nos. 11, 16-18).

Although a decrease in temperature is good for $NO_x$ control and slagging, it could have negative effects on the rate of carbon burnout and the amount of unburned carbon-in- ash. Biomass however is able to ignite the whole fuel body due to its relatively lower pyrolysis temperatures (Vamvuka et al, 2006; Kastanaki et al, 2006). The macromolecular structure of biomass is made up of polymers of cellulose, hemicelluloses and lignin which are linked together by weak bonds (bond energy of 380-420 kJ/mol). These bonds are less resistant to heat at low temperatures (400-500 ℃), in contrast to more resistant coal which consists mostly of polycyclic aromatic hydrocarbons linked together by aromatic (C=C) bonds with bond energy of 1000kJ/mol (Vuthaluru, 2004).

Despite the low temperature, the early and rapid release of volatiles increases the rate of carbon burnout near the flame zone, this is indicated by the fact that all grass co-firing ratios indicate higher combustion efficiency at port 9 (see Table 4.6 for port layout information) than that of coal (Table 5.3 and Fig. 6.13). The combustion efficiency for 10 % grass at ports 15 and 21 however, is below that of coal. This may be attributed to the amount of volatiles in grass being used up quickly before they can sufficiently ignite the rest of the predominantly coal char at lower temperature than that of baseline coal. For 15% and 20% grass the carbon burnout is higher than that of the baseline coal. This is so because the decreasing amount of coal and increasing amount of biomass in the burning fuel, associated with these co-firing ratios, releases enough volatiles to ignite the rest of the fuel. It has to be noted that 15% grass gives a better carbon burnout than 20% grass and this would suggest that there is an optimum point between 10% and 20% grass. This can be expected because higher co-firing ratios would mean lower flame temperature and although there would be more volatiles, it would be increasingly difficult to break the bonds as the temperature drops, and as a result a drop in carbon burnout can be expected.

The combustion profiles for the original sawdust tests (Fig. 6.4) indicate better burnout rate than that of the baseline coal and better than that of grass-based co-firing. This is apparently contrary to the PSCTF results (Figs. 6.7-6.12) which indicate that grass-based co-firing has a better burnout than that of sawdust. This discrepancy can be explained in terms of the particle size distribution of the biomass fuels co-fired at the Pilot Scale Combustion Test Facility (Table 4.3). Sawdust has finer particles than those of grass. The relatively large aspect ratio of grass particles combined with larger particle sizes slows the rate of carbon burnout. Particles with higher aspect ratio tend to burn first and fast on the edges and slowly towards the belly. The bigger particle size would be typically the case in commercial power stations, because the cost of higher size reduction is prohibitive. In the case of DTF feed fuels size reduction is required to be below 150 µm which can be easily achieved for smaller quantities (about 500g) of feed fuels. In this case, the very thin, less dense grass particles with reduced aspect ratio burn better than dense sawdust particles.

There is also a noted decrease in combustion efficiency for the repeated tests Fig. 6.12, compared with the tests that were run earlier, Fig. 6.11. This reduction might be due to lack of air for complete combustion coupled with short residence time.

### 6.1.6 Ignition Behaviour shown by DTF results

The ignition parameters: volatile matter as determined by DTF ($VM_{DTF}$), calorific value of the volatile matter ($CV_{vm}$), heat in volatiles (HIV) and energy ratio were used to assess the ignition properties of the fuels burned. These parameters were calculated using the respective moisture content, ash content and calorific values of fuel (Table 5.8) and char (Table 5.9). Energy ratio is the ratio of the amount of energy required for

ignition relative to the amount of energy being liberated during combustion (Wagner, 2008). Table 6.7 displays ignition parameters for the seven tests conducted on the DTF. $VM_{DTF}$ gives a better representation of the volatiles that will be released in full scale boiler than the volatile matter indicated by the proximate analysis. From Eskom coal characterisation database, $VM_{DTF}$ ranges from 20% to 35% with an average of 27%, the $CV_{vm}$ has an average value of 26 MJ/kg and ranges from 17 to 30 MJ/kg while HIV has an average value of 36% with a lower boundary of 20% (Wagner, 2008).

Table 6.7 Ignition parameters of the fuels combusted in the DTF

| **Ignition Parameter** | **Unit** | **100% Coal (T1)** | **10% Sawdust (T2)** | **15% Sawdust (T3)** | **20% Sawdust (T4)** | **10% Grass (T5)** | **15% Grass (T6)** | **20% Grass (T7)** |
|---|---|---|---|---|---|---|---|---|
| **Volatile Matter by DTF ($VM_{DTF}$)** | % | 30 | 39.2 | 41.5 | 43.5 | 37.4 | 40.2 | 43.8 |
| **Calorific Value of Volatile Matter ($CV_{VM}$)** | MJ/ kg | 24.1 | 23.8 | 23.2 | 22.1 | 24.4 | 22.7 | 22.0 |
| **Heat in Volatiles (HIV)** | % | 33.5 | 44.1 | 45.5 | 45.6 | 43.2 | 43.1 | 46.0 |
| **Activation Energy ($E_a$ )** | kJ/ mol | 73.0 | 66.8 | 65.7 | 72.7 | 69.0 | 70.2 | 62.5 |
| **Energy ratio ($E_r$)** | - | 3.1 | 5.2 | 5.7 | 5.2 | 4.8 | 4.9 | 6.2 |
| **Burnout time ($B_t$)** | s | 1.1 | 2.6 | 2.5 | 1.5 | 2.5 | 2.4 | 1.7 |

$E_a$ in excess of 100 kJ/mol indicates unstable ignition properties (Wagner, 2008) and $E_r$ which is less than 1 indicates poor ignition because of inadequate energy available in volatiles to support ignition (Twala in Wager, 2008). Burnout time is the time required to achieve 98% combustion efficiency at 1400 ℃. Burnout time in excess of 3 sec leads to boiler problems and poor combustion efficiency (Wagner, 2008).

**Sawdust-based blends Ignition**

For sawdust/coal blends tests (2-4), $VM_{DTF}$ increases with the co-firing ratio and it is higher than that of the coal alone for all sawdust-based co-firing ratios (Table 6.7). With $VM_{DTF}$ used as ignition indicator, it shows that sawdust/coal blends would have better ignition than coal alone and the ignition would improve with increasing co-firing ratio when fired in a boiler. CVvm decreases with the co-firing ratio and it is below that of coal for all sawdust/coal blends (Table 6.7). The CVvm values obtained indicate that 100% coal will burn better than its blends with sawdust. All CVvm values including that of 100% coal (tests 1-4) are below Eskom's average of 26 MJ/kg (Wagner, 2008) but are still within the set criterion. HIV increases with co-firing ratio and is higher than that of baseline for all sawdust/coal co-firing ratios. The values of HIV for the blends are above Eskom average and indicate that the sawdust blends have better ignition properties than those of coal alone.

Energy ratio for tests (1-4) is above 1. The variation of energy ratio (Er) with increasing co-firing ratio is not clear but for all sawdust based co-firing ratios, Er is higher than that of the baseline (Table 6.7).

Burnout time decreases with co-firing but for all sawdust based co-firing ratios it is longer than that of coal alone. The burnout time for 20% co-firing ratio is notably shorter than that of the other two co-firing ratios

suggesting that higher co-firing ratios could result shorter burnout times. For tests 1-4, burnout time is less than 3 sec.

**Grass-based blends Ignition**

For grass/coal blends tests (5-7), $VM_{DTF}$ increases with the co-firing ratio and it is higher than that of the coal alone for all grass-based co-firing ratios (Table 6.7). This shows that grass/coal blends would have better ignition than coal alone and the ignition would improve with increasing co-firing ratio when fired in a boiler. The amount of $VM_{DTF}$ however is generally less than that of sawdust-based cofiring. $CV_{vm}$ decreases with the co-firing ratio and it is below that of coal for all grass/coal blends except for the 10% grass blend (Table 6.7). The $CV_{vm}$ values obtained indicate that ignitability will deteriorate more steeply as co-firing rate is increased, compared to sawdust. All $CV_{vm}$ values including that of 100% coal (tests 5-7) are below Eskom's average of 26 MJ/kg (Wagner, 2008) but are still within the set criterion. HIV increases with co-firing ratio and is higher than that of baseline for all grass/coal co-firing ratios. The values of HIV (Table 6.7) for the blends are above Eskom average and indicate that the grass blends have better ignition properties than those of coal alone. HIV values for grass are generally lower than those of sawdust.

Energy ratio for tests 5-4 is above 1. The energy ratio ($E_r$) increases with co-firing ratio and for all grass based co-firing ratios, $E_r$ is higher than that of the baseline (Table 6.7). For the first two co-firing ratios (tests 5 and 6) $E_r$ is lower than that of sawdust but for the last co-firing ratio (test 7), $E_r$ is significantly higher than that of sawdust. This can be attributed to variation in activation energy ($E_a$) since $E_r$ depends on $E_a$.

Burnout time decreases with co-firing ratio, but for all grass based co-firing ratios it is longer than that of coal alone. The burnout time for 20% co-firing ratio is notably shorter than that of the other two co-firing ratios. For

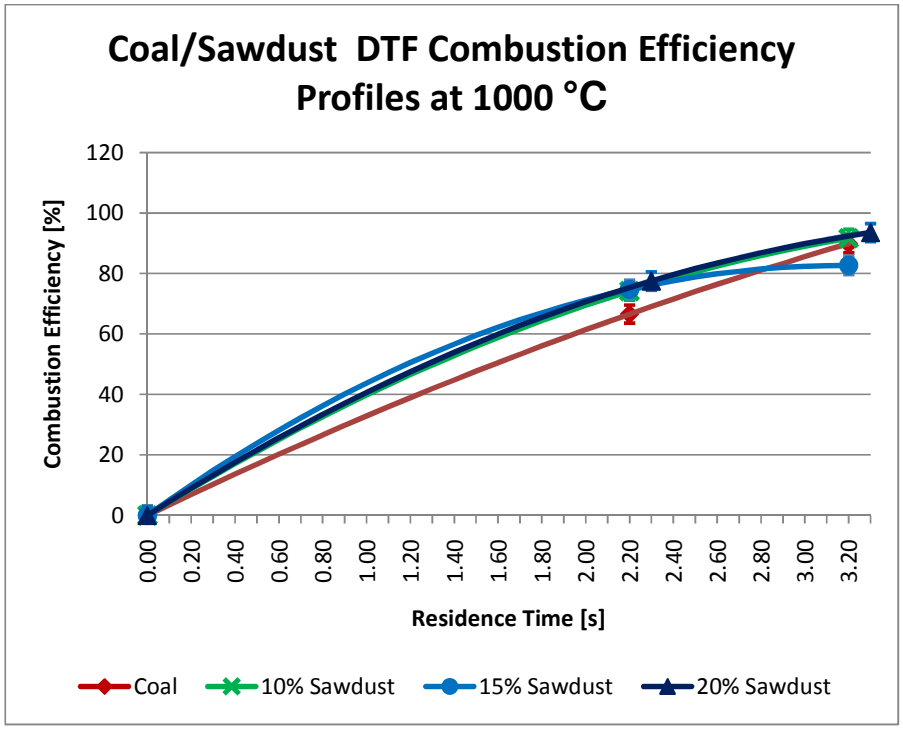


Figure 6.14 Sawdust based co-firing burnout profiles from the DTF at 1000 ℃

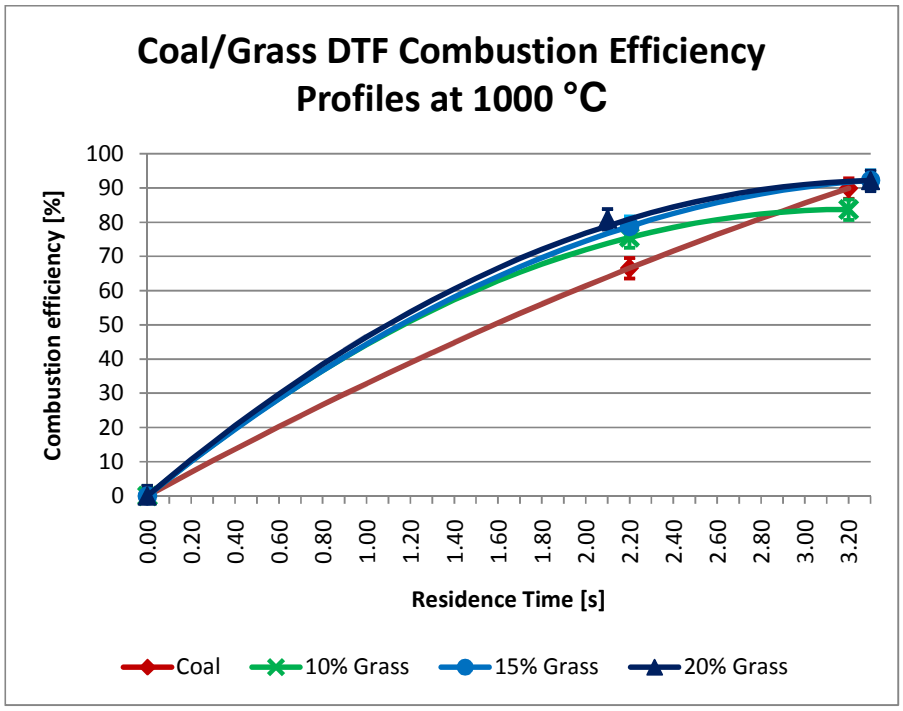


Figure 6.15 Grass-based co-firing burnout profiles from the DTF at 1000

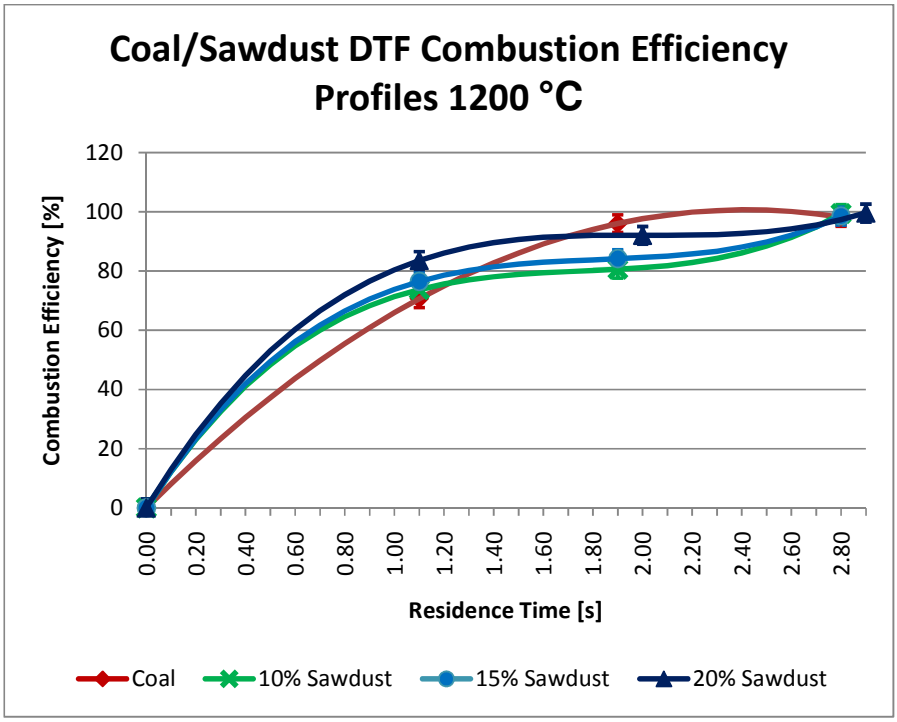


Figure 6.16 Sawdust based co-firing combustion efficiency profiles from DTF at 1200 ℃

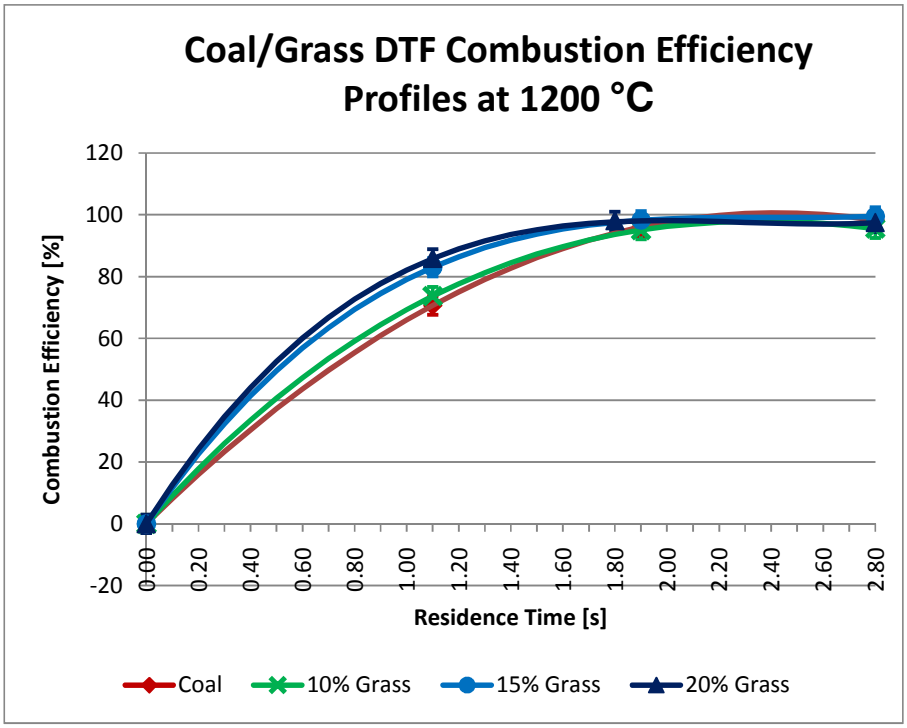


Figure 6.17 Grass based co-firing combustion efficiency profiles from DTF at 1200 ℃

tests 5-7, burnout time is less than the set standard of 3 sec. Burnout times for grass-based co-firing are slightly lower than those of sawdust for 10% and 15% co-firing ratios suggesting that grass is slightly more reactive than sawdust.

As far as the ignition parameters considered above are concerned, sawdust/coal blends show better ignition properties than those of grass although grass is more reactive than sawdust. These observations should be considered together with the behaviour of combustion efficiencies considered next.

**Combustion efficiency profiles**

Table 5.11 shows the combustion efficiencies at each of the probe positions as explained in section (4.3.2). The combustion efficiency profiles were generated from these figures (Table 5.11) by fitting the best curve (using Matlab) through them. An exponential curve fitting algorithm of the form $y=ae^{bt}+ce^{dt}$ was the one found to give the best fit, where a,b,c and d are the coefficients and t is the residence time (calculated in Appendix J) as shown in the sample calculation in section 4.3.4. Such curves are shown on Figs. 6.14-6.19. Each curve has three points beside the origin. These points represent in the order from left to right, the combustion efficiencies at P5, P3 and P1 respectively.

Fig. 6.14 and 6.15 show the burnout/combustion efficiency profiles at 1000 ℃ for sawdust/coal and grass/coal blends respectively. At this temperature, grass and sawdust show better carbon burnout than coal at P3 for all blends due to reactivity of biomass in the blends. At P1 however, for one blend in each case, burnout falls below that of coal. These are 15% sawdust and 10% grass. The reasons for this drop are not obvious.

Sawdust profiles at 1200 ℃ (Fig. 6.16) show better carbon burnout than that of coal at P5 for all its blends with coal. At P3 however, the burnout is below the baseline for all blends. Coal and all blends have nearly the same combustion efficiency at P1. This would suggest that the rate of char reaction for the sawdust/coal blends is inhibited by certain factors at high temperatures. There are several possible methods by which mineral matter can inhibit combustion. The most common mechanism is, the presence of an inorganic-rich layer on the char surface acting as a barrier of oxygen diffusion to the reacting surface. This layer of ash may form when the char is oxidized on or near the external surface of the particle, leaving behind the mineral constituents on the char surface (Lunden, et al,1998,Li,et al, 2009);

When char conversion occurs below ash flow temperatures, the char transforms to dry unmelted ash particles, whereas when the temperature is above the ash flow temperature, the char transforms to a molten slag in the late stage of char oxidation (Li et al, 2009). At the early stages of combustion, the included minerals in the char matrix are shielded from the high temperature by carbon because carbon does not melt at typical combustion temperatures. During the late stages of combustion (about 80% conversion), when almost all carbon has been converted, the included minerals appear on the surface of the char and are no longer protected by the residual carbon in the char particle. The included minerals get exposed to the high temperature and melt (Li et al, 2009), forming a microscopic ash film that blocks oxygen access to active carbon sites and reducing the total available carbon per surface area in the char matrix (Lunden et al, 1998).

The situation for grass (Fig. 6.17) at 1200 ℃ however is different in that it has better carbon burnout than baseline at positions P5 and P3 and nearly the same as that of baseline at P1 for all co-firing ratios. Grass blends at this temperature are not as negatively affected as those of

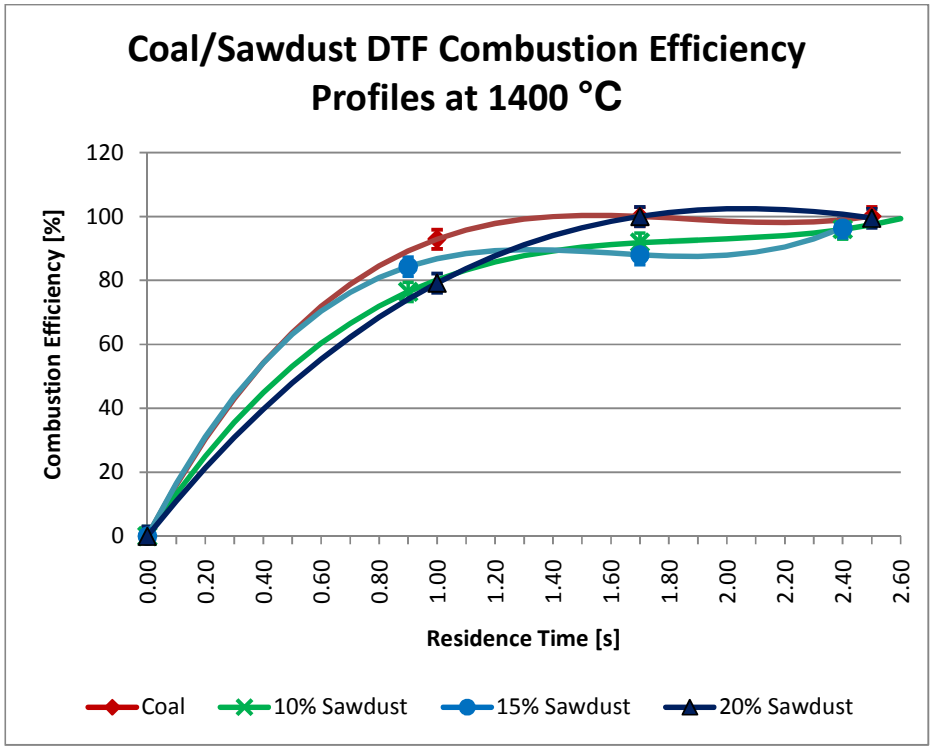


Figure 6.18 Sawdust based co-firing combustion efficiency profiles from DTF at 1400 ℃

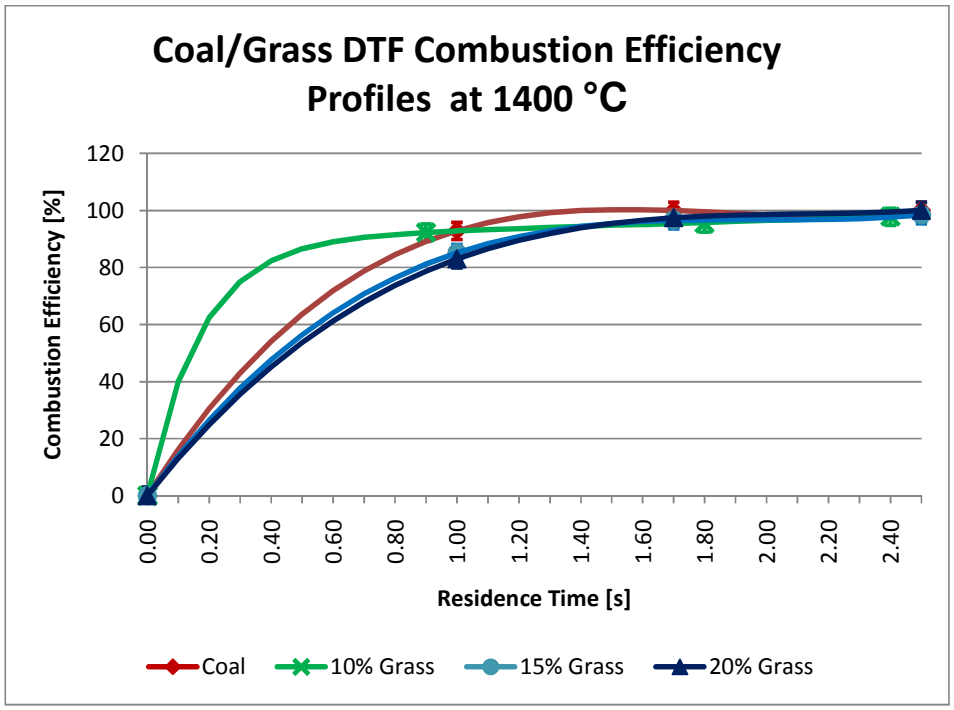


Figure 6.19 Grass based co-firing combustion efficiency profiles from DTF at 1400 ℃

sawdust due to comparatively low amount of fluxing elements in grass. At this temperature carbon burnout increases with increasing co-firing ratio for both biomass blends.

The behaviour of combustion efficiency observed in Figs 6.16, 6.18 and 6.19 indicate the influence of high temperature on the char-slag transformation. The addition of biomass lowers the ash fusion temperatures of the coal due to increased fluxing agents (Ca, Fe, Na and K). This is more so for sawdust-based co-firing as the amounts of Ca ,Fe and Na are higher than those in grass-based co-firing. Although from Table 5.1 grass has more potassium than sawdust, it has lower Fe, Na and much less Ca than sawdust. Unlike sawdust, grass has much more Si which tends to increase ash fusion temperatures.

The combustion efficiency profiles indicate that grass/coal blends burned more efficiently than those of sawdust. Although sawdust/coal blends showed better ignition properties than grass/coal blends, the fluxing elements in sawdust had a dramatic effect in the combustion efficiency of these fuels due to partial or total carbon encapsulation by molten ash.

### 6.1.7 Analysis of slag deposits

Ash samples collected from ports 9, 15 and 21 for test nos. 11,13-18 and slag deposit samples for test nos. 14 – 18 were submitted to Van Alphen Consultancy for detailed mineralogical analysis using QEMSCAN. QEMSCAN is a Scanning Electron Microscope (SEM) based system which is configured to automatically quantify and qualify the mineral and amorphous phase proportions in fuel, fly ash and clinkers. The mineral and amorphous phase discrimination is based on the elemental proportions (van Alphen, 2008). The slag deposits for Test no. 11 (coal A)

and Test 13 (10% sawdust) as well as fouling deposits for all tests could not be sampled (See section 5.2).

The chemical analysis data (5.1) obtained was used to predict the mineralogy of the samples (Table 6.8). The mineral prediction is a normative calculation based on the known mineral composition of South African coals (van Alphen, 2008).

Table 6.8 Calculated normative mineral proportions based on chemical analysis (van Alphen, 2008)

| Estimated Mineral Proportions | Formula | Coal A | Sawdust | Grass |
|---|---|---|---|---|
| Pyrite | $FeS_2$ | 2.9 | 0.08 | 0.09 |
| Calcite | $CaCO_3$ | 1.7 | 0.5 | 0.00 |
| Dolomite | $CaMg(CO_3)_2$ | 3.4 | 0.00 | 0.7 |
| Apatite | | 0.4 | 0.06 | 0.2 |
| Microcline | | 0.2 | 0.1 | 0.7 |
| Muscovite/illite | | 1.1 | 0.6 | 4.4 |
| Kaolinite | $Al_2Si_2(OH)_5$ | 17.4 | -0.2 | -2.66 |
| Quartz | $SiO_2$ | 2.3 | 0.00 | 4.3 |
| Siderite/Fe-oxide | $FeCO_3$ | 0.00 | 0.1 | 0.00 |
| Rutile | $TiO_2$ | 0.4 | 0.6 | 0.00 |
| Coal | C,O and H | 70.2 | 98.15 | 92.28 |
| Total mineral matter | | 29.8 | 1.85 | 7.72 |
| Mineral volatiles | | 6.46 | 0.33 | 0.46 |
| Ash% (DB) – calculated | | 23.34 | 1.53 | 7.26 |
| Ash% (DB) – measured | | 23.85 | 1.38 | 6.50 |

Coal A is characterised by a high proportion of kaolinite, and a lower proportion of dolomite, pyrite and quartz (Table 6.8).

Sawdust is characterised by a high proportion of calcite, rutile and muscovite/illite (Table 6.8). K is a common organically bound element in biomass, and it is unlikely that there are any K-bearing minerals (muscovite/illite and microcline) in the sawdust (van Alphen, 2008).

The grass is characterised by a high quartz and correspondingly high proportion of K-bearing minerals (Table 6.8). In sugar cane, amorphous $SiO_2$ in the cell cavity strengthens the plant. It is conceivable that grass will also have amorphous $SiO_2$ in this form. Quartz and kaolinite are common constituents of soil and will account for the comparatively high ash content of the grass. Potassium is probably organically bound and is unlikely to be in the form of K-bearing minerals (microcline and muscovite/illite) (van Alphen, 2008).

**Slag deposits from the sawdust-based co-firing**

The analysis of the slag obtained for 15% sawdust (Fig. 6.20) shows that it is a solid consolidated clinker deposit. Glass formed is predominantly Ca-Fe bearing aluminosilicate (see Table 6.9) derived from coalescence of pyrite, carbonates and kaolinite (Van Alphen, 2007). Glass refers to any phase which was molten at some stage. Si and Al are the basic constituents of the glass and occur in varying proportions. “Alumino” glass refers to a glass with similar Si and Al proportions, whereas quartz glass is a phase with a high Si content relative to Al. There is an evidence of crystallisation of anorthite which is indicative of sintering and cooling. This deposit is hard and will be difficult to remove by sootblowing (Van Alphen, 2008). It is conceivable that this deposit underwent rapid cooling and the anorthite crystallisation was halted (Van Alphen, 2008).

The slag obtained for 20% sawdust (Fig. 6.14) is different from that obtained for 15% sawdust. The difference between these two is the temperature each was subjected to. Fig 6.11 reveals that 15% sawdust slag was subjected to a much higher temperature than that of 20% sawdust. This might be due to the uneven supply of coal and biomass as already explained in section 6.1.3. Sawdust has a higher tendency to slag than grass due to its lower ash fusion temperatures. Compared to grass,

sawdust has very low ash content such that its tendency to slag is diluted by high ash content of coal (Zheng et al, 2007).

**Table 6.9** Clinker deposit mineral and phase proportions - volume % (van Alphen, 2008)

| | **15% SD T14** | **20% SD T15** | **10% GS T16** | **15% GS T17** | **20% GS T18** |
|---|---|---|---|---|---|
| Fe-oxide | 0.8 | 6.6 | 3.1 | 7.6 | 2.9 |
| CaOxide | 0.2 | 4.9 | 3.5 | 3.7 | 3.8 |
| CaMg-oxide | 0.0 | 0.4 | 0.4 | 0.5 | 0.8 |
| Quartz | 3.1 | 9.7 | 11.4 | 12.3 | 15.3 |
| Aluminosilicate (kaolinite) | 1.1 | 4.6 | 9.6 | 10.0 | 11.8 |
| K-aluminosilicate (muscovite/illite) | 0.0 | 0.4 | 1.2 | 1.4 | 2.7 |
| Quartz_Kaolinite | 0.9 | 0.3 | 0.4 | 0.5 | 0.7 |
| Alumino-glass (Ca-Fe, and Ca-bearingAluminosilicate glass) | 52.2 | 25.6 | 27.8 | 24.4 | 24.0 |
| Anorthite | 0.2 | 30.9 | 28.9 | 26.7 | 22.8 |
| Quartz_glass (Ca-Fe, and Ca-bearing Si Rich glass) | 39.6 | 15.7 | 13.1 | 12.1 | 14.7 |
| Rutile | 0.0 | 0.1 | 0.1 | 0.1 | 0.0 |
| Holes | 1.6 | 0.9 | 0.5 | 0.4 | 0.5 |
| Other | 0.1 | 0.1 | 0.1 | 0.1 | 0.1 |
| | 100 | 100 | 100 | 100 | 100 |

The 20% sawdust deposit is dominated by a high proportion of thin walled cenospheres, very much similar to grass slag deposits. The deposit has high proportions of Ca-Fe bearing alumino and quartz glass (see table 6.9). The slag is friable and should be easily removed by sootblowing.

Although the sawdust-based slag deposits had a comparatively higher proportion of fluxing element based aluminosilicates, the slag deposition rate was lower than the grass-based slag deposits. This is in part attributed to the comparatively higher ash percentage content of the grass compared to the sawdust and the higher proportion of “solid” ash particles (quartz, aluminosilicate, Fe-oxide and Ca/CaMg-oxide) in the grass-based slag deposits.

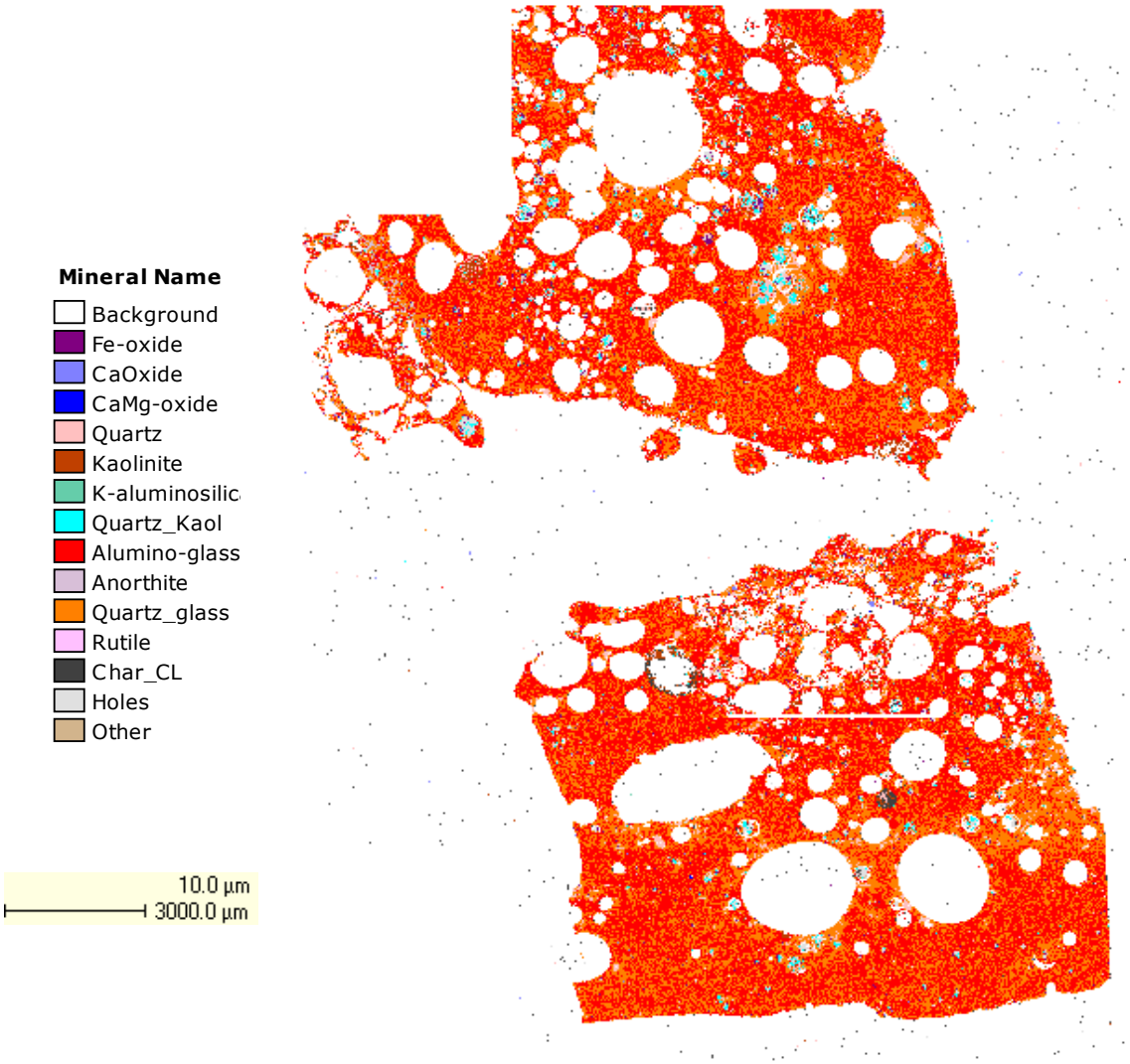


Figure 6.20 Test 14: 85% coal and 15% sawdust. Solid clinker samples dominated by Ca-Fe aluminosilicate and Ca-Fe quartz glass (van Alphen, 2008).

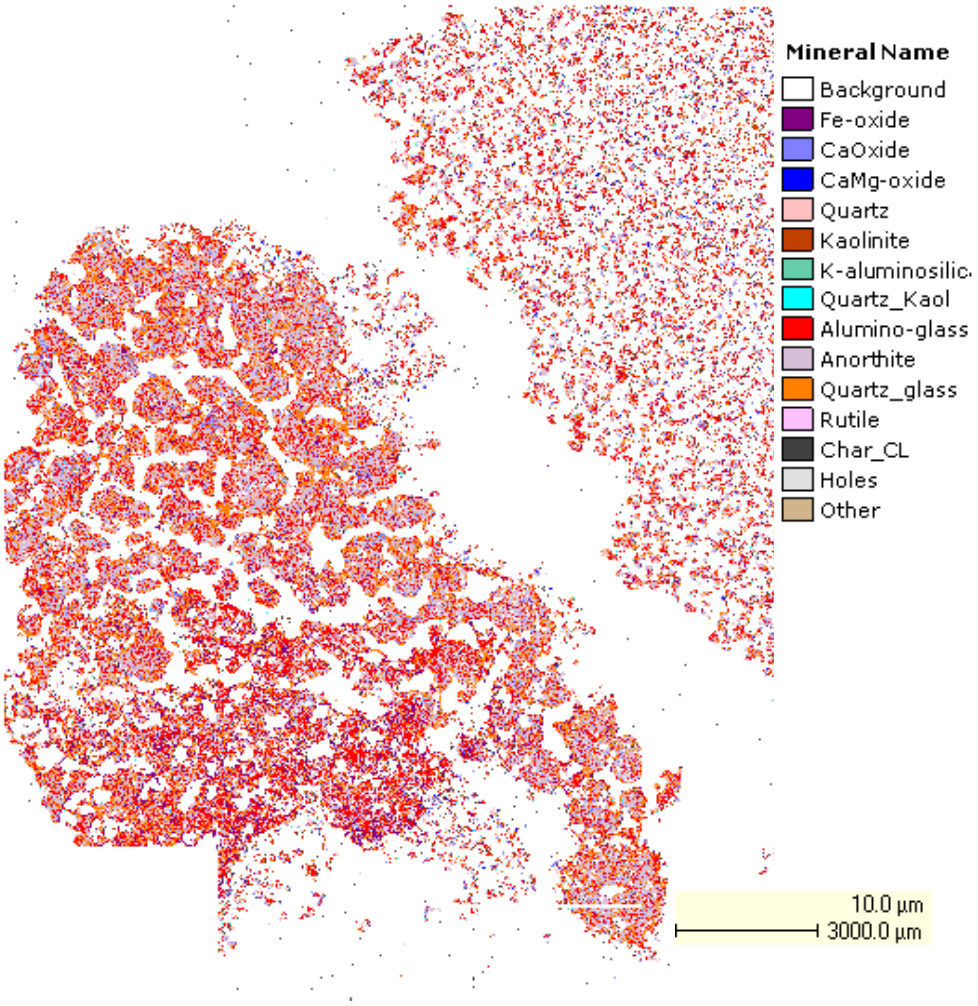


**Figure 6.21** Test 15 80% coal and 20% sawdust. Note the "consolidated" clinker deposit (bottom left) compared to the clinker deposit with a high proportion of voids (van Alphen, 2008).

The rate of deposition as a function of co-firing ratio could not be determined as the baseline and 10% sawdust slag deposit was not available. The rates of slagging for 15% and 20% co-firing ratios are 17.5 g/hr and 13.9 g/hr respectively (Table 5.3). Sawdust co-firing depicts powdery type deposit as well as molten fused type deposit. This results are in line with Annamalai et al, (2003).

**Slag deposits from the grass-based co-firing**

The slag deposits for 10% to 20% percent grass (Fig. 6.22), unlike those of sawdust, are similar. They consist of Ca-Fe bearing alumino and quartz glass but with a comparatively higher proportion of anorthite that has crystallised out of the melt. Discrete spherical Fe-oxide grains, angular

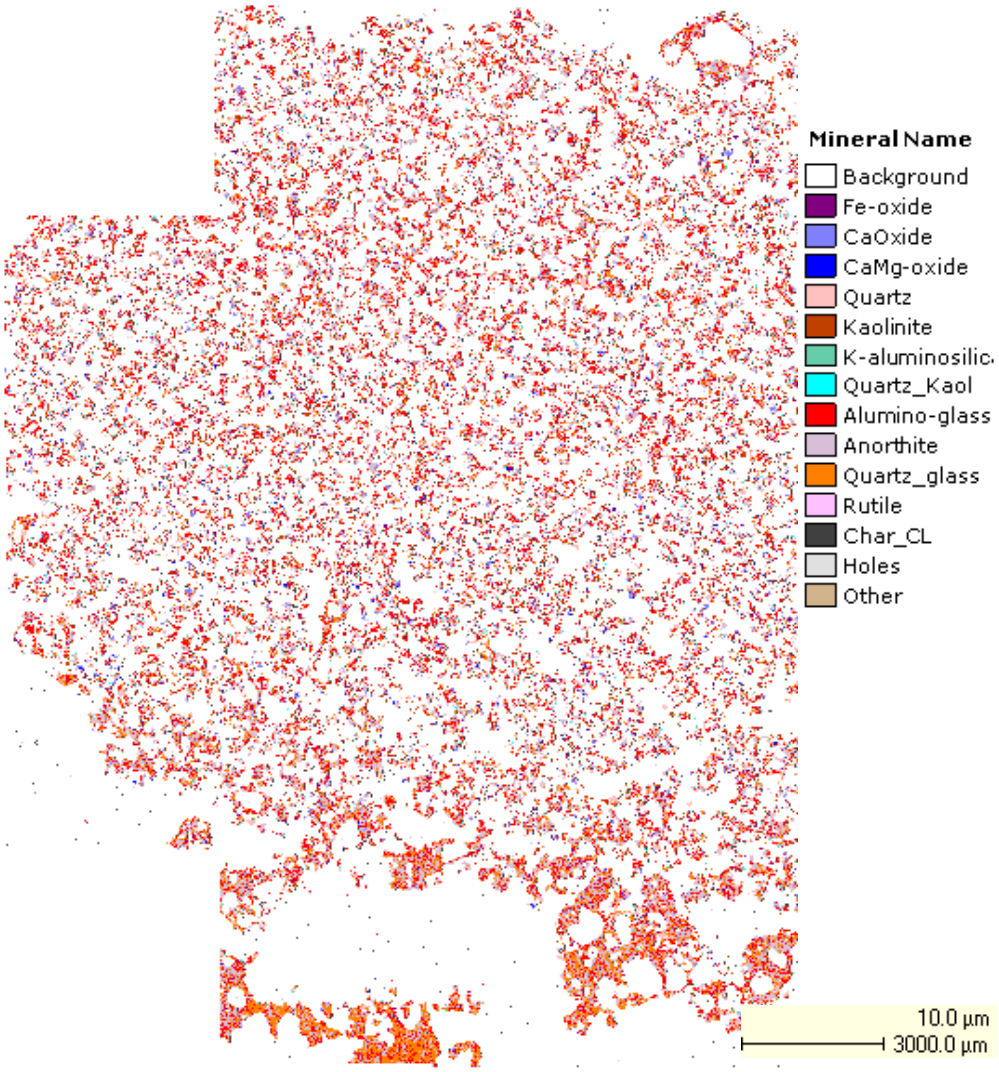


**Figure 6.22** Test 16: 10% Grass and 90% Coal. Clinker deposit mainly consists of thin walled- cenospheres. Consolidated clinker deposit appears at the bottom of the deposit (van Alphen, 2008).

quartz, aluminosilicate (kaolinite) and Ca-oxide/CaMgOxide grains encapsulated in the glass matrix are common (Fig.6.23). These are mainly derived from minerals in the coal and represent the transformation products of pyrite, quartz, kaolinite and carbonates (calcite/dolomite), respectively. A comparatively higher proportion of Fe-oxide, Ca-oxide, CaMg-oxide, quartz and aluminosilicate (kaolinite) has been observed. These are derived not only from coal minerals but from quartz and kaolinite in the grass as well. Quartz and kaolinite are common constituents of soil and will account for the comparatively high ash content of the grass.

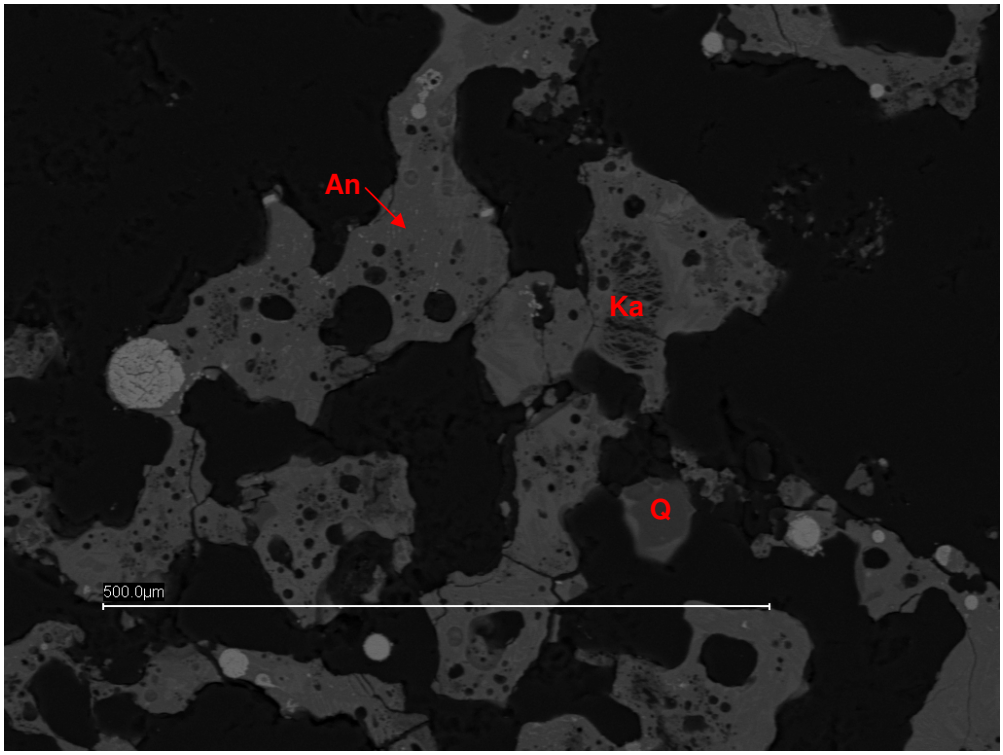


**Figure 6.23** Backscatter electron micrograph of T18 clinker deposit. Note the spherical Fe-oxide grains (light grey), angular quartz (Q), aluminosilicate (Ka) and anorthite laths in light grey "glass". Scale bar is 500 µm. The dark background is epoxy resin (van Alphen, 2008).

It is noted that there is a comparatively high proportion of anorthite relative to glass. This suggests that the deposits were not cooled rapidly, which facilitated anorthite crystallisation. This clinker deposit (Fig. 6.22) is

characterised by a high proportion of voids. It is friable and should be easily removed by soot blowing (Van Alphen, 2008).

The rates of slagging for grass-based co-firing for 10%, 15% and 20% co-firing ration were 31.3, 32.4 and 19.2 g/hr respectively. The deposits for 10% and 15% co-firing ratios slightly increase as the co-firing ratio increases. Zheng et al, (2007) report that deposition rate when ash content of baseline coal is high (>15%) deposition rate was constant. This argument might work for the first two co-firing ratios but not for 20% ratio which shows significantly low deposition rate. Grass has significant amount of potassium (Table 5.1) which would mean an increase in biomass share to 20% would increase slagging tendency as reported by some researchers (Heinzel et al,1998; Wigley et al, 2007; Annamalai et al, 2003a, Fradson, 2005; Pronobis 2005, Zheng et al, 2007) but increased potassium sometimes does not result in increased deposition Pederson et al, 1996). Grass has high fusion temperature owing to the high amount of silica in its ash (Table 5.1) and this coupled with the lowest gas temperature associated with 20% grass (Fig. 6.13), allowed a certain portion of ash not to melt thereby decreasing deposition efficiency. Grass has higher rate of slag deposition than that of sawdust due to relatively high ash content. The slag deposits of grass however are preferable because they are powdery and would be easily removed by soot blowing. Gil et al, (2009) also found soft deposits when co-firing cynara with South African coal.

These results (T14-T18) should be interpreted in the context of South African coal, bearing in mind that slagging is whole system specific. It is a function of coal mineralogy, mineral deportment (Van Alphen, 2007) and operating conditions of the boiler. Six groups of slag deposits have been identified for South African coals, namely, aluminosilicate with Al/Si ratio similar to kaolinite source with no fluxing elements(Ca, Fe, Mg, K and Na), Ca-Fe bearing aluminosilicate glass, K-bearing aluminosilicate glass,

quartz and Si-rich glasses (with minor proportions of Al,Ca, Fe and Mg), Ca(Mg)-rich oxides (with minor concentrations of Al and Si) and Fe-rich oxides with minor concentrations of Al and Si (Van Alphen, 2007).

## 6.2 Model validation

The results of the numerical simulation (Chapter 3) are compared with the actual experimental results to assess the accuracy of the predictions. Numerical simulation was used to predict the emissions ($CO_2$, $SO_2$ and $NO_X$) and temperature profiles.

### 6.2.1 Nitrogen Oxide ($NO_X$) Emissions

Fig. 6.24 shows $NO_X$ simulation profiles for sawdust-based co-firing. The trend of the predicted $NO_X$ emissions is similar to the experimental $NO_X$ but underpredicts it. The amounts of percentage difference for the tests between predicted and actual $NO_X$ emissions are 17% for baseline (coal A), 17% for 10% sawdust, 18% for 15% sawdust and 19 for 20% sawdust. The reason for the under prediction may be attributed to the excess air and fuel flow rate. In the model the flow rate is constant and perfect but in the experiment the supply of fuel fluctuates and is on average slightly above the set point (see section 6.1.3). There is no excess air provision in the model, the reactions are assumed to occur at stoichiometric conditions and yet in the experiment there is excess air and has influence on $NO_X$ (see section 6.1.1).

The predicted and experimental $NO_X$ emissions for grass-based co-firing are shown in Fig. 6.25. The trend of simulation is similar to that of experimental $NO_X$ emissions. The differences between predicted and experimental values are as follows: 17% for baseline (coal A), 3% for 10% grass, 11% for 15% grass and 21% for 20% grass. The reasons for the gap are the same as for sawdust that is excess air and fuel flow, only to the lesser extend for grass (Table 6.4).

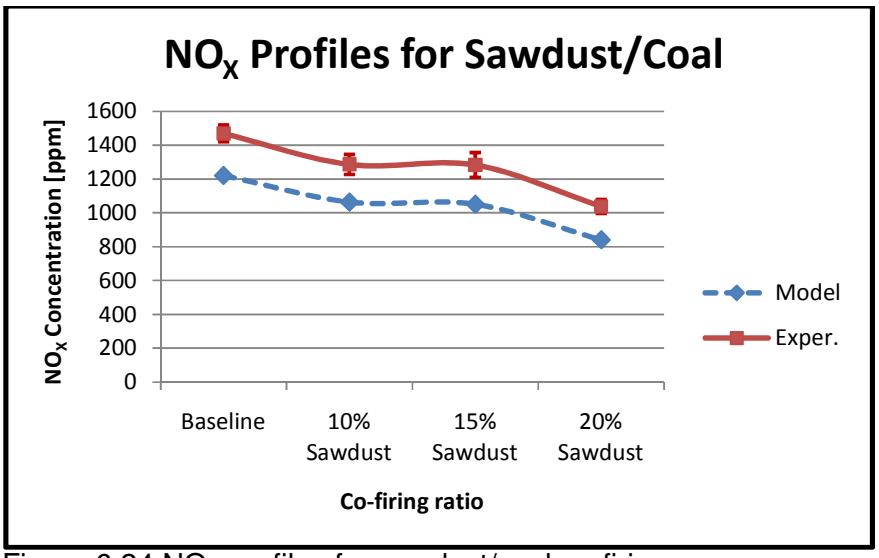


Figure 6.24 $NO_X$ profiles for sawdust/coal co-firing

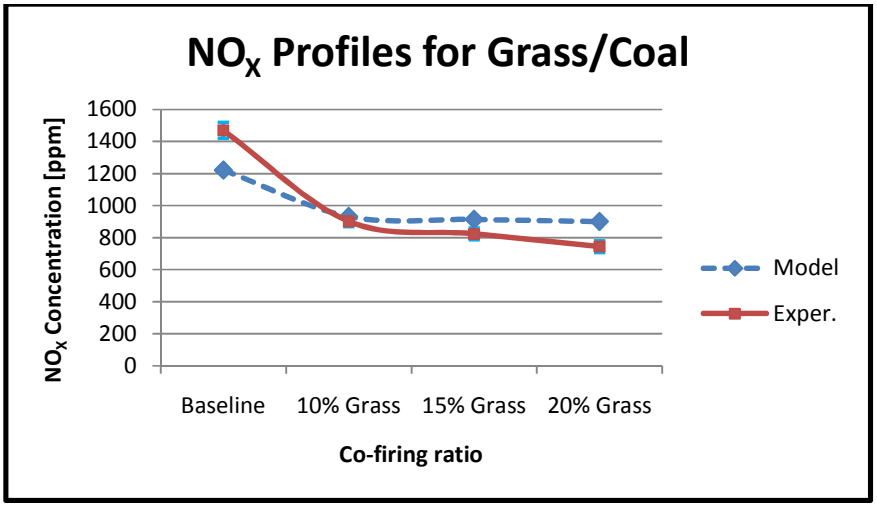


Figure 6.25 $NO_X$ profiles for grass/coal co-firing

The simulation results for both sawdust and grass based co-firing, show a trend that is similar to that of the experimental results and there is a good agreement with them. Profiles of sawdust are different from those of grass because sawdust has higher nitrogen content than that of coal whereas grass has lower nitrogen content than that of coal, hence there are more pronounced reduction effects for grass.

### 6.2.2 Carbon dioxide ($CO_2$) Emissions

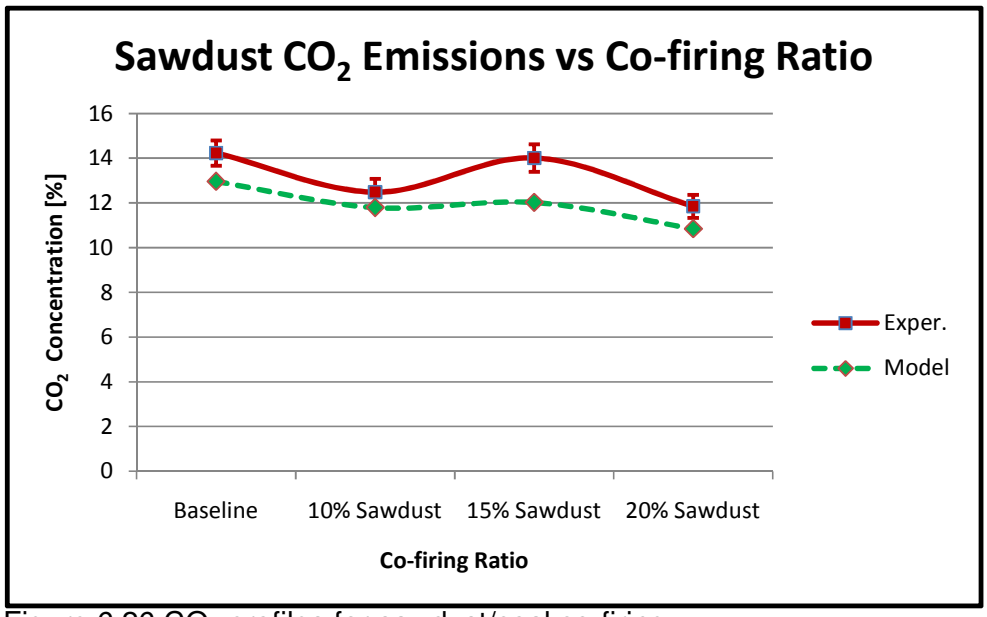


Figure 6.26 $CO_2$ profiles for sawdust/coal co-firing

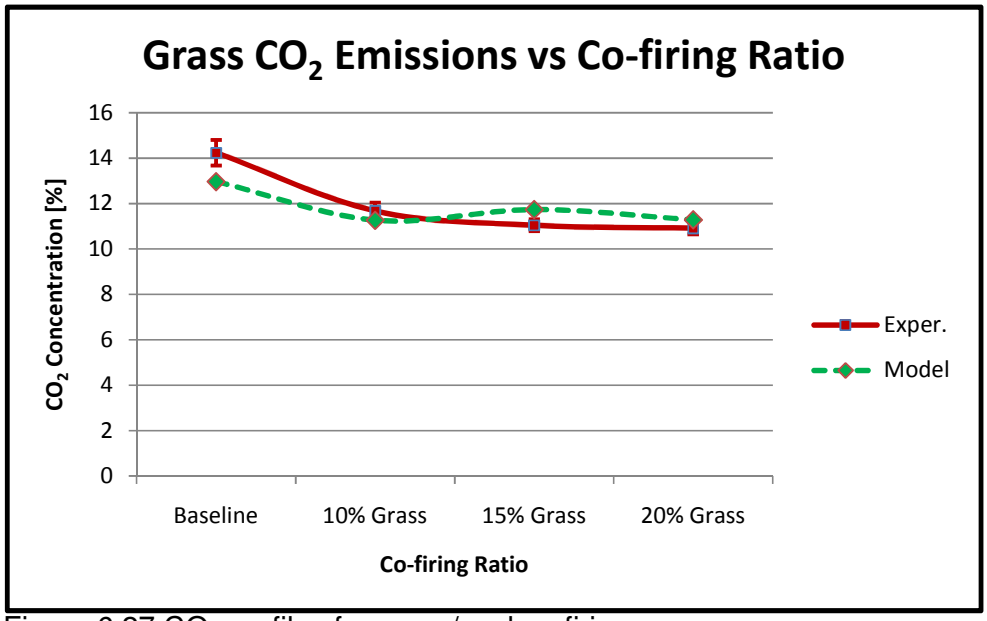


Figure 6.27 $CO_2$ profiles for grass/coal co-firing

Fig. 6.26 shows the comparison of predicted and experimental $CO_2$ emissions. The percentage differences are 9%, 6%, 14% and 9% for baseline (coal A), 10% sawdust, 15% sawdust, 20% sawdust respectively.

The biggest difference is corresponding to 15% sawdust which has already been explained in section 6.1.3 that it may be regarded as an outlier.

Fig. 6.27 shows the simulated $CO_2$ profiles plotted with those from experimental data for comparison. The differences in percentage are: 9%, 4%, 6% and 3% for baseline (coal A), 10% grass, 15% grass, 20% grass respectively. There is a very small margin between the two profiles and it can be said the prediction is good.

The model agrees with the experimental data in terms of the amount of concentrations predicted and the general trend of the profiles. With the exception of 15% sawdust it can be said that the predictions agree well with experimental results.

### 6.2.3 Sulphur Dioxide ($SO_2$) Emissions

The percentage differences between the simulated and experimental $SO_2$ emissions are as follows: 64%, 2%, 2% and 9% for baseline (coalA), 10% sawdust, 15% sawdust and 20% sawdust respectively (Fig. 6.28) and 64%, 40%, 46% and 37% for baseline (coalA), 10% grass, 15% grass and 20% grass respectively (Fig. 6.29).

Considering the $SO_2$ profiles for sawdust in Fig 6.28, one might be inclined to say that they agree well with the experimental results but it must be remembered that the experimental results for 10% and 15% sawdust themselves are suspect. Since the sulphur content of sawdust is less than that of coal, the overall effect should have resulted in lower $SO_2$ concentrations than those of the baseline. There is no reason to assume that 20% sawdust (Fig 6.28) has not been predicted correctly. If 10% and 15% were lower as already argued, it would be about the same margin as 20% sawdust from the predicted values. It has also been argued (section 6.1.3) that $SO_2$ readings for the baseline should have been higher, the

reasons for this low reading are not obvious. If that was the case, then the comparison with the model would be similar to that of Fig. 6.29 for grass except that the gap between predicted values and experimental ones would be small compared to those of grass.

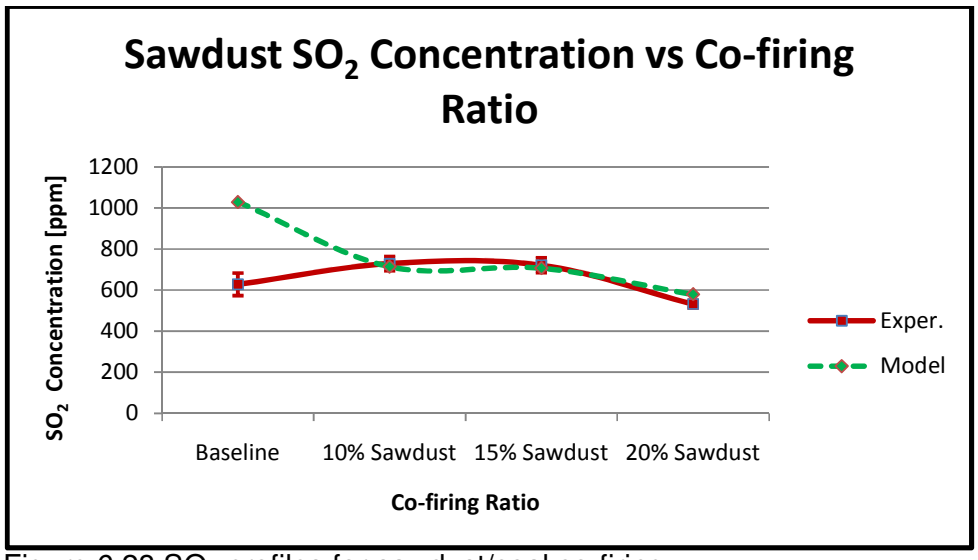


Figure 6.28 $SO_2$ profiles for sawdust/coal co-firing

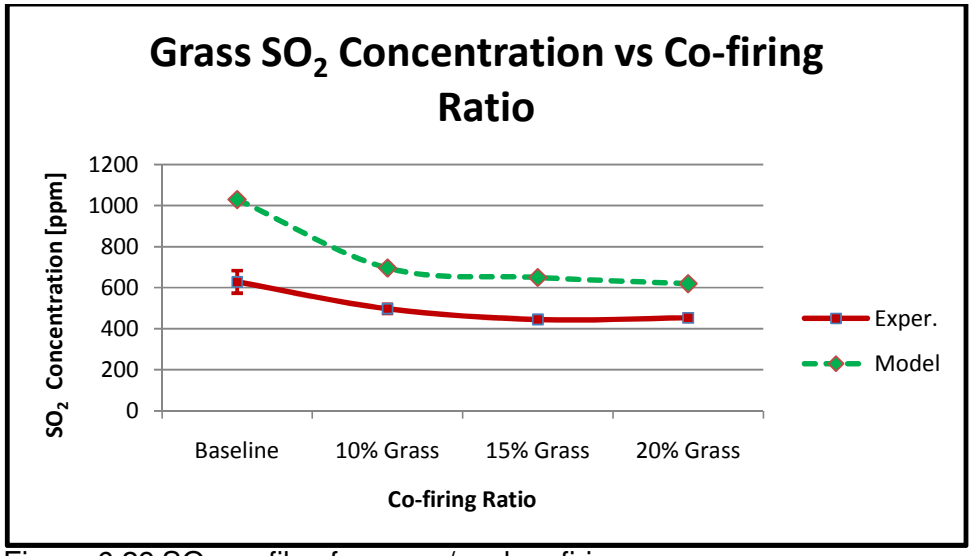


Figure 6.29 $SO_2$ profiles for grass/coal co-firing

Considering the $SO_2$ profiles for grass in Fig 6.29, the $SO_X$ model over-predicts the $SO_2$ concentration by 47% on average, which is unsatisfactory. This over prediction can be attributed to the capture of $SO_2$

by alkaline ash in the furnace (Spliethoff et al, 1998). Due to higher potassium content of grass coupled with higher ash content than those of sawdust, higher $SO_2$ capture by ash during grass-based co-firing can be expected. The $SO_X$ model on the other hand does not take $SO_2$ capture by ash into consideration. The predicted trend of $SO_2$ emission for grass, however agrees with that of the experimental results.

### 6.2.4 Temperature Profiles

Temperature is one of the important parameters which influences the success in simulating the combustion parameters, especially $NO_X$ emissions. Figs. 6.30-6.35 show plots of simulated flue gas temperature and the experimental data for comparison. Next to each plot is the colour map from Fluent showing temperature field predictions in the computation domain. The temperature profile comparisons shown in the figures indicate good correspondence (Table 6.10) between the predicted and the measured temperatures at the various ports along the flue gas path, for all the co-firing conditions.

Table 6.10 Percentage error in predicting flue gas temperatures.

| | % difference between simulation and experimental data | | | |
|---|---|---|---|---|
| | Port 4 | Port 10 | Port D | Port 28 |
| Baseline | 1 | 1 | 0 | 6 |
| 10% SD | 1 | 2 | 1 | 3 |
| 15% SD | 1 | 5 | 0 | 5 |
| 20% SD | 1 | 5 | 2 | 4 |
| 10% GS | 8 | 4 | 4 | 2 |
| 15% GS | 10 | 3 | 4 | 2 |
| 20% GS | 9 | 2 | 5 | 3 |

Table 6.10 shows for each test the difference in percentage between the predicted and experimental temperature values vertically downwards along the radiative section from port 4 to port 28 (see table 4.6 for ports information). All errors are within 10%.

Temperature along the radiative section is expected to rise quickly near the burner mouth to reach a maximum at a short distance from it (port 10 in this case) and then fall gradually along the radiative section. For coal this trend is evidenced by both predicted and experimental temperature profiles. The trend for sawdust-based co-firing is that the simulation peak temperatures are slightly lower than the experimental ones. These might be due to the particle size. The small particle size helps the particles to release more volatiles at a higher rate (Tillman, 2000) promoting high heat release rate and a faster reaction such that when model port D is reached the temperature would be decreasing because it would have peaked earlier upstream of model port D.

Temperature profiles for grass-based co-firing show behaviour of higher simulation temperatures than experimental on the same port. This is because grass particles are even smaller (Table 3.3) and more reactive than those of sawdust and will increase temperatures rapidly right at the beginning of the radiative section. The actual particle size distribution of grass is easier to misrepresent than that of sawdust in modelling because of the following reasons. Firstly grass particle shape is cylindrical with high aspect ratio.

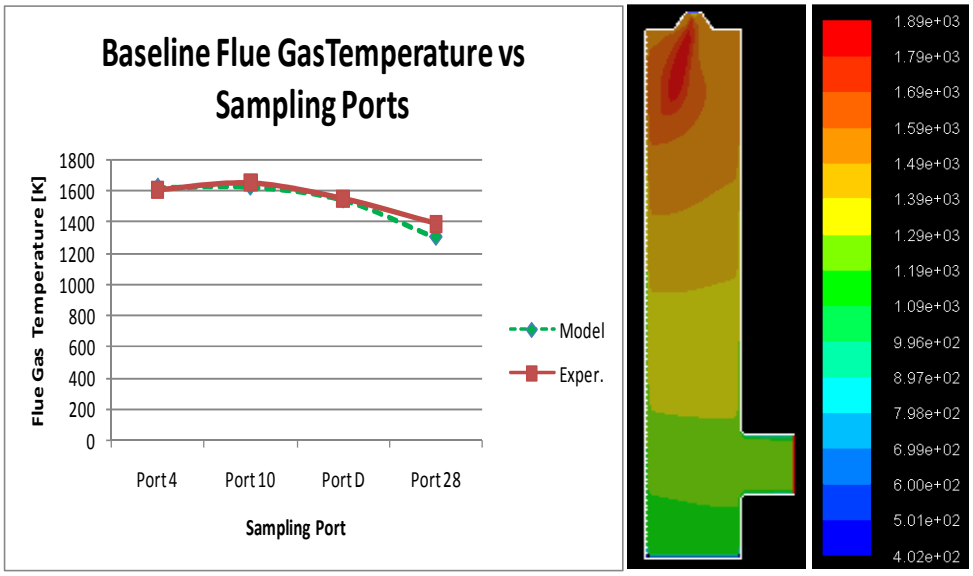


Figure 6.30 Temperature distribution for baseline coal A

For instance, a particle with 0.5 mm by 2cm can go through a 0.5 mm sieve and be classified as less than 0.5 mm while in actual fact it is a big particle because of its length. Secondly Fluent models biomass particles as ellipses using a shape factor. When a value 0.5 mm is entered in the particle size panel, it is treated as an ellipse whose surface area is equal to that of a 0.5 mm sphere. Thirdly Fluent does not allow the shape factors to be defined separately for each fuel stream. Grass has higher aspect ratios than sawdust that is why the discrepancies are more significant than in the charts for sawdust. The predictions are nevertheless good.

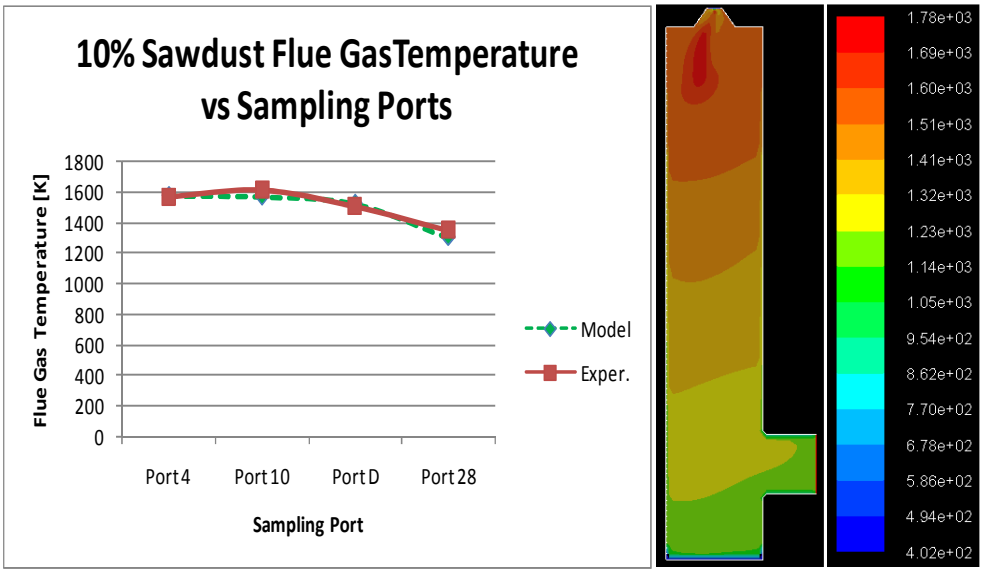


Figure 6.31 Temperature distribution for 10% sawdust / 90% coal A

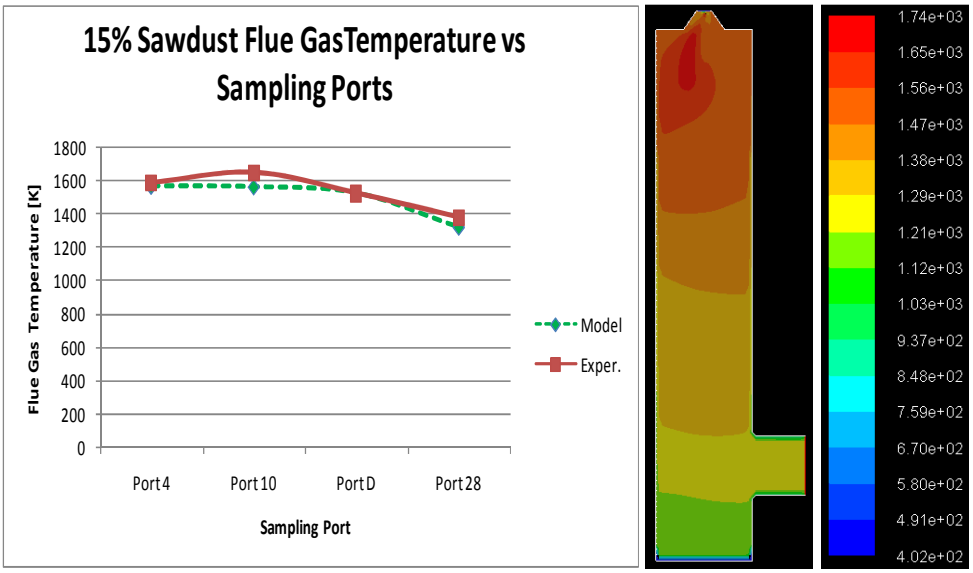

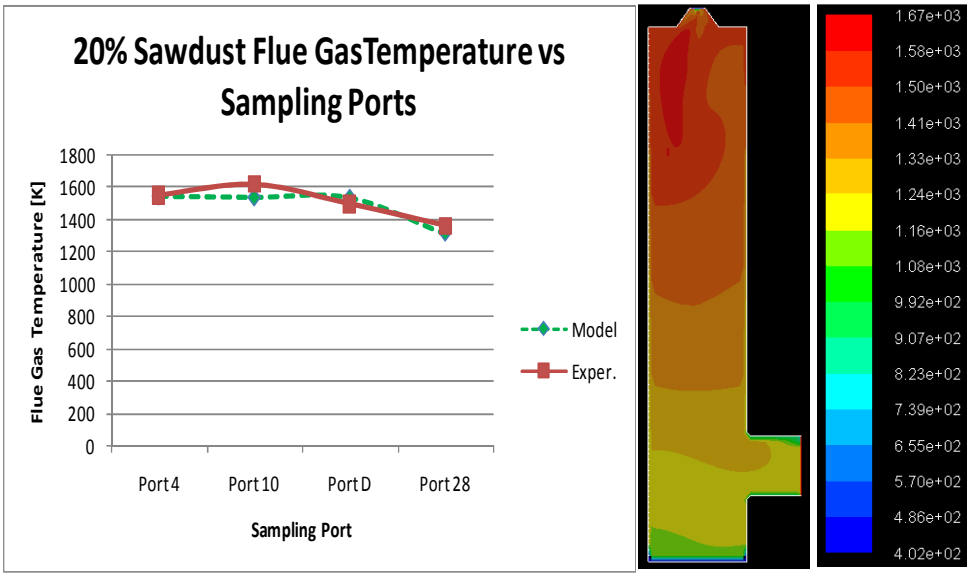


Figure 6.32 Temperature distribution for 20% sawdust / 80% coal A

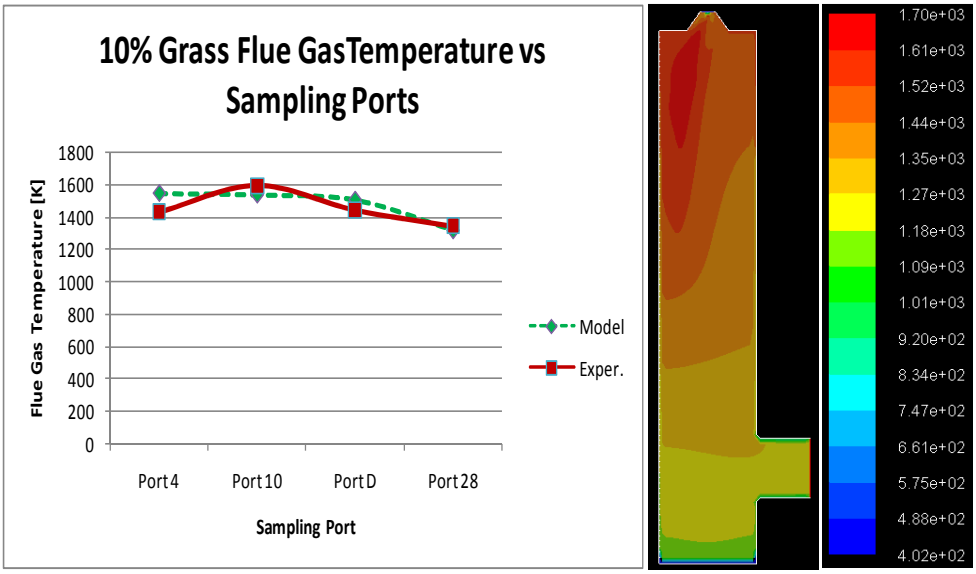


Figure 6.33 Temperature distribution for 10% grass / 90% coal A

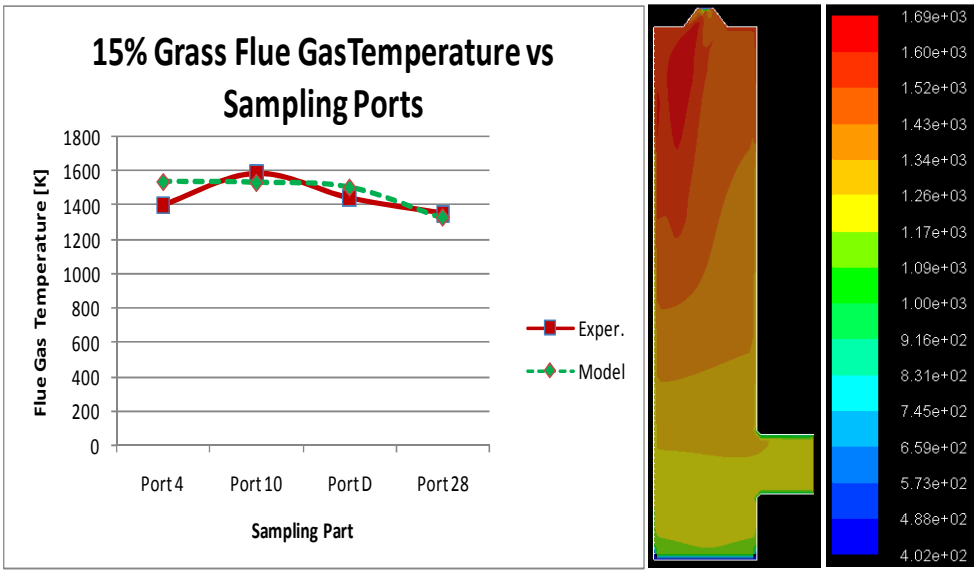


Figure 6.34 Temperature distribution for 15% grass / 85% coal A

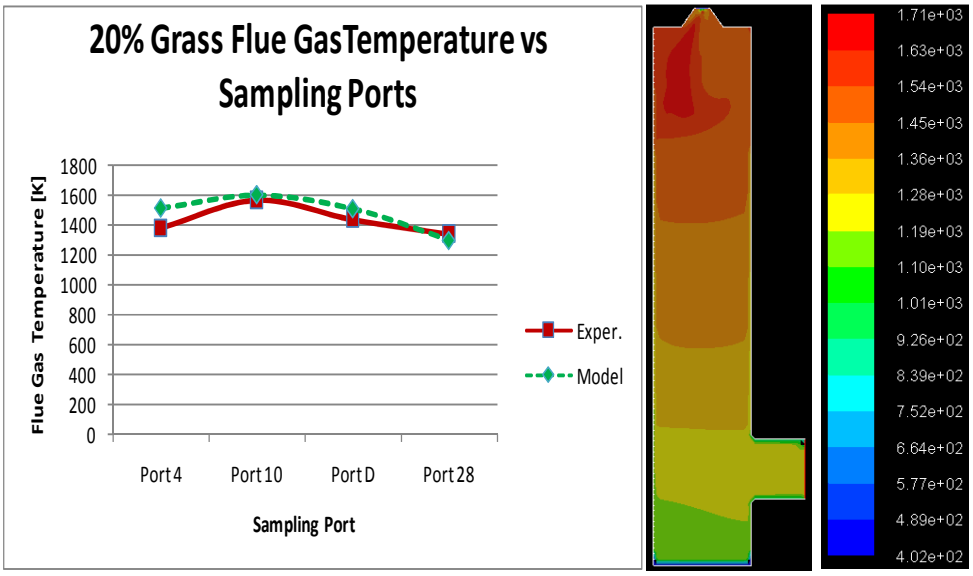


Figure 6.35 Temperature distribution for baseline coal A

# 7 CONCLUSION AND RECOMMENDATIONS

## 7.1 CONCLUSIONS

This project is the first to report on a pilot-scale experimental programme into the effects of co-firing biomass (of two types) with typical South African power station coal using a pulverised-fuel burner. The project included running computer simulations which were validated by the data from the Eskom Pilot Scale Combustion Test Facility (PSCTF). In general it may be said that the project was successfully completed. The achievements may be summarized with reference to the scope and objectives contained sections 1.3 as follows:

### 7.1.1 Percentage Reduction as Function of Co-firing Ratio

Tests were carried out using both herbaceous (grass) and ligneous (sawdust) types of biomass. For both types tests and simulations were carried out for three co-firing ratios, namely with 10%, 15% and 20% of biomass in the fuel blend, on an energy basis. It was found that the reduction in emissions increased as the biomass proportion was increased, in a non-linear manner. The reductions achieved for CO2, SO2 and NOx emissions at a co-firing ratio of 20% are summarised below for each type of biomass:

Table 7.1 Emissions of grass and sawdust at 20%

| | Grass | Sawdust |
|---|---|---|
| CO2 | 23% | 17% |
| SO2 | 28% | 15% |
| NOx | 49% | 29% |

### 7.1.2 Best Type of Biomass Based on Percentage Reduction in Emissions With Tolerable Slagging and Fouling Propensities

Grass (herbaceous) biomass is the best type of biomass as it resulted in greater emissions reductions than sawdust (ligneous). The QEMSCAN analysis of grass slag deposits indicated that they should be weak enough to be handled by soot blowing equipment. Sawdust co-firing produced a powdery type deposit dominated by a high proportion of thin walled cenospheres consisting of Ca-Fe bearing alumino and quartz glass, as well as molten fused type deposit which might be difficult to remove. Grass slag deposists on the other hand consist of Ca-Fe bearing alumino and quartz glass but with a comparatively higher proportion of anorthite that has crystallised out of the melt and have high proportion of voids which make them friable and easy to clean by soot blowing.

### 7.1.3 Optimum Biomass Ratio Based on Carbon Burnout for the Best Type of Biomass

The optimum co-firing ratio with grass would appear to be about 15% on an energy basis, but this would need to be confirmed by a detailed technical and economic feasibility study. The 15% grass has a better carbon burnout compared to 20% as shown in Table 7.2 below. The unburned carbon of 15% grass is 0.1 higher than that of 20% at port 21, but this difference is small and might very well be within lab tolerance compared to the difference in the other two ports. Although 20% grass has highest reductions in $NO_X$ emissions, 15% grass has highest emission reductions in $CO_2$ and $SO_2$.

Table 7.2 Unburned carbon for 15% and 20% grass along the radiative section

| | Port 9 | Port 15 | Port 21 |
|---|---|---|---|
| 15% grass | 4.6 | 1.7 | 1.1 |
| 20% grass | 4.9 | 2.0 | 1.0 |

### 7.1.4 The Effect of Biomass on the Ignitability of Low-volatile Coal

Biomass was found to improve ignitability. There were no perceived problems with flame stability, but no camera was available for image recording. Biomass co-firing was found to improve the ignitability of the typical power station coal used, at 1000 – 1200 ºC (DTF results) and during all the PSCTF tests except during that of 10% grass where a drop of 0.65% combustion efficiency was observed. The combustion efficiency determined from DTF results for this range indicate an improvement of between 0.1% and 1.4% for grass and between 0.8% and 2.45% for sawdust.

### 7.1.5 Validation of Simulation Technique Using the Experimental Results

The simulation procedure used was based on commercially-available CFD software ('Fluent' in this case) with additional specialist packages for emission calculations. The input data required for the simulations included reaction kinetics obtained from Drop-Tube Furnace tests. Comparison of the combustion and emissions characteristics with experimental data from the PSCTF showed that the simulation procedure was capable of predicting these characteristics with generally good accuracy.

## 7.2 RECOMMENDATIONS

This project is the first pilot-scale experimental investigation into the co-firing of biomass with coal in the South African context. The initial results from this project are positive towards using biomass co-firing as a

greenhouse mitigating strategy as well as a pollution control strategy. Based on the fundamental results of this initial project, the next step if biomass co-firing is to be investigated further would need to cover a full system economic and technical study. There are many aspects of power station design that would have to be considered, as well as the fuel collection, transportation and processing.

Currently there is no corrosion assessment system available on the PSCTF. Although South African coal generally has little chlorine and/or alkali (major elements which are associated with corrosion) (Kershaw et al, 1992), it is useful to monitor corrosion when testing a wide range of fuels including biomass and its mixtures with coal especially in view of fuel diversification strategy employed by Eskom. Biomass fuels can contain significant amounts of chlorine and alkali that may cause high temperature corrosion of steam tubes in a boiler.

The high volatile characteristics of biomass can be ideal for reburning. This mode of co-firing could not be tested because the PSCTF was not equipped for it. While modification of the plant may interrupt a busy schedule of important tests, it is recommended that time should be created so that the plant could be modified to include this mode.

The fouling probe installed on the system (which was not functioning at the time of the tests) gives qualitative assessment of fouling by monitoring temperatures. In future it is strongly recommended that the sampling should include the fouling deposits derived from the individual tests. The analyses of fouling and slagging deposits together with that of the fly ash/flue dust will provide a comprehensive assessment of the impact of co-firing coal with biomass. There is a lot of settling in the convective section, so careful design of the fouling probe is required to avoid contamination of the fouling deposits.

The flame monitoring camera (not functional at the time of testing) should be improved to quantitatively measure the physical characteristics of the flame such as geometric (size, shape and location), luminous parameters (brightness and non-uniformity) and thermodynamic parameters (flicker and temperature). These measurements will give a comprehensive assessment of the flame stability.

Gathering data regarding the amount of biomass and types that are present in South Africa for use in power stations is one of the important starting points. Earlier work done by the CSIR and Eskom on a Renewables Database in 1996 needs to be updated so that it can provide information on the types of biomass as opposed to the blanket distribution it had adopted. Development of heuristic models should be initiated, with a stochastic approach to take into account random factors such as wild fires, drought, and competition for biomass fuel with existing and future technologies. There is also little information about devolatilisation and char reactivity for biomass in the literature in general. For South Africa to engage in a meaningful co-firing research and development programme, a reaction kinetics database for different biomass types would need to be built.

The electricity generation industry in South Africa has been dominated by coal as the main source of energy. The existing technology and the standards for sampling and testing have been developed and fine-tuned for coal as the fossil fuel. The introduction of biomass co-firing would require changes in terms of system design, storage, safety requirements, transport and fuel preparation. Because biomass is a solid fuel there are similarities with coal but some properties differ, such as bulk density which is much lower than that of coal. The relatively lower calorific value puts more strain on the handling equipment per unit power output because of larger volumes that would have to be handled.

The non-friable nature of biomass poses challenges of grinding, especially for automated systems with a closed loop feedback control system. It would require biomass to be passed through a number of grinding machines to ensure the progressive reduction in size as it moves through the cascade until the required fineness is achieved. Biomass dust is both a health and safety hazard. The dust particles can easily be inhaled and cause respiratory illnesses, or cause allergic reactions to skin, eyes and nose, unless prevented by protective clothing. Dust clouds associated with handling volumes of biomass can cause explosions if extraction fans are not installed. It would be necessary to invest in personnel training to handle the new fuel.

Co-firing biomass with coal can reduce emissions but judicious choices of fuels and operating systems are required to accomplish that (Robinson et al, 1998). Some of the key elements in controlling emissions is the accurate fuel control flow. Traditional weight-loss feeders used in power stations fall under the category of proportional controllers characteristic of saw tooth response and steady state error. The development of innovative process control systems such as fuzzy logic control for biomass combustion technologies can improve and stabilize system operation and further reduce personnel costs.

Further expansion of and improvement of basic data and models is necessary. Commercially available databases contain information on properties of almost all relevant elements and compounds. However, there are still blanks in the information available on thermodynamic and physical properties of certain compounds and multi-component system which complicate the simulation of chemical reactions and processes at high temperatures.

# 8 LIST OF RERERENCES


Abbas, T.; Costa, M.; P. Costen, Godoy, S.; Lockwood, F.C. ; Ou, J.J. ; Romo-Millares, C. ; Zhou, J. (1994) NOx formation and reduction mechanisms in pulverized coal flames, Fuel, Volume 73, Issue 9, Sep 1994, pp 1423-1436.

Aho, M., Ferrer, E. (2005) *Importance of coal ash composition in protecting the boiler against chlorine deposition during combustion of chlorine-rich biomass*, Fuel, v 84, n 2-3, Jan-Feb, pp 201-212.

Annamalai, K.; Sweeten, J.; Freeman, M.; Mathur, M.; O'Dowd, W.; Walbert, G.; Jones, S. (2003) *Co-firing of coal and catle feedlot biomass (FB) fuels. Part III: fouling results from a 500, 000 BTU/h pilot plant scale boiler burner*, Fuel, v 82, February, pp 1195 – 1200.

Annamalai, K.; Thien, B.; Sweeten, J. (2003) *Co-firing of coal and catle feedlot biomass (FB) fuels. Part II. Performance results from 30 $kW_t$ (100, 000) BTU/h laboratory scale boiler burner, Fuel, v 82, pp 1183 -1193.*

Barroso, J.; Ballester, J.; Pina, A. (2007) *Study of coal ash deposition in an entrained flow reactor: Assessment of traditional alternative slagging indices, Fuel Processing Technology*, v 88, pp 865 – 876.

Battista, J.J.Jr; Hughes, E.E.; Tillman, D.A. (2000) *Biomass cofiring at Seward Station, Biomass and Bioenergy*, v 19, n 6, Dec. p 419-427.

Baukal, C.E.; Schwartz, R.E. (2001) *The John Zink Combustion Handbook*, Technology & Engineering.

Baxter, L.L.; Miles, T.R.; Miles Jr. T.R.; Jenkins, B. M.; Milne, T.; Dayton, D.; Bryers, R.W.; Oden L.L. (1998) *The behavior of inorganic material in biomass-fired power boilers: field and laboratory experiences*, Fuel Processing Technology, v 54, n 1-3, Mar, pp 47-78.

Baxter, Larry (2005) *Biomass-coal co-combustion: Opportunity for affordable renewable energy*, Fuel, v 84, n 10, July, pp 1295-1302.

Bebar, L.; Kermes, V.; Stehlik, P.; Canek, J.; Oral, J. (2002) *Low NOx burners – prediction of emissions concentration based on design*, measurements and modelling, Waste Mnagement, v 22, pp 443 – 451.

Beér, J.M. (1995) Minimizing $NO_x$ emissions from stationary combustion; *Reaction engineering methodology, Chemical Engineering Science*, v 49, n 24A, pp 4067 – 4083.

Boylan, D. ; Bush, V.; Bransby, D. I. (2000) *Switchgrass cofiring: pilot scale and field evaluation,* Biomass and Bioenergy, v 19, n 6, Dec, pp 411-417.

Bryers, R.W. (1996) *Fireside slagging, fouling, and high-temperature corrosion of heat-transfer surface due to impurities in steam-raising fuels*, Progress in Energy and Combustion Science, v 22, n 1, pp 29-120.

Cope, R.F.; Arrington, C.B.; Hecker, W.C. (1994) *Effect of CaO Surface Area on Intrinsic Char Oxidation Rates for Beulah Zap Chars*, Energy & Fuels, v 8, n 5, pp 1095 – 1099.

Demirbas, A. **(**2003) *Sustainable cofiring of biomass with coal***,** Energy Conversion and Management, v 44, n 9, June, pp 1465-1479.

Demirbas, Ayhan (2004) *Combustion characteristics of different biomass fuels,* Progress in Energy and Combustion Science, v 30, n 2, pp 219-230.

Di Nola, G.; De Jong, W.; Spliethoff, H. (2008) *The fate of main gaseous and nitrogen species during fast heating rate devolatilization of coal and secondary fuels using a heated wire mesh reactor*, Fuel processing technology, doi:10.1016/j.fuproc.2008.10.009.

Dong, L.; Gao, S.; Song, W.; Xu, G. (2007) *Experimental study of NO reduction over biomass char, Fuel Processing Technology*, v 88, pp 707 – 715.

EIA. (2005). South Africa Country Analysis Brief. INTERNET. http://www.eia.doe.gov/emeu/cabs/safrica.html. Cited 16 March 2005.

Engineering Toolbox (2007) Emissivity coefficients. INTERNET. http://www.engineeringtoolbox.com/emissivity-coefficients-d_447.html. Cited 22 Jan 2007.

Essenhigh, R.H., Misra, M.K., Shaw D.W. (1989) Ignition of coal particles: A review, Combustion and Flame, v 77, n 1, Jul, Pp 3-30.

Everson, R. C.; Neomagus, H. W.J.P. ; Kaitano, R.; Falcon, R.; van Alphen C.; du Cann V. M. (2008) *Properties of high ash char particles derived from inertinite-rich coal: 1. Chemical, structural and petrographic characteristics,* Fuel, v 87, n 13-14, Oct, pp 3082-3090.

Falcon, R. (2006) The South African coal industry – An introduction overview, Coal Ash conference, 15 – 17 Feb, Johannesburg.

Falcon, R. (2007) *Impact of coal quality on combustion and power generation, Coal Combustion conference*, 5-9 Nov, Johannesburg.

Field, M.A. (1970) *Measurements of the effect of rank on combustion rates of pulverised coal*, Combustion and Flame, v14, pp 237-248.

Fluent Inc. (2006) *FLUENT 6.3 User's Guide*, Flunt Inc., Lebanon.

Frandsen, F.J. (2005) Utilizing biomass and waste for power production—a decade of contributing to the understanding, interpretation and analysis of deposits and corrosion products, Fuel, v 84, n 10, July, pp 1277-1294.

Gani, A; Morishita, K; Nishikawa, K; Naruse, I. (2005) *Characteristics of Co-combustion of Low-Rank Coal with Biomass*, Energy and fuels, v 19, n 4, May, pp 1652 – 1659.

Gil, A., Bartolomé, C., Ramos, I. (2009) Co-firing cynara biomass residues with two coals in a PF Furnace.INTERNET.http://www.combustion.org.uk/ ECM_2009/ P810153.pdf. Cited 18 March 2010.

Grotkjær, T., Dam-Johansen, K., Jensen, A.D., Glarborg, P. (2003) *An experimental study of biomass ignition*, Fuel, v 82, n 7, May, pp 825-833.

Gungor, A. (2008) Two-dimensional biomass combustion modeling of CFBFuel, v 87, n 8-9, Jul, pp 1453-1468

Gungor, A. (2009) Prediction of SO2 and NOx emissions for low-grade Turkish lignites in CFB combustors, Chemical Engineering Journal, v 146, n 3, Feb, pp 388-400.

Hatt, Roderick M. (1990) *Fireside Deposits in Coal-Fired Utility Boilers*, Progress in Energy and Combustion Science, Vol 16, pp 235-241.

Heinzel, T.; Siegle, V.; Spliethoff, H. ; Hein K. R. G. (1998) *Investigation of slagging in pulverized fuel co-combustion of biomass and coal at a pilot-scale test facility,* Fuel Processing Technology, v 54, n 1-3, Mar 1998, pp 109-125.

Haider, A. ; Levenspiel , O. (1989) Drag coefficient and terminal velocity of spherical and nonspherical particles, Powder Technology, v 58, n 1, May, pp 63-70.

Hughes, E. (2000) *Biomass cofiring: Economics, policy and opportunities, Biomass and Bioenergy*, v 19, n 6, Dec, p 457-465.

Hus, P. J.; Tillman, D. A. (2000) *Cofiring multiple opportunity fuels with coal at Bailly Generating Station,*Biomass and Bioenergy, v 19, n 6, Dec, pp 385-394.

Kastanaki, E.; Vamvuka, D. (2006) *A comparative reactivity and kinetic study on the combustion of coal–biomass char blends,* Fuel, v 85, n 9, Jun, pp 1186-1193.

Kaufmann, H., Nussbaumer, T., Baxter, L., Yang, N. (2000) *Deposit formation on a single cylinder during combustion of herbaceous biomass*, Fuel, v 79, n 2, Jan, pp 141-151.

Kazagic, A.; Smajevic I. (2007) *Experimental investigation of ash behavior and emissions during combustion of Bosnian coal and biomass*, Energy, v 32, n 10, Oct, pp 2006-2016.

Kazagic, A.; Smajevic, I. (2009) *Synergy effects of co-firing wooden biomass with Bosnian coal, Energy*, v 34, n 5, May, pp 699-707.

Kershaw, J.R., Taylor, G.H. (1992) *Properties of Gondwana coals with emphasis on the Permian coals of Australia and South Africa*, Fuel Processing Technology, n 31, n 2, Jul, pp 127-168.

Khan, M.R. (1989) Prediction of sulphur distribution in products during low temperature coal pyrolysis and gasification, Fuel, v 68, pp 1439-1449.

Khan, A.A.; de Jong, W.; Jansens, P.J.; Spliethoff, H.; (2009) Biomass combustion in fluidized bed boilers: Potential problems and remedies, Fuel Processing Technology, v 90, n 1, Jan 2009, pp 21-50.

Kokkinos, A.; Wasyluk, D.; Boris, M. (2002). Comparison of NOx Emissions Reductions with PRB and Bituminous Coals on Tangentially-Fired Boilers.INTERNET.http://www.babcock.com/pgg/tt/pdf/BR-1734.pdf. Cited 7 June 2005.

Kuo, K.(1986) *Principles of combustion*, John Wiley & Sons, New York.

Kupka, T.; Mancini,M.; Irmer, M.; Weber, R. (2008) *Investigation of ash deposit formation during co-firing of coal with sewage sludge, saw-dust and refuse derived fuel*, Fuel, Volume 87, Issue 12, September 2008, pp 2824-2837.

Kwong, P.C.W.; Chao, C.Y.H.; Wang, J.H.; Cheung, C.W.; Kendall, G. (2007) *Co-combustion of coal with rice husks and bamboo*, Atmospheric Environment, v 41, May, pp 7462-7472.

Leppälahti J. (1995) *Formation of NH3 and HCN in slow-heating-rate inert pyrolysis of peat, coal and bark*, Fuel, v74, n9, pp 1363 – 1368.

Li, C-Z.; Tan, L.L. (2000) *Formation of $NO_x$ and $SO_x$ precursors during the pyrolysis of coal and biomass. Part III. Further discussion on the formation of HCN and NH3 during pyrolysis*, Fuel, v 79, pp 1899 – 1906.

Li, S., Whitty, K.J. (2009) *Investigation of Coal Char–Slag Transition during Oxidation: Effect of Temperature and Residual Carbon*, Energy Fuels, v 23 n 4, pp 1998–2005, DOI: 10.1021/ef801082j.

Lunden, M.M., Yang, N.Y.C, Headley, T.J., Shaddix, C.R. (1998) *Mineral-char interactions during char combustion of a high-volatile coal*, Symposium (International) on Combustion, v 27, n 2, pp 1695-1702.

Ma, L.; Jones, J.M.; Pourkashanian, M.; Williams, A. (2007) Modelling the combustion of pulverized biomass in an industrial combustion test furnace, Fuel, v 86, n 12-13, Aug 2007, pp 1959-1965

Ma, L.; Gharebaghi, M.; Porter, R.; Pourkashanian, M.; Jones, J.M. ; Williams, A. (2009) Modelling methods for co-fired pulverised fuel furnaces, Fuel, doi:10.1016/j.fuel.2009.02.030.

Maciejewska, A.; Veringa, H.; Sanders, J.; Peteves, S.D. (2006) *Co-firing of biomass with coal: Constraints and role of biomass treatment, Institute of Energy*. ISBN 92-79-02989-4/ISSN 1018-5593.

Meesri, C.; Moghtaderi, B. (2002) *Lack of synergetic effects in the pyrolytic characteristics of woody biomass/coal blends under low and high heating rate regimes*, Biomass and Bioenergy, v 23, n 1, Jul, pp 55-66.

Michelsen, H.P., Frandsen, F., Dam-Johansen, K., Larsen, O.H. (1998) *Deposition and high temperature corrosion in a 10 MW straw fired boiler*, Fuel Processing Technology, v 54, n 1-3, Mar, pp 95-108.

Moghtaderi , B. (2007) *A study on the char burnout characteristics of coal and biomass blends,*Fuel, v 86, n 15, Oct, pp 2431-2438.

Molcan, P., Lu, G., Le Bris, T., Yan, Y., Taupin, B., Caillat, S. (2009) *Characterisation of biomass and coal co-firing on a 3 MWth Combustion Test Facility using flame imaging and gas/ash sampling techniques*, Fuel, v 88, n 12, Dec, pp 2328-2334.

Mondi.(2005).Mondi Energy Generation from Biomass Project.INTERNET.http://www.southsouthnorth.org/country_project_details.asp?country_id=5&project_id=76&project_type=1. Cited 23 March 2005.

Narayanan, K.V.; Natarajan, E. (2007) *Experimental studies on cofiring of coal and biomass blends in India*, Renewable Energy, v 32, n 15, Dec, pp 2548-2558.

Nutalapati, D., Gupta, R., Moghtaderi, B., Wall T.F. (2007) *Assessing slagging and fouling during biomass combustion: A thermodynamic approach allowing for alkali/ash reactions*, Fuel Processing Technology, v 88, n11-12, Dec, pp 1044-1052.

Obernberger, I. (1998) *Decentralized biomass combustion: State of the art and future development*, Biomass and Bioenergy, v 14, n1, pp33-56.

Pan, Y. G.; Velo, E.; Puigjaner, L. (1996) Pyrolysis of blends of biomass with poor coals,Fuel, v 75, n 4, Mar 1996, pp 412-418.

Pallarés, J., Gil, A., Cortés,C., Herce, C. (2009) *Numerical study of co-firing coal and Cynara cardunculus in a 350 MWe utility boiler*, Fuel Processing Technology, v 90, n10, Oct, pp 1207-1213.

Pedersen, L.S.; Nielsen, H.P.; Kiil, S.; Hansen, L.A.; Dam-Johansen, K.; Kildsig, F.; Christensen, J.; Jespersen, P. (1996) Full-scale co-firing of straw and coal, Fuel, v 75, n 13, Oct, pp 1584-1590.

Phong-Anant, D. (1985) *Nitrogen Oxide Formation from Australian Coals, Combustion and Flame*, v 62, pp 21 – 30.

Pronobis M. (2005) *Evaluation of the influence of biomass co-combustion on boiler furnace slagging by means of fusibility correlations,* Biomass and Bioenergy, v 28, n 4, Apr, pp 375-383.

Pronobis, M. (2006) *The influence of biomass co-combustion on boiler fouling and efficiency*, Fuel, v 85, n 4, March, pp 474-480.

Ren, Q.; Zhao, C.; Wu, X.; Liang, C.; Chen, X.; Shen, J.; Tang, G.; Wang, Z. (2008) *Effect of mineral matter on the formation of NOX precursors during biomass pyrolysis*, Journal of Analytical and Applied Pyrolysis, doi:10.1016/j.jaap.2008.08.006.

Robinson, A. L.; Junker, H.; Buckley, S. G. ; Sclippa, G.; Baxter, L. L. (1998) *Interactions between coal and biomass when cofiring*, Symposium (International) on Combustion, v 27, n 1, pp 1351-1359.

Robinson, A.L.; Rhodes, J.S.; Keith, D.W. (2003) *Assessment of Potential Carbon Dioxide Reductions Due to Biomass-Coal Cofiring in the United States,* Environmental Science and Technology, v 37, n 22, Nov 15, pp 5081-5089.

Robinson, A.L; Junker, H.; Baxter, L.L. (2002) Pilot-Scale Investigation of the Influence of Coal-Biomass Cofiring on Ash Deposition, Energy and Fuels, v 16, pp 343-355.

Robinson, Allen; Gera, D.; Mathur, M.P.; Freeman, M.C. (2002) *Effect of large aspect ratio of biomass particles on carbon burnout in a utility boiler*, Energy and Fuels, v 16, n 6, Nov/Dec, pp 1523-1532.

Sabastian, T.(2002).Modern Boiler Types and Applications.INTERNET. http://eny.hut.fi/library/steam_Boilers_demo/Mordern_boiler_applications/Mordern_boiler_types_and_applications.pfd . Cited 22 March 2005.

Salmenoja, K., Makela, K., Hupa, M., Backman, R. (1996) *Superheater corrosion in environments containing potassium and chlorine*, Journal of the Institute of Energy, v 69, n 480, Sep, pp 155-162.

Scaroni, A.W; Walker Jr., P.L.; Essenhigh, R.H. (1981) Kinetics of lignite pyrolysis in an entrained-flow isothermal furnace, Fuel, v 60, n 1, Jan 1981, pp 71-76.

Sami, M.; Annamalai, K.; Wooldridge, M. (2001) *Co-firing of coal and biomass fuel blends*, Progress in Energy and Combustion Science, v 27, n 2, pp 171-214.

Savolainen, K. (2003) *Co-firing of biomass in coal-fired utility boilers, Applied Energy, v 74, n 3-4, Mar-Apr, pp369-381.*

Skodras, G.; Grammelis, P.; Samaras, P.; Vourliotis, v; Kakaras, E.; Sakellaropoulos, G.P. (2002) *Emissions monitoring during coal waste wood co-combustion in an industrial steam boiler,* Fuel, v 81, n 5, March , pp 547-554.

Sondreal, E.A.; Benson, S.A.; Hurley, J.P.; Mann, M.D.; Pavlish, J.H.; Swanson, M.L.; Weber, G.F.; Zygarlicke, C.J. (2001) *Review of advances in combustion technology and biomass cofiring*, Fuel Processing Technology, v 71, n 1-3, June, pp 7-38.

Spliethoff, H.; Greul, U.; Rüdiger, H.; Hein, K. R.G. (1996) *Basic effects of $NO_x$ emissions in air staging and reburning at a bench-scale test facility*, Fuel, v 75, n 5, pp 560 – 564.

Spliethoff, H.; Hein, K.R.G. (1998) *Effect of co-combustion of biomass on emissions in pulverized fuel furnaces*, Fuel Processing Technology, v 54, n 1-3, Mar, pp 189-205.

Stubenberger, G.; Scharler, R.; Zahirovic, S.; Obernberger, I. (2008) *Experimental Investigation of nitrogen release from different solid biomass fuels as a basis for release models*, Fuel, v 87, pp 793 - 806.

Su, S.; Pohl, J.H.; Holcombe, D.; Hart, J.A. (2001) Techniques to determine ignition, flame stability and burnout of blended coals in p.f.

power station boilers, Progress in Energy and Combustion Science, v 27, pp 75-98.

Tarr, R.; Els, C.; Müller, M.; Mbangeleli, A.; Van Vyk, C.; Theron, J.; Strauss, J.J.; Hahn, W.; (2006) *The South African coal industry – An introduction overview*, Coal Ash conference, 15 – 17 Feb, Johannesburg.

Tillman, D.A. (2000) *Biomass cofiring: the technology, the experience, the combustion consequences*, Biomass and Bioenergy, v 19, pp 365 -384.

Tsubouchi, N; Ohtsuka, Y. (2007) Nitrogen Chemistry in coal pyrolysis: Catalytic roles of metal cations in secondary reactions of volatile nitrogen and char nitrogen, Fuel Processing Technology, v 89, pp 379 – 390.

Vamvuka, D. ; Kakaras, E.; Kastanaki, E.; Grammelis ,P. (2003) *Pyrolysis characteristics and kinetics of biomass residuals mixtures with lignite,* Fuel, v 82, n 15-17, Oct-Dec, pp 1949-1960.

Vamvuka, D; Troulinos, S.; Kastanaki, E. (2006) *The effect of mineral matter on the physical and chemical activation of low rank coal and biomass materials,*Fuel, v 85, n 12-13, Sep, pp 1763-1771.

Van Alphen, C. (2005). *Factors influencing fly ash formation and slag deposit formation (slagging) on combusting a South African pulverised fuel in a 200 MWe boiler*. PhD thesis, University of Witwatersrand.

Van Alphen C. (2007) *Automated mineralogical analysis of coal and ash products – Challenges and requirements, Minerals Engineering*, v 20, Feb, pp 496 – 505.

Van Alphen, C. (2008). Co-firing coal and biomass - clinkers:*Technical Memorandum FR 02, Corporate Services Division Eskom Research and Innovation Department (ERID) (unpublished)*.

Van der Riet, M. (1998) Drop Tube Furnace (DTF) Kinetic Theory, *Corporate Services Division Eskom Research and Innovation Department (ERID) (unpublished)*.

Van Dyk, J.C., Baxter, L.L., van Heerden, J.H.P., Coetzer, R.L.J. (2005) *Chemical fractionation tests on South African coal sources to obtain species-specific information on ash fusion temperatures (AFT)*, Fuel, v 84, n 14-15, Oct, pp 1768-1777.

Van Loo, S.; Koppejan, J. (2002) *Handbook of Biomass Combustion and Co-firing*, Twente University Press, Enschede.

Vuthaluru, H.B. (2004) *Investigations into the pyrolytic behaviour of coal/biomass blends using thermogravimetric analysis*, Bioresource Technology, v 92, pp 187 – 195.

Wagner, N.J. (2008) *The characterization of weathered discard coals and their behaviour during combustion*, Fuel, v 87, n 8-9, Jul, pp 1687-1697.

Watson, H.; Sibanda, D. (2008) *GIS mapping of areas suitable for various biofuel crops in SADC countries*, Biofuel and Renewable Energy Conference, 12 June, Johannesburg.

Wieck-Hansen, Kate; Overgaard, Peter; Larsen, Ole Hede (2000) *Cofiring coal and straw in a 150 $MW_e$ power boiler experiences*, Biomass and Bioenergy, v 19, n 6, Dec, pp 395-409.

Wigley, F.; Williamson, J.; Malmgren, A.; Riley G. (2007) Ash deposition at higher levels of coal replacement by biomass, Fuel Processing Technology, v 88, n 11-12, Dec, pp 1148-1154

*Wistrom, K (2005***)** The Importance of Damper Drive Performance For Clean Air. INTERNET. http://www.electricity-today.com/et/issue0702/i07_ performance.htm. Cited 7 June 2005.

Wu, C.; Tree D.; Baxter, L.; (2007) *Reactivity of NH3 and HCN during low-grade fuel combustion in swirling flow burner*, Proceedings of the combustion Institute, v 31, pp 2787 – 2794.

Zheng, Y.; Jensen, P. A.; Jensen, A.D.; Sander, B.; Junker, H. (2007) *Ash transformation during co-firing coal and straw*, Fuel, v 86, n 7-8, May 2007, pp 1008-1020.

# 9 LIST OF APPENDICES

APPENDIX A : Data Logs for the tests conducted in September 2007 (First Tests).

APPENDIX B: Tables of averages from the data logs of the first tests.

APPENDIX C: Curve fitting data for the first data.

APPENDIX D: Handwritten log sheets and combustible data for the first tests.

APPENDIX E: Data Logs for the tests conducted in August 2008 (Repeat Tests).

APPENDIX F: Tables of averages from the data logs of the repeat tests.

APPENDIX G: Curve fitting data for the repeat tests.

APPENDIX H: Handwritten log sheets for repeat tests.

APPENDIX I: Printout of the output from the DTF program.

APPENDIX J: Printout of the spreadheet that was used to correct the DTF program and summary of reaction kinetics.